

ICP-MS ANALYSIS OF FISSION PRODUCT DIFFUSION IN GRAPHITE FOR HIGH-TEMPERATURE GAS-COOLED REACTORS

A DISSERTATION

Presented to the Faculty of the Graduate School

at the

University of Missouri

In Partial Fulfillment of the Requirements for the Degree of

Doctor of Philosophy

By:

LUKAS M. CARTER

Dr. J. David Robertson, Committee Chair

December, 2015

The undersigned, appointed by the Dean of the Graduate School, have examined the dissertation entitled:

REAL TIME ANALYSIS OF FISSION PRODUCT DIFFUSION IN GRAPHITE IN HIGH-TEMPERATURE GAS-COOLED REACTORS

Presented by LUKAS M. CARTER,

A candidate for the degree of Doctor of Philosophy,

And hereby certify that, in their opinion, it is worthy of acceptance.

Dr. J. David Robertson

Dr. C. Michael Greenlief

Dr. Justin R. Walensky

Dr. William H. Miller

Dr. John D. Brockman

DEDICATION

For my mom and my sister, who have supported me since before I carried out my first science experiment (which took place on my elementary school playground, and for which I was sent home)

ACKNOWLEDGEMENTS

I'd like to express my gratitude to those who helped me on my journey through graduate school. First I'd like to thank my advisors, Dr. J David Robertson and Dr. John Brockman, for believing in me and providing support during every triumph, and advice and encouragement during every roadblock I've encountered. I can't thank either of you enough, and I can't express the magnitude of the impact either of you have made on my development as a chemist.

I'd like to thank Dr. Sudarshan Loyalka for his invaluable assistance and many helpful discussions. Dr. Loyalka's mathematical talent still leaves me in awe at times.

Much of my work would have been impossible without the excellent work done by the machinists at the MURR Science Instrument Shop. Dr. Rajesh Gutti and David Nicolaus provided tremendous assistance with the design of the experiment components used in my research.

Thanks to Barry Higgins and Jim Guthrie for ICP-MS support at MURR, and to Dr. Steve Morris and Dr. Mike Glascock for helpful discussions and use of laboratory equipment.

Finally I'd like to thank my committee members, Dr. Mike Greenlief, Dr. Justin Walensky, and Dr. Bill Miller, for your immensely helpful input and support.

TABLE OF CONTENTS

Acknowledgements	ii
List of Figures	xii
List of Tables	xvi
List of Symbols and Abbreviations	xvii
Abstract	xviii
CHAPTER 1: INTRODUCTION	1
1.1. HTGR design and capabilities	2
1.1.1. TRISO fuel concept	5
1.2. Core structural materials and fission product release mechanisms	7
1.3. References	9
CHAPTER 2: DIFFUSION THEORY	11
2.1. Overview	11
2.2. Fick's laws of diffusion	11
2.3. Solutions of the diffusion equation	13
2.4. Diffusion models	13
2.4.1. Barrier model	13

2.4.2. Booth model	14
2.4.2.1. Short time solutions	18
2.4.2.2. Non-uniform initial distributions	19
2.4.3. Sandwich model	20
2.4.4. Exact multilayer model	22
2.5. Deviations from Fickian behavior	24
2.6. Factors affecting diffusion in HTGRs	25
2.6.1. Graphite structural considerations	25
2.6.2. Radiological considerations	27
2.6.3. Chemical considerations	28
2.6.3.1. Concentration effects	28
2.6.3.2. Multicomponent systems	28
2.6.3.3. Graphite oxidation	28
2.6.4. The nature and state of diffusing fission products	29
2.6.5. Mechanisms of diffusion in graphite	29
2.6.5.1. Lattice diffusion	29
2.6.5.2. Grain boundary diffusion	30
2.6.5.3. Surface diffusion	30
2.6.5.4. Gas-phase diffusion	30
2.6.5.5. Convection	30
2.6.5.6. Combined mechanisms	31

2.7. References	31
CHAPTER 3: PREVIOUS WORK	33
3.1. Leyers' experiments	33
3.1.1. Sample preparation	33
3.1.2. Experimental	34
3.1.3. Results	34
3.2. Fukuda's experiments	35
3.2.1. Sample preparation	35
3.2.2. Concentration profile measurements	36
3.2.3. Results	37
3.3. Hayashi's experiments	37
3.3.1. Sample preparation	37
3.3.2. Diffusion measurements	37
3.3.3. Results	38
3.4. References	38
CHAPTER 4: ANALYTICAL TECHNIQUES	40
4.1. Diffusion cell	41
4.1.1. Overview	42
4.1.2. Design features	42

4.1.2.1. Aerosol inlet/outlet tubes	42
4.1.2.2. Sample chamber	43
4.1.2.3. Tube furnace	44
4.1.2.4. Aremco 890 cement	45
4.1.2.4.1. Graphite bonding experiments	45
4.1.2.5. SiC construction	48
4.1.3. Diffusion cell temperature testing	48
4.1.4. Diffusion cell assembly, disassembly, and maintenance	50
4.1.5. Diffusion cell development history	51
4.2. Gas-jet system	54
4.2.1. Overview	54
4.2.2. PALAS GFG-1000 aerosol generator	56
4.2.3. Aerosol characterization	56
4.3. ICP-MS	58
4.3.1. Overview	58
4.3.2. Nexion 300X ICP-MS	59
4.3.3. Dual-inlet spray chamber	59
4.4. Neutron activation analysis	60
4.4.1. Overview	61
4.4.2. ICP-MS calibration	61
4.5. References	63

CHAPTER 5: TIME-LAG MEASUREMENTS OF CESIUM DIFFUSION IN GRAPHITE	64
5.1. Overview	64
5.2. Theoretical	64
5.3. Sample preparation	64
5.4. Diffusion measurements	67
5.5. Data analysis	67
5.6. Results	67
5.7. Discussion of experimental error	70
5.8. Conclusion	71
5.9. Proposed experimental design modifications	72
5.10. References	74
CHAPTER 6: DETERMINATION OF DIFFUSION COEFFICIENTS FOR CESIUM IN IG-110 GRAPHITE VIA SPHERICAL RELEASE METHOD	75
6.1. Highlights	75
6.2. Abstract	75
6.3. Introduction	76
6.4. Materials and methods	77
6.4.1. The release model and method	77
6.4.2. Materials and sample preparation	80

6.5. Experimental	82
6.6. Data and analysis	86
6.7. Discussion	91
6.8. Conclusions	93
6.9. Acknowledgements	93
6.10. References	94
CHAPTER 7: CALIBRATION OF A SYSTEM FOR MEASUREMENTS OF FISSION PRODUCT DIFFUSION COEFFICIENTS IN GRAPHITE	96
7.1. Abstract	96
7.2. Introduction	97
7.3. Theory	98
7.4. Experimental	101
7.4.1. Overview	101
7.4.2. Specific methods	104
7.5. Results and discussion	106
7.6. Conclusion	107
7.7. Acknowledgements	108
7.8. References	108
CHAPTER 8: DETERMINATION OF DIFFUSION COEFFICIENTS FOR CESIUM IN NBG-18 GRAPHITE VIA SPHERICAL RELEASE METHOD	110

8.1. Highlights	110
8.2. Abstract	110
8.3. Introduction	111
8.4. Theory	112
8.5. Experimental	116
8.5.1. Instrumentation	116
8.5.2. Specific methods	118
8.5.2.1. Sample preparation	118
8.5.2.2. Initial Cs content analysis	119
8.5.2.3. Diffusion measurements	120
8.5.2.4. Final Cs content analysis	120
8.6. Results	121
8.7. Discussion	124
8.8. Conclusion	128
8.9. Acknowledgements	129
8.10. References	129
8.11. Appendix	130
CHAPTER 9: SILVER AND STRONTIUM INFUSION EXPERIMENTS	135
9.1. Overview	135
9.2. Gas-phase infusion	135

9.3. Powdered graphite infusion	137
9.3.1. Quartz container	137
9.3.2. Molybdenum container	140
9.3.3. Graphite container	143
CHAPTER 10: DETERMINATION OF DIFFUSION COEFFICIENTS FOR IODINE IN IG-110 VIA SPHERICAL RELEASE METHOD	146
10.1. Highlights	146
10.2. Abstract	146
10.3. Introduction	147
10.4. Theory	147
10.5. Experimental	148
10.5.1. Instrumentation	148
10.5.2. Specific methods	149
10.5.2.1. Sample preparation	149
10.5.2.2. Initial iodine content analysis	149
10.5.2.3. Diffusion measurements	150
10.5.2.4. Final iodine content analysis	150
10.6. Results	153
10.7. Discussion	156
10.8. Conclusion	160
10.9. References	160

CHAPTER 11: CONCLUSIONS AND FUTURE WORK	161
CHAPTER 12: APPENDICES	164
12.1. Derivation of commonly used equations	165
12.1.1. Fick's second law	165
12.1.2. Spherical release series	165
12.1.3. Spherical release short time	172
12.2. Development of a MS Excel program for calculation of diffusion coefficients	177
12.2.1. Introduction	178
12.2.2. ICP-MS data analysis spreadsheet	178
12.2.3. Spherical release diffusion calculator/simulator	183
12.2.4. Spherical infusion calculator/simulator	186
VITA	190

LIST OF FIGURES

1.1: Fuel design and fabrication and core schematic for prismatic block and pebble bed HTGRs. Adapted from [1]

2.1: Initial configuration of the finite barrier model. Dots represent diffusant particles (FPs).

2.2: Typical curve from a lag time analysis experiment. The blue curve corresponds to experimental data. The red curve is an extrapolation of the steady-state portion of the curve, and the t-intercept is the lag time used to calculate the diffusion coefficient

2.3: Initial configuration of the spherical release model. Dots represent diffusant particles (FPs).

2.4: Initial configuration of the sandwich model. Dots represent diffusant particles (FPs).

2.5: Initial configuration of the exact multilayer model

2.6: Graphite molecular structure. Basal plane top view is at left; side view at right. Adapted from [7].

2.7: General fabrication process and resulting variance in microstructural features of graphite grades used previously (top left and right, historical reference H-451) and current candidate graphites (bottom left and right, IG-110 and NBG-18, respectively) for HTGRs. Adapted from [8].

3.1: Leyers' experimental setup for cesium release in flowing helium [1]

3.2: Schematic of Fukuda's sample design [2]

4.1: Schematic of experimental setup (release configuration)

4.2: Actual experimental setup

4.3: SiC diffusion cell schematic

4.4: Close-up of sample holder region in permeation configuration

- 4.5:** Close-up of sample holder region in release configuration. Dots in spherical pebble represent diffusant particles dispersed within the pebble.
- 4.6:** Close-up of sample holder region in profile configuration. The helium flow is present to prevent oxidation of the graphite donor and acceptor specimens; no aerosol is present as transport is not monitored in real time. In this scheme, the diffusant concentration profile in the acceptor specimen would be analyzed by a sectioning technique.
- 4.7:** Aremco 890 SiC-Graphite seal at start (top) and end (bottom) of 900° C, 10 hr heating cycle under argon atmosphere
- 4.8:** Aremco 890 graphite-SiC seal during helium permeation experiment.
- 4.9:** Interior of tube furnace at 1200K. The diffusion cell is at center.
- 4.10:** Interior of diffusion cell post-temperature test. The vertical marks spanning the length of the SiC outside tube are friction marks from insertion of the interior components. Note the Aremco 890 seal appears intact and the graphite surface shows minimal signs of oxidation.
- 4.11:** Quartz cell design which was to be fabricated by Technical Glass. The base of the cell is designed to be removable
- 4.12:** Quartz cell designed at MURR
- 4.13:** Graphite disc bonded to quartz tube using Aremco Graphi-bond, after curing procedure. Note cracking in quartz tube at 2 o'clock position and air bubbles distributed around the edges of the barrier.
- 4.14:** Stability of aerosol production over experimental timescale
- 4.15:** Dual-inlet spray chamber with connections to diffusion cell (left) and 1ppb indium standard (right)
- 5.1:** Sealed sample chamber containing 1.0 µg cesium behind 1.0 mm IG-110 graphite barrier (uncured cement)
- 5.2:** Time-lag analysis of cesium diffusion in 0.1cm commercial graphite at 1200K

5.3: Time-lag analysis of cesium diffusion in 0.1cm commercial graphite at 1300K

5.4: Proposed time-lag design modifications

6.1: The release experiment takes place inside SiC tube that is closed at one end and mounted vertically in a Lindberg tube furnace. The arrows show the helium jet path.

6.2: Schematic of the release experiment setup. The graphite sphere is located inside the SiC tube. Cs that is released is transported to the ICP-MS by a He-jet system.

6.3: Dual inlet spray chamber. Inlet 1 (left) from He-jet with He flow rate of 1 L/min. Inlet 2 (right) from nebulizer that injects 200 $\mu\text{L}/\text{min}$ of 1.00 ng/g In as an internal standard.

6.4: Sphere 10 release flux plot (left) and fractional release plot (right) with best fit theoretical curve corresponding to $D=1.3\times 10^{-12}$ m^2/s .

6.5: The measured diffusion coefficients from this experiment plotted versus reciprocal temperature with other values for various graphites reported in the literature.

7.1: Experimental setup

8.1: ICP-MS sensitivity as a function of carbon aerosol generator spark frequency (Hz) or carbon particle aerosol density in the He carrier gas

8.2: Initial Cs concentration profile measured by LA-ICP-MS

8.3: Fractional release curves for six $R=0.3$ cm NBG-18 graphite spheres as measured by ICP-MS

8.4: Fractional release curves and respective fit of Eqn. 11 for $R=0.30$ cm NBG-18 graphite spheres at 1290 and 1185 K.

8.5: The measured diffusion coefficients from this experiment plotted versus reciprocal temperature with other values for various graphites reported in the literature.

8.6: The normalized infusion profile (mass concentration vs radius), measurements and theory.

9.1: Metal nitrate decomposition under vacuum in quartz tubing

- 9.2:** Sealed quartz tube containing 1 g graphite powder and five R=1/16" IG-110 spheres before annealing procedure
- 9.3:** Sealed quartz tube after annealing procedure
- 9.4:** Unused molybdenum container
- 9.5:** Molybdenum container filled with Sr laden graphite powder and IG-110 spheres
- 9.6:** Molybdenum container after annealing attempt, with dark purple MoO₂ oxidation layer visible
- 9.7:** Annealed graphite canisters
- 10.1:** I/IG-110, R=0.15 cm, T=873 K
- 10.2:** I/IG-110, R=0.15 cm, T=983 K
- 10.3:** I/IG-110, R=0.15 cm, T=1108 K
- 10.4:** I/IG-110, R=0.15 cm, T=1193 K
- 10.5:** I/IG-110, R=0.15 cm, T=1293 K
- 10.6:** Variation of D as function of T

LIST OF TABLES

- 1.1:** Early and contemporary HTGR design specifications [2]
- 1.2:** Summary of TRISO fuel failure mechanisms [2]
- 5.1:** Diffusion data for time-lag measurements
- 6.1:** Selected previous measurements of Cs diffusion in various graphites
- 6.2:** The table lists the diffusion coefficients calculated by fitting solutions of eqn. 6 to the experimental data using a regression algorithm. The initial and final Cs content was measured using INAA.
- 6.3:** Pre-exponential and activation parameters for diffusion of Cs in IG-110 graphite between 1100K and 1300K.
- 7.1:** Cs release calibration factors obtained using 50 Hz spark generation frequency and 0.7 bar He aerosol generation parameters. ICP-MS Cs counts were normalized relative to 2000 cps In
- 8.1:** Cs diffusion coefficients in NBG-18 graphite in the temperature range of 1090K to 1395K.
- 8.2:** Pre-exponential and activation parameters for diffusion of Cs in NBG-18 graphite between 1090K and 1395K.
- 9.1:** Graphite canister annealed IG-110 sphere elemental component analysis (2 min irradiation at 5×10^{13} n_{th}/cm²/s, 5 hr count).
- 10.1:** IG-110 sphere iodine content and effective diffusion coefficients calculated from Eqn. 10.3.

LIST OF SYMBOLS AND ABBREVIATIONS

FP: Fission Product

HTGR: High Temperature Gas-Cooled Reactor

HTTR: High Temperature Test Reactor

ICP-MS: Inductively Coupled Plasma Mass Spectrometry

INAA: Instrumental Neutron Activation Analysis

LA-ICP-MS: Laser Ablation Inductively Coupled Plasma Mass Spectrometry

MURR: University of Missouri Research Reactor

MWt: Megawatt Thermal

NSEI: University of Missouri Nuclear Science and Engineering Institute

PBMR: Pebble Bed Modular Reactor

PyC: Pyrocarbon

SiC: Silicon Carbide

TRISO: Tri-Structural Isotropic

VHTR: Very High Temperature Reactor

ABSTRACT

Release of radioactive fission products from nuclear fuel during normal reactor operation or in accident scenarios is a fundamental safety concern. Of paramount importance are the understanding and elucidation of mechanisms of chemical interaction, nuclear interaction, and transport phenomena involving fission products. Worldwide efforts to reduce fossil fuel dependence coupled with an increasing overall energy demand have generated renewed enthusiasm toward nuclear power technologies, and as such, these mechanisms continue to be the subjects of vigorous research.

High-Temperature Gas-Cooled Reactors (HTGRs or VHTRs) remain one of the most promising candidates for the next generation of nuclear power reactors. An extant knowledge gap specific to HTGR technology derives from an incomplete understanding of fission product transport in major core materials under HTGR operational conditions. Our specific interest in the current work is diffusion in reactor graphite. Development of methods for analysis of diffusion of multiple fission products is key to providing accurate models for fission product release from HTGR core components and the reactor as a whole.

In the present work, a specialized diffusion cell has been developed and constructed to facilitate real-time diffusion measurements via ICP-MS. The cell utilizes a

helium gas-jet system which transports diffusing fission products to the mass spectrometer using carbon nanoparticles. The setup was designed to replicate conditions present in a functioning HTGR, and can be configured for real-time release or permeation measurements of single or multiple fission products from graphite or other core materials.

In the present work, we have analyzed release rates of cesium in graphite grades IG-110, NBG-18, and a commercial grade of graphite, as well as release of iodine in IG-110. Additionally we have investigated infusion of graphite samples with Cs, I, Sr, Ag, and other surrogate fission products for use in release or profile measurements of diffusion coefficients.

CHAPTER 1:

INTRODUCTION TO HTGR TECHNOLOGY AND FISSION PRODUCT TRANSPORT

Release of fission products from nuclear fuel during normal operation or in accident scenarios is a fundamental safety concern in nuclear reactors. Such release is hazardous primarily because of radioactive fission product decay, in which harmful ionizing radiation is released from fission product nuclides. The severity of the hazard is dependent on multiple factors including the identity of the nuclides, the quantity released, and the physical and chemical forms of the fission product nuclides.

Reduction of the overall source term continues to be a subject of intense focus in the research and development of nuclear reactors, and accurate models for fission product release are vital to accomplish this objective. Measuring fission product release provides a way to monitor fuel integrity in addition to normal radiological surveillance.

The High Temperature Gas-Cooled Reactor (HTGR), one of six reactor designs currently undergoing research by the Generation IV International Forum, implements a novel fission product containment concept which offers multiple additional barriers to fission product release. Graphitic materials are key components in this technology, and serve roles in core structural elements as well as fission product containment. Diffusion is a primary mass transport processes governing the distribution and release of fission

products in the reactor; thus, understanding fission product behavior in graphite is critical to ensure safe and reliable operation of the reactor and to limit the source term during both normal operation and disaster scenarios.

The primary goal of this research is to develop and test a method for analyzing fission product diffusion in graphite under conditions present in the HTGR. Using a specialized diffusion cell in combination with inductively coupled plasma-mass spectrometry (ICP-MS) and an aerosol laden gas-jet system, we determined diffusion coefficients for fission products in various types of reactor graphite under reactor conditions. High-yield, medium-lived fission products have the potential to be most damaging to the environment and biological systems in the event of a breach of the core or primary coolant loop in HTGR operation. Cesium-137, strontium-90, iodine-131, and silver-110m are thus nuclides of primary focus.

In the following sections, an effort is made to outline the general factors and processes in HTGRs which affect diffusion.

1.1. HTGR design and capabilities

The gas-cooled reactor concept was conceived in the early days of nuclear energy development, and was eventually realized in commercial form with the construction of the first Magnox reactor, completed in 1955 in Calder Hall, UK. Magnox reactors utilized graphite moderators and a pressurized carbon dioxide gas coolant. Design specifications began to very closely resemble their modern forms in the late

1960's, with the advent of the experimental DRAGON reactor, Peach Bottom reactor, and AVR reactor, all of which utilized a pressurized helium coolant and coated fuel particle concepts. The High Temperature Test Reactor (HTTR) in Japan, and HTR-10 in China are examples of currently operational HTGRs.

HTGRs share a similar range of power ratings (typically 200 MWt to 625 MWt) and outlet temperatures (700°C to 850°C and higher) as well as coolant transport systems to provide process energy via high temperature fluids and/or thermal fluid expansion [1]. The exceptionally high outlet temperatures present in HTGRs increase thermal efficiency to values approaching 50% and afford the opportunity to use nuclear process heat to drive highly endothermic industrial processes including hydrogen production [1]. A summary of contemporary and historically relevant HTGR design specifications from IAEA-TECDOC-1645-CD is provided in table 1.1.

<i>Experimental HTGRs</i>					
	Peach Bottom (USA)	Dragon (UK)	AVR (Germany)	HTR (Japan)	HTR-10 (China)
Operational Status	1967-74 safe encl.	1968-75 safe encl.	1967-88 Defueled	1998-xx in operation	2000-xx in operation
Thermal/electric power [MW _{th} /MW _e]	115/40	20/-	46/15	30/-	10/-
Fuel element type	pin	pin	Spherical	pin-in-block	Spherical
Power density [MW _{th} .m ⁻³]	8.3	14	2.6	2.5	2
He-inlet/ outlet temperature [°C]	377/750	350/750	270/950	385/850 and 950	250/350/700/900
Mean He pressure [MPa]	2.5	2	1	4	3
Enrichment	HEU	HEU/LEU	HEU/LEU	LEU	LEU
Fuel	Carbide	Oxide	Carbide/Oxide	Oxide	Oxide
Coating	BISO	TRISO	BISO/TRISO	TRISO	TRISO
Pressure vessel	steel	steel	Steel	steel	Steel
<i>Prototype HTGRs</i>					
	Fort St. Vrain (USA)		THTR (Germany)		
Operational Status	1976-1989 Decommissioned		1986-1989 safe enclosure		
Thermal/electric power [MW _{th} /MW _e]	842/330		750/300		
Fuel element type	Prismatic		Spherical		
Power density [MW _{th} .m ⁻³]	6.3		6		
He-inlet/-outlet temperature [°C/°C]	405/784		270/750		
Mean He pressure [MPa]	4.5		3.9		
Steam temperature [°C]	530		530		
Electricity production [MWh]	5500		2890		
Enrichment	HEU		HEU		
Fuel	Carbide		Oxide		
Coating	TRISO		BISO		
Pressure vessel	PCRv		PCRv		
<i>Commercial HTGR Projects</i>					
	German designs		HTR-Modul	HTR-100	
Thermal/electric power [MW _{th} /MW _e]	PNP	HHT	HTR-500	HTR-Modul	HTR-100
Fuel element type	500/- spherical	1240/500 block/ spherical	1250/500 spherical	200/80 spherical	258/100 Spherical
Power density [MW _{th} .m ⁻³]	4	5,5	7	3	3
He-inlet/-outlet temperature [°C/°C]	300/950	440/850	280/700	250/750	250/740
He pressure [MPa]	3.9	5.0	4.7	5.0	7.0
Steam temperature [°C]	850	-	530	530	530
Enrichment	LEU	LEU	LEU	LEU	LEU
Fuel	Oxide	Oxide	Oxide	Oxide	Oxide
Coating	TRISO	TRISO	TRISO	TRISO	TRISO
Pressure vessel	PCRv	PCRv	PCRv	Steel	Steel
	International designs		VGM-400 (Russia)	PBMR (SA)	GT/MHR (USA/Russia)
Thermal/electric power [MW _{th} /MW _e]	MHTGR (USA)	VGR-50 (Russia)	VGM-400 (Russia)	PBMR (SA)	GT/MHR (USA/Russia)
Fuel element type	350/140 prismatic	136/50 spherical	1060/300 spherical	400/165 spherical	600/285 prismatic
Power density [MW _{th} .m ⁻³]	6	?	?	4.8	6.5
He-inlet/-outlet temperature [°C]	319/685	296/810	350/950	500/900	510/850
He pressure [MPa]	9	4	5	9	7
Enrichment	LEU	HEU	LEU	LEU	U/Pu
Fuel	UCO	Oxide	Oxide	Oxide	Oxide
Coating	TRISO	TRISO	TRISO	TRISO	TRISO
Pressure vessel	steel	steel	PCRv	steel	steel
	HTR-PM (China)	HTR/VHTR [ANTARES] (France)	NGNP (VHTR) (USA)		
Thermal/electric power [MW _{th} /MW _e]	2x250/ 200	600/-	600 (max)/-	500/200	
Fuel element type	spherical	prismatic	prismatic	spherical	
Power density [MW _{th} .m ⁻³]	3.215	?	undecided	6.0	
He-inlet/-outlet temperature [°C/°C]	250/700	400/1000	-/ 850 to 950	350/ 850 to 950	
He pressure [MPa]	7	5	undecided	9	
Enrichment	LEU	LEU	LEU	LEU	
Fuel	Oxide	UCO or UO ₂	UCO	UO ₂	
Coating	TRISO	TRISO	TRISO	TRISO	
Pressure Vessel	Steel	Steel	Steel	Steel	

Table 1.1: Early and contemporary HTGR design specifications [2]

1.1.1. TRISO fuel concept

The primary design objective for contemporary HTGRs mandates that no internal or external event could lead to a release of radiation from the plant that could threaten food or water supplies or force evacuation of the public [1]. This requirement is met through implementation of several necessary design features. Foremost, an HTGR must be equipped with multiple barriers to fission product release that will not fail under any normal or induced reactor condition. At the heart of the HTGR design is the TRISO (tri-structural isotropic) fuel concept. Each TRISO fuel particle contains a spherical pellet of uranium oxide or oxycarbide which is subsequently coated with three barriers to fission product release. These barriers are applied in sequence, and include (a) a porous carbon buffer layer, which attenuates fission recoils and serves as a void volume for expansion of fission product gases, (b) a pyrolytic carbon intermediate layer which retains gaseous fission products and alleviates stress on the other layers, and (c) a silicon carbide layer which retains metallic fission products, serves as the main source of protection from physical and chemical stresses encountered in the core, and is the primary barrier to fission product release. Fission product retention is supplemented by moderator graphite in the core, and finally by the reactor pressure vessel and containment.

Contemporary HTGRs typically fall under two main categories: pebble bed modular reactors (PBMRs) and prismatic block HTGRs. These reactors share very similar design characteristics but differ mainly in the way the core is constructed.

In the pebble bed design, TRISO pellets are uniformly dispersed in spherical graphite pebbles to form fuel spheres. The graphite matrix that comprises the bulk of the fuel sphere serves as the moderator in this design, and as an additional barrier to fission product release. Fuel spheres are arranged in a specific geometry in the core assembly to allow for criticality. Helium coolant circulates into the reactor core and through the void volume between the fuel spheres where heat exchange occurs. The coolant exits the reactor through the main coolant loop where inline turbines and heat exchangers extract mechanical and thermal energy from it. A detailed schematic of a PBMR core and main coolant loop may be found in [3].

The prismatic block design utilizes a more traditional fuel rod approach which itself incorporates the TRISO fuel. In this design, TRISO pellets are formed into cylindrical fuel compacts using a carbon-based resin. Fuel compacts are stacked within a graphite sleeve to form fuel rods and inserted into a prismatic graphite block which serves as the moderator and principal core component. Helium coolant circulates between pre-drilled channels in the prismatic core. A detailed schematic of the prismatic block core design is given in [1].

The following diagram outlines the fuel element fabrication schemes and general core/coolant loop layout for the pebble bed and prismatic block HTGRs:

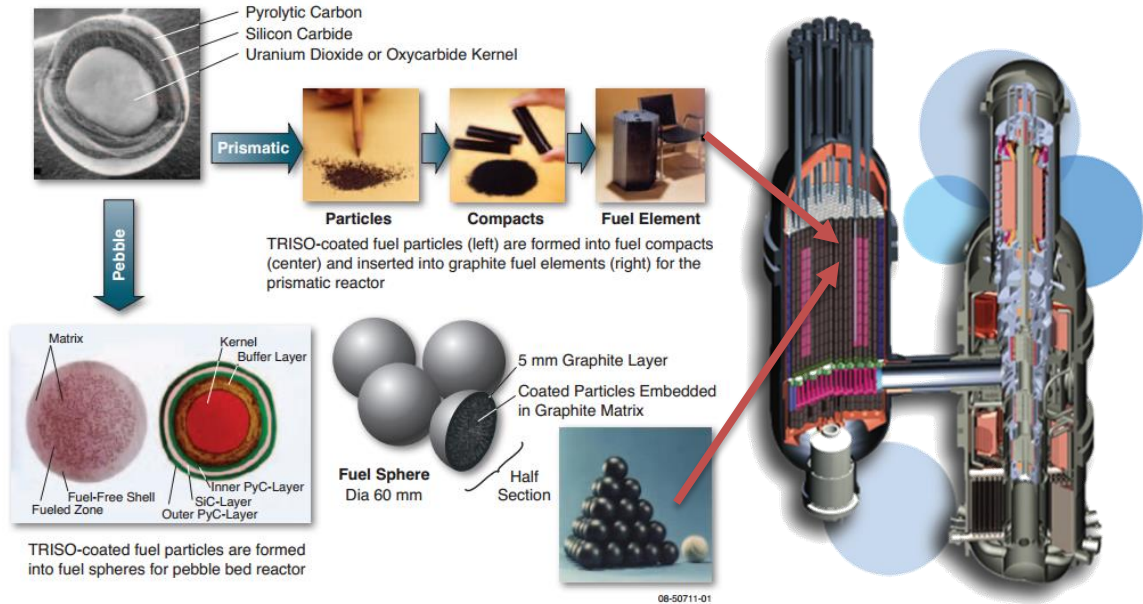


Figure 1.1: Fuel design and fabrication and core schematic for prismatic block and pebble bed HTGRs. Adapted from [1]

1.2. Core structural materials and fission product release

Fission product release involves several fundamental mass transport processes, including diffusion, sorption, and convection. Most fission products originate in the fuel kernels of TRISO pellets in HTGRs, and therefore must penetrate several barriers to fission product release before they can escape the reactor. The magnitude of this contribution depends on the chemical and physical properties of the particular fission product, as well as the nature of the materials with which it interacts. Damage to the coating layers of the TRISO fuel can result in fission product release in addition to the traditional transport phenomena. A summary of known TRISO failure mechanisms from IAEA-TECDOC-1645-CD is presented below:

Failure mechanism	Reactor conditions	service	Particle design and performance parameters that affect the failure mechanism	Comments
Pressure vessel failure	Temperature Burnup Fast fluence		Strength of SiC Buffer density (void volume) Fission gas release CO production Layer thicknesses Kernel type (UO ₂ , UCO)	
Irradiation-induced PyC failure	Fast fluence Temperature		Dimensional change of PyC Irradiation-induced creep of PyC Anisotropy of PyC Strength of PyC PyC thickness PyC density	Can be ameliorated by proper coating conditions
IPyC partial debonding	Temperature Fast fluence		Nature of the interface Interfacial strength Dimensional change of PyC Irradiation-induced creep of PyC	Can be ameliorated by proper coating conditions
Kernel migration	Temperature Burnup Temperature gradient		Layer thicknesses Kernel type	UO ₂ only. Not important for UCO. Reasonably well understood
Fission product attack	Temperature Burnup Temperature gradient Time at temperature		Fission product transport behavior Diffusion Buffer densification and cracking Chemical state/transport behavior of fission products Microstructure of PyC and SiC	Could be more important at high burnup in LEU fuels because of greater yields of palladium from plutonium fissions
Non-retentive SiC Layer: Diffusive release through intact layers	Temperature Burnup Temperature gradient Time at temperature		Chemical state/transport behavior of fission products Microstructure of SiC SiC thickness	More important at higher temperatures (> 1200°C) where existing data suggest diffusion will contribute to the source term.
Non-retentive SiC layer:	Burnup Temperature Fluence		Kernel type (UO ₂ , UCO)	CO is generated in particles with UO ₂ kernels.
SiC Corrosion by CO	Time at temperature		IPyC performance	At elevated temperatures, CO can attack the SiC layer if the IPyC layer is porous or has failed.
SiC degradation by cesium			Microstructure of SiC Thickness of SiC	Exact mechanism is unclear but limited data suggest cesium may degrade SiC layer
PyC thermal creep	Time at temperature		Thickness of PyC and stress state of PyC	Not important in traditional accident envelope (peak temperature < 1600°C)
SiC thermal decomposition	Temperature Time at temperature		SiC thickness Microstructure of SiC	Not important in traditional accident envelope (peak temperature < 1600°C)
Kernel Coating Mechanical Interaction (KCMi)	Burnup Fast Fluence Temperature		Initial Kernel – Coating Gas Gap Buffer properties IPyC Properties Kernel Swelling Rate	Failure of SiC Layer shortly after Gas Gap closed at sufficiently high Burn-ups

Table 1.2: Summary of TRISO fuel failure mechanisms [2]

Silicon carbide (SiC) is the primary barrier to fission product release from the fuel in HTGRs. Transport properties of SiC indicate that release should be much smaller than that which is observed from in-pile experiments [4]. This suggests the primary release mechanism from SiC is not a classical transport phenomenon, but rather damage to the SiC via mechanical stresses or degradation from radiation effects.

Graphitic materials are used extensively in HTGR core structures. Properties of graphite tend to vary widely (porosity, crystallinity, isotropy, density, grain size, $sp^2:sp^3$ hybridization ratio, oxidation resistance, purity) and properties are generally suited or optimized for a specific role. However, all graphites share certain properties; graphite is a porous material and therefore diffusion in graphite typically occurs at a much larger rate than crystalline solids. Graphite dust is also known to be present in HTGRs which facilitates transport by convective processes once fission products have sorbed onto dust particles.

1.3. References

[1] *The High Temperature Gas-Cooled Reactor: Next Generation Nuclear Energy*. Retrieved from: http://www.ngnpalliance.org/images/general_files/HTGR%20page%20individual%20040611.pdf

[2] IAEA-TECDOC-1645-CD. *High Temperature Gas-Cooled Reactor Fuels and Materials*. 2010.

[3] http://www.cecaust.com.au/election2013/policies/blueprintforeconomicdevelopment/nuclearpower/supersafe_pbmr.html

[4] T. Boyle. Measurement of Fission Product Diffusion in VHTR Materials. University of Missouri, 2010.

CHAPTER 2:

DIFFUSION THEORY

2.1. Overview

Diffusion is usually defined as the net flow of a material down a concentration gradient. At the molecular level, it is a statistical consequence of particulate random walks due to interactions with surrounding particles.

2.2. Fick's laws of diffusion

The general equations that govern classical diffusion processes are Fick's laws of diffusion. Specifically:

$$J = -D\nabla C \quad (2.1)$$

and

$$\frac{\partial C}{\partial t} = D\nabla^2 C \quad (2.2)$$

Where:

J = material flux ($g/cm^2 \cdot s$)

D = diffusivity (cm^2/s)

C = concentration (g/cm^3)

t = time (s)

The diffusivity or diffusion coefficient, D , is the constant of proportionality between the concentration gradient and the flux of material through a barrier. It is usually defined for a specific mobile diffusant (in our case, fission products) within a specific stationary medium (graphite), and is the primary parameter governing the rate at which diffusion occurs. The diffusion coefficient is potentially a function of many variables; in graphite, it can be a function of temperature, graphite type, porosity, diffusant concentration, concentration of impurities, irradiation, pressure, and oxidation, among others [1]. Some of these variables will be held constant in HTGR operation, simplifying mathematics considerably. In classical diffusion, the temperature dependence on the diffusion coefficient is described by an Arrhenius form:

$$D = D_0 e^{-\frac{Q}{RT}} \quad (2.3)$$

Where:

$D = \text{diffusivity } (cm^2/s)$

$D_0 = \text{diffusivity at infinite temperature } (cm^2/s)$

$Q = \text{activation energy } (J/mol)$

$R = \text{gas constant } (J/mol \cdot K)$

$T = \text{temperature } (K)$

Diffusion coefficients are commonly reported as the pre-exponential, D_0 , along with a corresponding Q -value. Diffusion in solids is often assumed to take place by a series of jumps (between vacancies in crystalline solids, for example) and Q represents the activation energy for a jump of one mole of particles.

Diffusion measurements in solids typically follow one of three different general design criteria: (a) permeation measurements, where an average concentration gradient is maintained and flux through a barrier is measured as a function of time, (b) profile measurements, where diffusion into, but not through, a solid occurs for a fixed time and the resulting concentration profile within the solid is measured (c) release measurements, where a solid is given an initial, uniform concentration of diffusant and release in time is measured [1]. In each case, a solution of the diffusion equation (or a manipulated form thereof) is typically fitted to the resulting data to obtain the diffusion coefficient.

2.3. Solutions of the diffusion equation

Solutions to Fick's laws may be obtained by integration under the appropriate boundary conditions for the system in question, yielding expressions for the concentration profile as a function of time. Expressions for flux, quantity of material diffused, fractional release, or other useful quantities may be obtained by further manipulation of the concentration profile solution. The following section contains some solutions of diffusion equations relevant to the current work.

2.4. Diffusion models

2.4.1. Finite barrier model

Consider the following system at $t=0$, involving an infinite reservoir of diffusant with concentration $C=C_0$, and an initially clean barrier of thickness l and area A , with upstream face located at $x=0$ and downstream face at $x=l$:

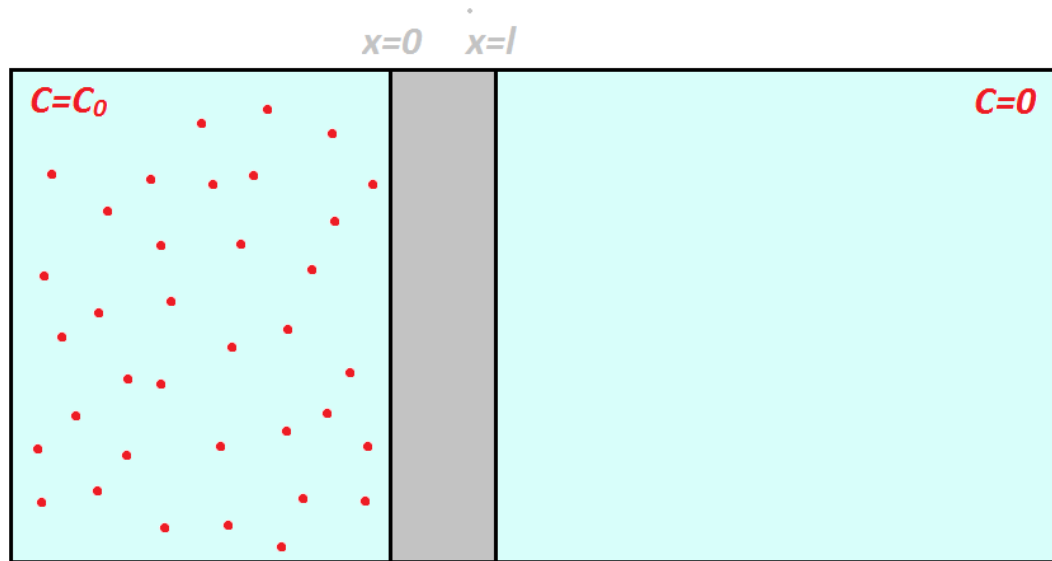


Figure 2.1: Initial configuration of the finite barrier model. Dots represent diffusant particles (FPs).

If diffusing material is continually removed from the downstream face of the barrier (i.e. $C=0$), when restricted to one dimension the diffusion equation becomes:

$$\frac{\partial C(x,t)}{\partial t} = D \frac{\partial^2 C(x,t)}{\partial x^2} \quad (2.4)$$

With initial condition:

$$C(x,0) = 0$$

and boundary conditions:

$$C(0,t) = C_0$$

$$C(l,t) = 0$$

Where: x = spatial coordinate in barrier

l = barrier thickness

The solution follows from integration, either by implementing a variable transformation to make the problem homogeneous followed by the method of separation of variables, or by Laplace's method. The solution is:

$$C(x, t) = C_0 - \frac{C_0 x}{\ell} - \frac{2C_0}{\pi} \sum_{n=1}^{\infty} \frac{1}{n} \sin\left(\frac{n\pi x}{\ell}\right) e^{-\left(\frac{n\pi}{\ell}\right)^2 Dt} \quad (2.5)$$

If the diffusivity is known, the concentration may be calculated at any time and distance within the barrier. If the diffusivity is unknown, it may be determined experimentally by lag-time analysis. In this method, the total amount of material (or a proportional fraction thereof) which has exited the downstream face of the barrier is measured as a function of time. The equation describing release from this face is obtained by application of Fick's first law to the concentration profile solution to find the flux, multiplication by the barrier cross-sectional area to find the rate, and subsequent integration in the time domain to obtain the desired solution. The solution is [2]:

$$Q(t) = \frac{ADC_0}{\ell} \left(t - \frac{\ell^2}{6D} + \frac{2\ell^2}{\pi^2 D} \sum_{n=1}^{\infty} \frac{(-1)^{n+1}}{n^2} e^{-\left(\frac{n\pi}{\ell}\right)^2 Dt} \right) \quad (2.6)$$

Where: $Q(t)$ = cumulative release from downstream barrier face

A = barrier area

At long times, the exponential term becomes negligibly small, and diffusion approaches a steady state as the concentration profile within the barrier becomes

linear. Extrapolation of the linear portion of a plot of $Q(t)$ vs. t to the t -axis yields the lag time, t_{lag} :

$$t_{lag} = \frac{\ell^2}{6D} \quad (2.7)$$

The value of the diffusion coefficient then follows from simple algebra. Lag time analysis is the most common method for determination of diffusion coefficients in solids. This method is very convenient experimentally, as the boundary conditions are easy to replicate and many methods are available for measurement of diffusing material. Additionally, only a fraction of the actual diffusing material must be measured, eliminating the need for separate calibration procedures for many such techniques.

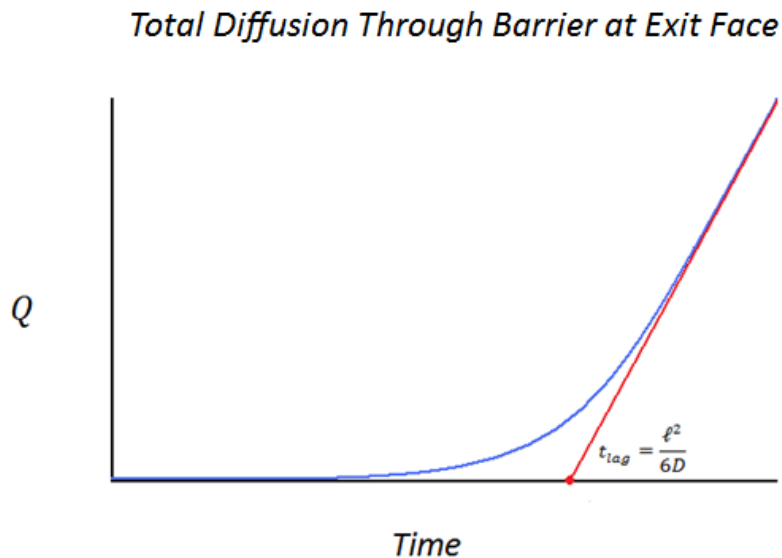


Figure 2.2: Typical curve from a lag time analysis experiment. The blue curve corresponds to experimental data. The red curve is an extrapolation of the steady-state

portion of the curve, and the t-intercept is the lag time used to calculate the diffusion coefficient

2.4.2. Booth model (spherical release model)

Most applicable to the research conducted in this work, the Booth model was developed for modeling fission product release from spherical uranium oxide fuel pellets for use in HTGRs. Consider the following system at $t=0$, where a spherical solid of radius $r=R$ contains a uniform fission product concentration $C=C_0$:

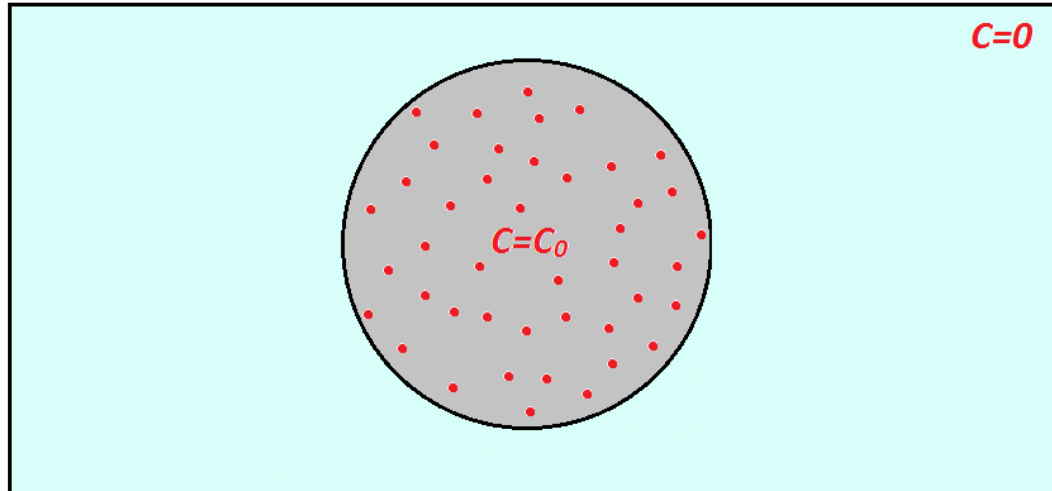


Figure 2.3: Initial configuration of the spherical release model. Dots represent diffusant particles (FPs).

If diffusing material is continually removed from the surface of the sphere, the diffusion equation (in spherical coordinates) becomes:

$$\frac{\partial C(r,t)}{\partial t} = \frac{1}{r^2} \frac{\partial}{\partial r} \left(D r^2 \frac{\partial C(r,t)}{\partial r} \right) \quad (2.8)$$

With initial condition:

$$C(r, 0) = C_0$$

and boundary conditions:

$$C(0, t) = \text{finite}$$

$$C(R, t) = 0$$

Where: r = radial coordinate in sphere

R = sphere radius

The solution is:

$$C(r, t) = \frac{2C_0R}{\pi r} \sum_{n=1}^{\infty} \frac{(-1)^{n+1}}{n} \sin\left(\frac{n\pi r}{R}\right) e^{-\left(\frac{n\pi}{R}\right)^2 Dt} \quad (2.9)$$

Through integration over the surface area, subtraction from the initial quantity, and division by the initial quantity of diffusant, Booth gives the fraction $F(t)$ of diffusant released from the sphere as [3]:

$$F(t) = 1 - \frac{6}{\pi^2} \sum_{n=1}^{\infty} \frac{1}{n^2} e^{-\left(\frac{n\pi}{R}\right)^2 Dt} \quad (2.10)$$

Evaluation of the diffusion coefficient typically follows via least squares fitment of this equation (through variation of D) to experimental fractional release data.

2.4.2.1. Short time solutions

The series solutions presented in the last section present practical problems when modeling release from spherical particles, as the series converges slowly at short times when a finite number of summation terms are used. Using Laplace's method to solve the diffusion equation affords the opportunity to construct simple analytical expressions for the flux or fractional release, for example, using the initial value theorem from calculus. Although "short time" approximations, they are often

extremely accurate over a wide range of fractional releases, greatly simplifying data analysis [4].

The short time flux at the sphere surface is:

$$J_R(t) = \frac{\left[3m_0 \left(\frac{Dt}{\pi R^2} \right)^{-1/2} \frac{D}{\pi R^2} - 3 \frac{m_0 D}{R^2} \right]}{A} \quad (2.11)$$

Where: A = sphere surface area

The short time fractional release is:

$$F(t) = 6 \sqrt{\frac{Dt}{\pi R^2}} - 3 \frac{Dt}{R^2} \quad (2.12)$$

The Booth model is the primary model used for calculation of diffusion coefficients in the present work, and the short time solutions are almost exclusively used in data fitting procedures.

2.4.2.2. Non-uniform initial distributions

In the case where the initial distribution of material within a spherical sample is non-uniform but spherically symmetric, the solution of Fick's law has the following form, under the boundary condition in which material is continually removed from the sphere surface:

$$C(r, t) = \frac{1}{r} \sum_{n=1}^{\infty} \frac{2}{R} \int_0^R r C(r) \sin\left(\frac{n\pi r}{R}\right) dr \cdot \left[\sin\left(\frac{n\pi r}{R}\right) e^{-\left(\frac{n\pi}{R}\right)^2 Dt} \right] \quad (2.13)$$

where $C(r)$ is the initial condition, the concentration profile in the sphere at $t=0$. The flux $J(r, t)$ of the diffusant or fission product is given by Fick's first law:

$$J(r, t) = -D \frac{\partial C(r, t)}{\partial r} \quad (2.14)$$

The flux of FP through the surface of the sphere is thus:

$$J_R(t) = -D \frac{\partial}{\partial r} \left\{ \frac{1}{r} \sum_{n=1}^{\infty} \frac{2}{R} \int_0^R r C(r) \sin\left(\frac{n\pi r}{R}\right) dr \cdot \left[\sin\left(\frac{n\pi r}{R}\right) e^{-\left(\frac{n\pi}{R}\right)^2 Dt} \right] \right\} \Big|_{r=R} \quad (2.15)$$

The total mass of FP $m(t)$ which has diffused from the surface in time t , is the product of the surface area of the sphere and the time integral of (7). The fractional release $F(t)$, defined as the ratio of mass of FP released from the sphere to the total initial FP mass, is thus:

$$F(t) = \frac{4\pi R^2 \int_0^t \left(-D \frac{\partial}{\partial r} \left\{ \frac{1}{r} \sum_{n=1}^{\infty} \frac{2}{R} \int_0^R r C(r) \sin\left(\frac{n\pi r}{R}\right) dr \cdot \left[\sin\left(\frac{n\pi r}{R}\right) e^{-\left(\frac{n\pi}{R}\right)^2 Dt} \right] \right\} \Big|_{r=R} \right) dt}{m_0} \quad (2.16)$$

If the initial distribution of FP is known, solutions of (7) or (8) may be fit to experimental release data to determine the diffusion coefficient.

2.4.3. Sandwich model

The sandwich method is a classical analysis for determination of diffusion coefficients by analysis of the concentration profile generated by a diffusion experiment [5]. There are several variations of this technique, but most involve an initially clean acceptor medium being placed in contact with a donor medium of the same material containing a uniform concentration of diffusant. The donor and acceptor specimens are pressed together to form a diffusion couple or “sandwich”.

Consider the following system at $t=0$, where the donor specimen is a cylindrical disc of finite thickness, and the acceptor specimen is a cylindrical disc of semi-infinite thickness (compared to the diffusion depth):

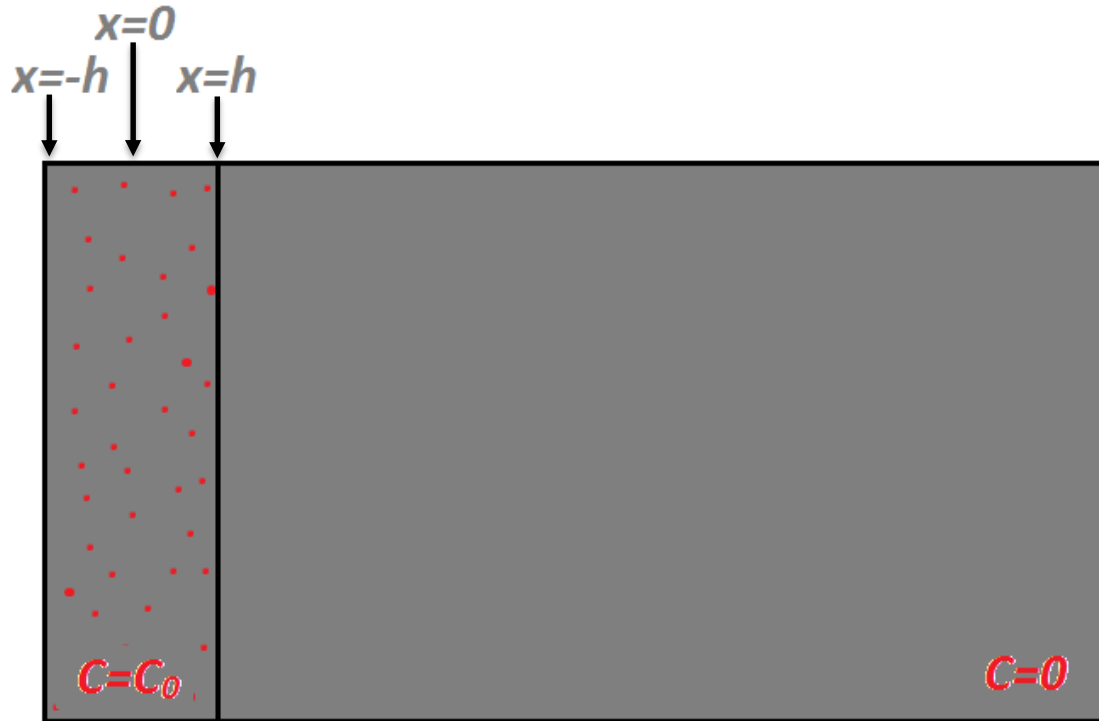


Figure 2.4: Initial configuration of the sandwich model. Dots represent diffusant particles (FPs).

If diffusion is restricted to one dimension, the diffusion equation becomes:

$$\frac{\partial C(x,t)}{\partial t} = D \frac{\partial^2 C(x,t)}{\partial x^2} \quad (2.17)$$

With initial condition:

$$C(x,0) = C_0 \text{ for } -h \leq x \leq h$$

$$C(x,0) = 0 \text{ for } x > h \text{ or } x < -h$$

Where: x = spatial coordinate

h = barrier half thickness

The solution is [5]:

$$C(x, t) = \frac{C_0}{2} \left\{ \operatorname{erf} \left(\frac{h-x}{\sqrt{4Dt}} \right) + \operatorname{erf} \left(\frac{h+x}{\sqrt{4Dt}} \right) \right\} \quad (2.18)$$

Where:

$$\operatorname{erf}(x) = \frac{2}{\sqrt{\pi}} \int_0^x e^{-\xi^2} d\xi \quad (2.19)$$

If the source disc is infinitesimally thin, it may be regarded as proportional to a delta function, whereby the concentration profile is described by:

$$C(x, t) = \frac{\alpha}{\sqrt{4\pi Dt}} e^{-x^2/4Dt} \quad (2.20)$$

Where:

α = number of atoms per unit area in source disc

2.4.4. Exact multilayer model

In describing fission product release from TRISO pellets for example, it is useful to consider solutions of the relatively simple forms described previously. Release from the central fuel kernel is accurately described by Booth's spherical release equations. Permeation through the PyC or SiC layers is analogous to the 1-D finite barrier model, but the proper solution for the concentration profile in these layers involves a change to spherical coordinates and a variable boundary condition. The exact solution for the concentration profile when considering fission product release from a single TRISO particle, and assuming a uniform distribution of the given fission product in the fuel kernel, is given by the exact multilayer model.

Consider the following system at $t=0$, which represents a four layer (three coating) TRISO pellet with an initial, uniform concentration of diffusant contained in the central fuel kernel:

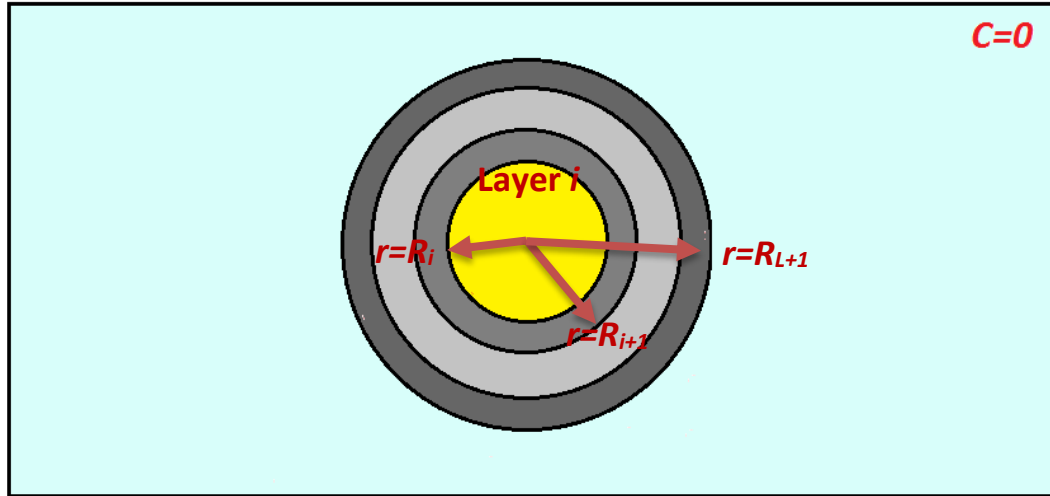


Figure 2.5: Initial configuration of the exact multilayer model.

The inner and outer radii for particular layer i are R_i and R_{i+1} , where $1 \leq i \leq L$ and $R_1=0$ (pellet center). The diffusion equation for each layer is thus [6]:

$$\frac{\partial C_i(r,t)}{\partial t} = \frac{D_i}{r^2} \frac{\partial}{\partial r} \left(r^2 \frac{\partial C_i(r,t)}{\partial r} \right) \quad (2.21)$$

With initial conditions:

$$C(r,0) = C_0, 0 < r < R_i$$

and boundary conditions:

$$C(0,t) = \text{finite}$$

$$C(R_{L+1},t) = 0$$

and interface conditions:

$$D_i \frac{\partial C_i(r,t)}{\partial r} = D_{i+1} \frac{\partial C_{i+1}(r,t)}{\partial r} \text{ and } \gamma_i C_i(r,t) = \gamma_{i+1} C_{i+1}(r,t), r = R_{i+1}, i = 1, 2, \dots, L-1$$

Where:

$$R_i < r < R_{i+1}, i = 1, 2, \dots, L$$

$D_i = \text{diffusivity in layer } i$

$\gamma = \text{partition factor}$

Interface conditions specify flux continuity along with the introduction of partition factor γ to accommodate discontinuity of the concentration profile at the interfaces. The solution is [6]:

$$C_i(r, t) = \sum_{n=1}^{\infty} \frac{C_n e^{-t\beta_n^2}}{r} \left[A_{i,n} \sin\left(\frac{r\beta_n}{\sqrt{D_i}}\right) + B_{i,n} \cos\left(\frac{r\beta_n}{\sqrt{D_i}}\right) \right] \quad (2.22)$$

where $A_{i,n}$, $B_{i,n}$, and C_n are constants determined by the initial conditions and β_n are eigenvalues determined by the boundary conditions. The overall fractional release is then given by [6]:

$$F(t) = 1 - \frac{\left(\sum_{i=1}^L 4\pi \sum_{n=1}^{\infty} C_n e^{-t\beta_n^2} \left[A_{i,n} \left\{ \frac{D_i}{\beta_n^2} \sin\left(\frac{r\beta_n}{\sqrt{D_i}}\right) - \frac{r\sqrt{D_i}}{\beta_n} \cos\left(\frac{r\beta_n}{\sqrt{D_i}}\right) \right\} + B_{i,n} \left\{ \frac{D_i}{\beta_n^2} \cos\left(\frac{r\beta_n}{\sqrt{D_i}}\right) - \frac{r\sqrt{D_i}}{\beta_n} \sin\left(\frac{r\beta_n}{\sqrt{D_i}}\right) \right\} \right]_{R_i} \right)^{R_{i+1}}}{m_0} \quad (2.23)$$

When diffusion coefficients are known for each layer, the expression can be evaluated after determination of the constants $A_{i,n}$, $B_{i,n}$, and C_n , and the eigenvalues β_n . This expression is particularly useful for describing fission product release from TRISO particles after experimental determination of diffusion coefficients for fission products in each layer.

2.5. Deviations from Fickian behavior

Additional modeling is required to account for deviations from Fickian behavior. Deviations may be a consequence of irregular structural features of a material, concentration or time dependence of the diffusion coefficient, or impurities in the medium. Common approaches for modeling anomalous (non-Fickian) diffusion include adding additional mass transport terms to the classical diffusion equation, or alternatively, attempting to account for a variable diffusivity. The forms these modifications should take is often widely debated, as assumptions must be made regarding the fundamental mechanisms responsible for the deviations. These assumptions are often very difficult to verify experimentally. Additionally, solutions typically require numerical methods to utilize.

In practice, diffusion is often assumed to be Fickian, and diffusion is described using an effective diffusion coefficient.

2.6. Factors affecting diffusion in HTGRs

2.6.1. Graphite structural considerations

Nuclear graphite is composed of crystalline grains aligned to varying degrees, forming a network of open and closed pores, cracks, and grain boundaries. Wide variation exist among grain size, porosity, isotropy, and crystallinity in graphite types, and depends largely on manufacturing techniques and raw material composition. The primary raw materials used in fabrication of nuclear graphite include coke, binder material, impregnants, and other additives.

A variety of graphite types have been used in HTGRs which have structural characteristics optimal for particular roles. Diffusion is known to proceed primarily through pore volume and along pore surfaces, thus diffusion coefficients are generally larger in more porous materials. Impregnation can be used to reduce porosity and increase density, which increases the material's capacity for moderation as well as fission product retention. Grain size is widely variable among graphite types, with modern manufacturing technologies capable of producing much smaller grain sizes and greater uniformity than was previously possible. Differences in binder composition can also affect structure, and the nature of the binder has additional chemical effects on mass transport processes in graphite. Although it is clear that structural variations have an effect on diffusion behavior and fission product retention, few correlations have been established.

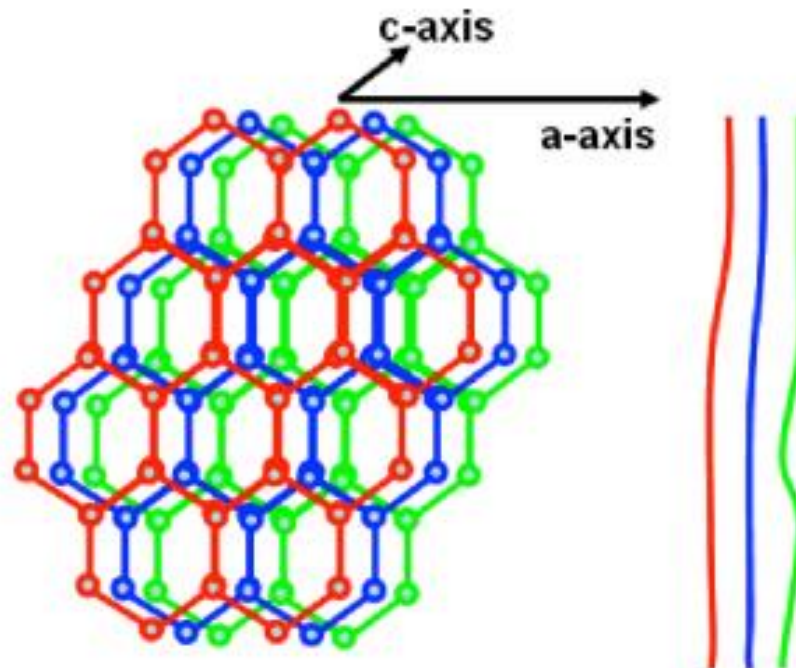


Figure 2.6: Graphite molecular structure. Basal plane top view is at left; side view at right. Adapted from [7].

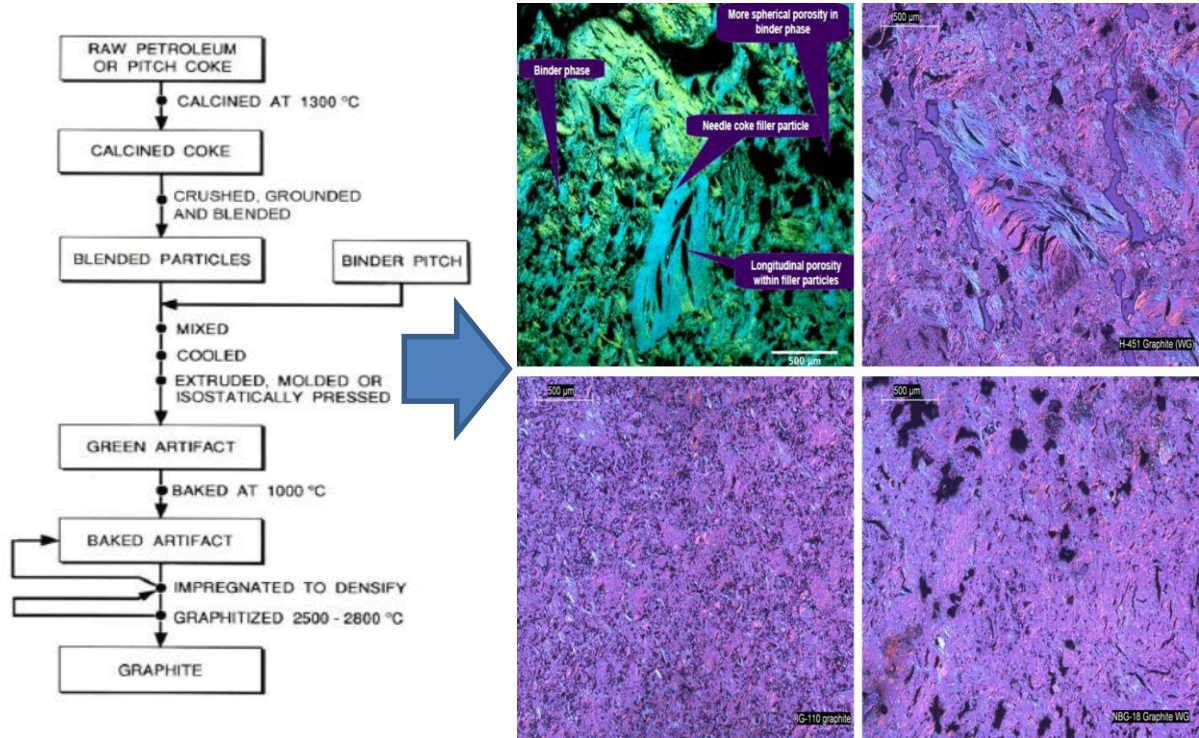


Figure 2.7: General fabrication process and resulting variance in microstructural features of graphite grades used previously (top left and right, historical reference H-451) and current candidate graphites (bottom left and right, IG-110 and NBG-18, respectively) for HTGRs. Adapted from [8].

2.6.2. Radiological considerations

Mechanisms of radiation damage in graphitic materials are well understood, and typically result in displacement of carbon atoms from lattice positions and into interstitial regions, causing expansion of the graphite grains in the c-axis and contraction

along the a-axis as displaced atoms form new basal planes in the interstitial regions [8].

The resulting stress forces imparted as a result of grain expansion may in turn induce cracks or other defects in the microstructure leading to structural compromise.

Irradiation history may result in sufficient structural change to induce deviations from Fickian behavior in fission product diffusion.

2.6.3. Chemical considerations

2.6.3.1. Concentration effects

It is well known that the diffusion coefficient can be concentration dependent. The concentrations of fission products in HTGRs, however, remain small enough such that concentration effects on diffusion behavior are usually negligibly small [1].

2.6.3.2. Multicomponent systems

In a multicomponent system with multiple mobile diffusants, each diffusant may have an effect on the diffusion of other species. The most weakly adsorbing species are typically affected the most, where such species exhibit accelerated diffusion rates, and the effect is magnified at larger concentrations when competition for binding sites becomes more important [1].

The opposite effect (slowed diffusion) may also occur, for example, when an immobile impurity or structural feature irreversibly sorbs or incorporates a particular component.

2.6.3.3. Graphite oxidation

Graphite oxidation has been shown to increase diffusion rates of cesium, and has varying effects on the diffusion of silver and strontium [1]. These changes are primarily attributed to increases in the porosity and preferential oxidation of binder materials.

Molecular oxygen, carbon dioxide, and water impurities in the coolant are the primary sources of oxidative stress in HTGRs. Accidents involving air or water ingress compound this effect. The relevant chemical reactions are [8]:



Radiolytic oxidation by activated carbon dioxide has been shown to be unimportant in HTGRs [8].

2.6.4. The nature and state of diffusing fission products

The predominant form of diffusing cesium in graphitic systems is Cs^+ [9] due to the low first ionization potential (3.79 eV) [10] of Cs^0 . The first ionization potential of silver (7.58 eV) [10] is much higher than the work function of graphitic materials (≈ 5.0 eV), and thus silver diffuses in its neutral form, Ag^0 . The presence of impurities may cause the formation of salts or other crystallites with varying degrees of mobility.

2.6.5. Mechanisms of diffusion in graphite

2.6.5.1. Lattice diffusion

Bulk diffusion within individual graphite grains (crystals) is assumed to take place via a classical lattice diffusion type mechanism. Due to the anisotropic nature of graphite crystals, diffusion coefficients vary depending on crystallographic direction. Diffusion of fission products within graphite grains is not a primary mechanism of transport for fission products in graphite and therefore this mechanism is rarely incorporated into diffusion models [1].

2.6.5.2. Grain boundary diffusion

Grain boundary diffusion is commonly observed in non-porous crystalline materials. It is essentially flow of diffusant around and in-between grains of the medium as opposed to through the grains (lattice diffusion).

2.6.5.3. Surface diffusion

Surface diffusion is generally applicable to porous crystalline materials, and entails diffusion along pore surfaces. Mechanistically, it is assumed to occur via series of “jumps” between diffusion sites on pore surfaces (desorption and adsorption), where a particular activation energy is required for each jump. Surface diffusion has been shown to be the primary mechanism for diffusion of cesium in certain graphites [1].

2.6.5.4. Gas phase diffusion

Flow of diffusant in vapor form through the open pore volume is termed gas phase diffusion. Gas phase diffusion has been shown to be a primary mechanism of transport of silver in certain graphites [1].

2.6.5.5. Convection

Convective transport is largely unimportant due to the small pore dimensions in most graphites.

2.6.5.6. Combined mechanisms

Due to the complicated structure of graphite, mechanisms may compete with one another, particularly in high radiation environments or when oxidative stresses are present which can alter the pore distribution and material makeup of the graphite. In graphite, many diffusion mechanisms and deterministic parameters are difficult to determine experimentally. Because of this and related uncertainty, and because most historical codes for predicting FP release from HTGR cores (e.g. FRESCO) assume one mode of transport in reactor graphite dominates, data are typically modelled using an overall effective diffusion coefficient which combines transport coefficients for different migration channels into one parameter.

2.7. References

- [1] B. F. Meyers. "A Review of the Diffusion of Selected Fission Product Metals in Polycrystalline Graphite". 1983. E. Hoinkis. *Transport of Fission Products in Matrix and Graphite: Proceedings of a Colloquium Held at the Hahn-Meitner Institut Berlin from 9-11 November 1981*
- [2] Rutherford, S. W. & Do, D. D. *Review of Time Lag Permeation Technique as a Method for Characterization of Porous Media and Membranes*. Adsorption 3, 283-312 (1997).
- [3] Booth, A. H. *A Method of Calculating Fission Gas Diffusion from UO₂ Fuel and its Application to the X-2-F Loop Test*. 1957.
- [4] Olander, D. R. *Fundamentals of Nuclear Reactor Fuel Elements*. 1976.

[5] Hayashi, Kimio, & Fukuda, Kousaku . (1989). Diffusion coefficients of cesium in un-irradiated graphite and comparison with those obtained from in-pile experiments. *Journal of Nuclear Materials*, 168(3), 328-336.

[6] Gelbard, Fred. (2003). *Analytical Modeling of Fission Product Releases by Diffusion from Multicoated Fuel Particles*. DOI:10.2172/809605

[7] HTGR Graphite Core Component Stress Analysis Research Program – Task 1. Technical Letter Report. 2011. Obtained from:
<http://pbadupws.nrc.gov/docs/ML1127/ML11276A009.pdf>

[8] HTGR Technology Course for the Nuclear Regulatory Commission May 24 – 27, 2010 Module 9 Graphite. 2010.

[9] E. Hoinkis. “The Determination of Diffusion Coefficients of Cesium and Silver by the Release Method in As-Received, Oxidized and Neutron Irradiated Graphitic Matrix”. E. Hoinkis. *Transport of Fission Products in Matrix and Graphite: Proceedings of a Colloquium Held at the Hahn-Meitner Institut Berlin from 9-11 November 1981*.

[10] HCP on the web: CRC Handbook of Chemistry and Physics, 87th ed, 2006-2007. <http://www.hbcnetbase.com>

CHAPTER 3:

PREVIOUS WORK

Diffusion of fission products in graphite has been a subject of intense interest since the early developmental stages of HTGRs. As diffusion is affected by many variables, there have been a wide variety of experimental approaches to analyzing diffusion behavior. Experimental agreement among the results are widely variable as well.

Several studies relevant to the present work are summarized in this section.

3.1. Leyers' experiments

H. J. Leyers [1] conducted spherical release experiments to measure the diffusion coefficient of cesium in the graphitic matrix A3, which was used in AVR fuel elements. The Booth model described in (2.4.2) was used in determination of the diffusion coefficient.

3.1.1. Sample preparation

Cesium was applied to the surface of 1cm diameter spherical pebbles of matrix A3 via application of CsNO₃ solution. The doped A3 samples were dried, sealed in an evacuated molybdenum container, and annealed at 1400°C to homogeneously

distribute metallic cesium within the matrix. The spheres contained a cesium concentration of 7×10^{-1} mg/g after the annealing procedure. An irradiation was performed to generate Cs-134 so release could be analyzed via gamma spectroscopy; after the irradiation the spheres contained approximately 6 μ Ci of Cs-134 activity.

3.1.2. Experimental

The experimental setup was arranged such that the activity remaining in a sample could be analyzed by gamma spectroscopy. A system for flowing helium over the sample was implemented so material diffusing out of the sphere would be swept away from the sample chamber, maintaining the boundary conditions necessary for description of diffusion by the Booth model.

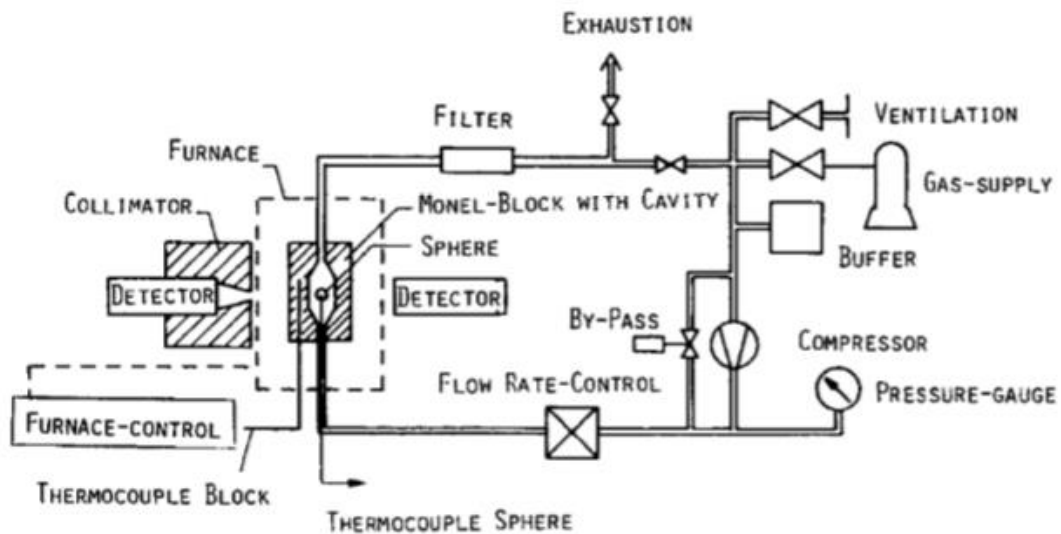


Figure 3.1: Leyers' experimental setup for cesium release in flowing helium [1]

3.1.3. Results

Diffusion coefficients were measured in the range of 900°C to 1100°C. Leys gives the parameters D_0 and Q for cesium in matrix A3. In Arrhenius form:

$$D_{Cs} = \left(2.01 \text{ cm}^2/\text{s}\right) e^{-\left(\frac{198,000 \text{ J/mol}}{RT}\right)} \quad (3.1)$$

Where: $R = 8.314 \text{ J/K} \cdot \text{mol}$

3.2. Fukuda's experiments

K. Fukuda [2] determined diffusion coefficients for strontium and barium in graphite matrix (pyrocarbon). These were fueled experiments which measured concentration profiles of fission products which had simultaneously diffused during annealing after irradiation of a spherical graphitic sample containing a central UO_2 fuel kernel.

3.2.1. Sample preparation

Spherical UO_2 fuel kernels approximately 0.6mm in diameter were coated with a spherical pyrocarbon shell fabricated similarly to pyrocarbon used in HTGR fuel compacts. The outside diameter of the finished samples was 10mm. The position of the central fuel kernel was verified using X-ray radiography. A schematic of a representative sample is below:

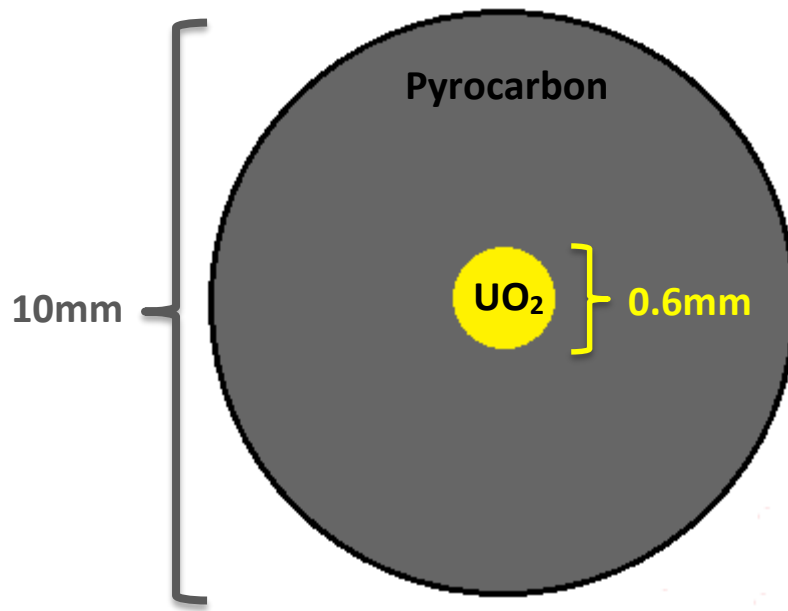


Figure 3.2: Schematic of Fukuda's sample design [2]

The samples were irradiated to generate an initial distribution of fission products in the pyrocarbon shell via fission recoil [2]. Finally, the samples were annealed for periods of 9hr to 51hr at temperatures between 1175°C and 1375°C to allow fission products to redistribute themselves via diffusion.

3.2.2. Concentration profile measurements

Grooved sections of known depth and thickness were removed from the pyrocarbon by a lathe. The resulting powder from each stepwise removal was weighed and counted via γ -spectrometry to determine the fission product concentration in each section. Measurement of the Strontium-90 content required additional preparation for

β -counting procedures. Data from each section was then assimilated to give the concentration profile in the sample.

3.2.3. Results

Fukuda gives the diffusion coefficients for barium and strontium as:

$$D_{Ba} = \left(7.3 \times 10^{-1} \text{ cm}^2/\text{s}\right) e^{-\left(\frac{2.2 \times 10^5 \text{ J/mol}}{RT}\right)} \quad (3.2)$$

$$D_{Sr} = \left(2.8 \times 10^1 \text{ cm}^2/\text{s}\right) e^{-\left(\frac{2.1 \times 10^5 \text{ J/mol}}{RT}\right)} \quad (3.3)$$

3.3. Hayashi's experiments

Hayashi [3] and Fukuda determined diffusion coefficients for cesium in IG-110 graphite using the profile method described in (2.4.4) and gamma spectroscopy.

3.3.1. Sample preparation

Thin cylindrical graphite source discs were impregnated with elemental cesium by immersion in a ^{137}Cs tagged CsNO_3 solution and subsequent heating to 800-900°C to decompose the nitrate and uniformly distribute the cesium.

3.3.2. Diffusion measurements

In each analysis, a source disc was placed in contact with a clean receiving specimen and the couple was annealed for up to an hour in a diffusion cell designed to house the samples in a high temperature inert atmosphere.

After the diffusion anneal the acceptor specimen was sectioned and the concentration profile was determined using γ spectroscopy. Diffusion coefficients were determined by fitting solutions of equation (2.4.3-2) to the concentration profile.

3.3.3. Results

Hayashi and Fukuda report diffusion coefficients for cesium in IG-110 graphite as [3]:

$$D_{Cs,series [A]} = \left(1.2 \times 10^{-4} \text{ m}^2/\text{s}\right) e^{-\left(\frac{1.12 \times 10^5 \text{ J/mol}}{RT}\right)} \quad (3.4)$$

$$D_{Cs,series [B]} = \left(1.7 \times 10^{-4} \text{ m}^2/\text{s}\right) e^{-\left(\frac{9.5 \times 10^5 \text{ J/mol}}{RT}\right)} \quad (3.5)$$

Variation of over an order of magnitude in diffusion coefficients was observed between identical runs and was attributed to sample dependence. Diffusion coefficients obtained from both series of data were 3-4 orders of magnitude larger than those obtained from a study of cesium diffusion in irradiated IG-110 graphite [3].

3.4. References

- [1] Leyers, H. J. "Cesium Release out of Matrix A3 in Flowing Helium". E. Hoinkis. *Transport of Fission Products in Matrix and Graphite: Proceedings of a Colloquium Held at the Hahn-Meitner Institut Berlin from 9-11 November 1981.*
- [2] K. Fukuda, T. Sawai, K. Ikawa. "Diffusion of Fission Products in Matrix Graphite." *Journal of Nuclear Science and Technology.* 21(2) (1984) 126.

[3] Hayashi, Kimio, & Fukuda, Kousaku . (1989). Diffusion coefficients of cesium in un-irradiated graphite and comparison with those obtained from in-pile experiments. *Journal of Nuclear Materials*, 168(3), 328-336.

CHAPTER 4:

ANALYTICAL TECHNIQUES

This section focuses on the instrumentation, apparatus, and techniques used in the present work for real-time analysis of fission product diffusion in graphite. A schematic outlining the experimental setup is presented below, and the components therein are discussed in the proceeding paragraphs.

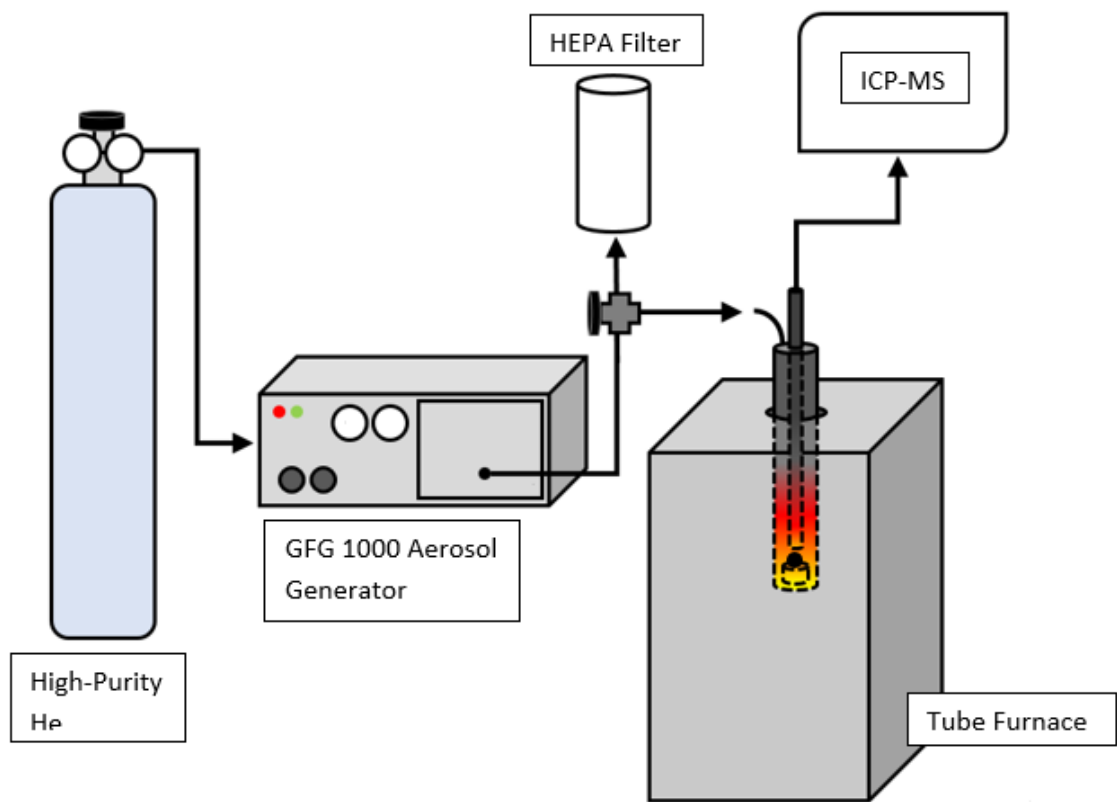


Figure 4.1: Schematic of experimental setup (release configuration)

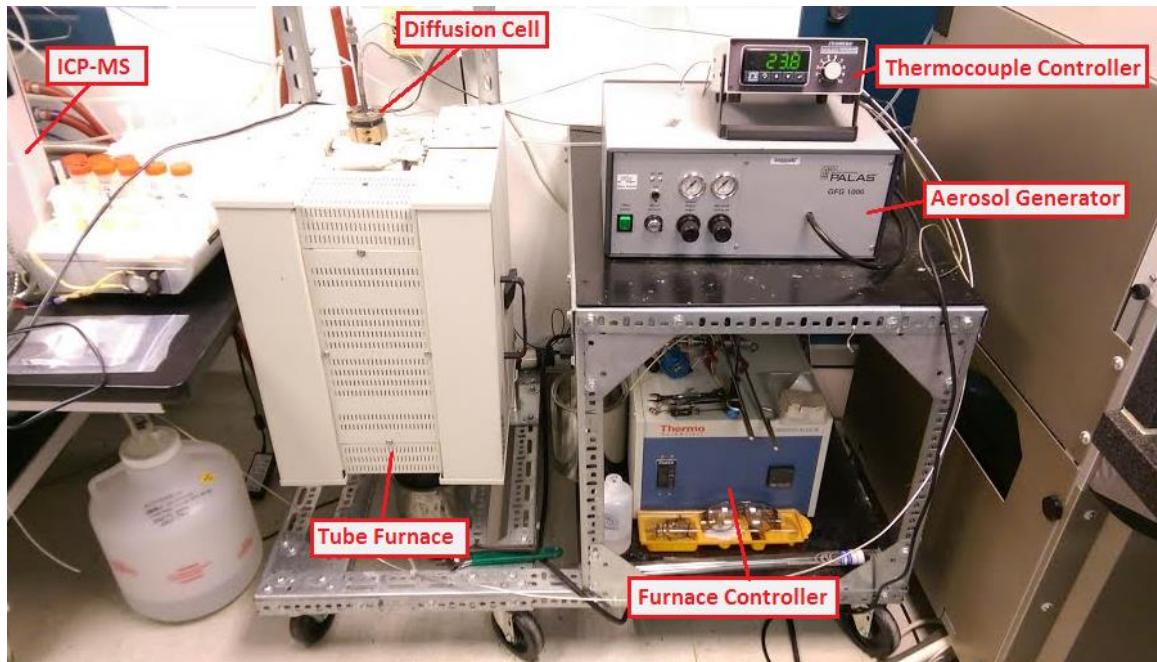


Figure 4.2: Actual experimental setup

4.1. Diffusion cell

In collaboration with the University of Missouri Nuclear Science and Engineering Institute (NSEI), a specialized diffusion cell has been developed for the present work. The cell was originally designed to house a designed-to-fail TRISO fuel (essentially TRISO pellets manufactured without their SiC barrier layer) in its sample chamber. The fuel could then be subject to a variety of irradiation schemes to generate fission products. The cell is compatible with simultaneous irradiation/diffusion measurements.

In the present work, cold isotopes or radiotracer levels of activity will be used which is appropriate for determination of diffusion coefficients.

A schematic of the diffusion cell is presented below:

All dimensions are in inches

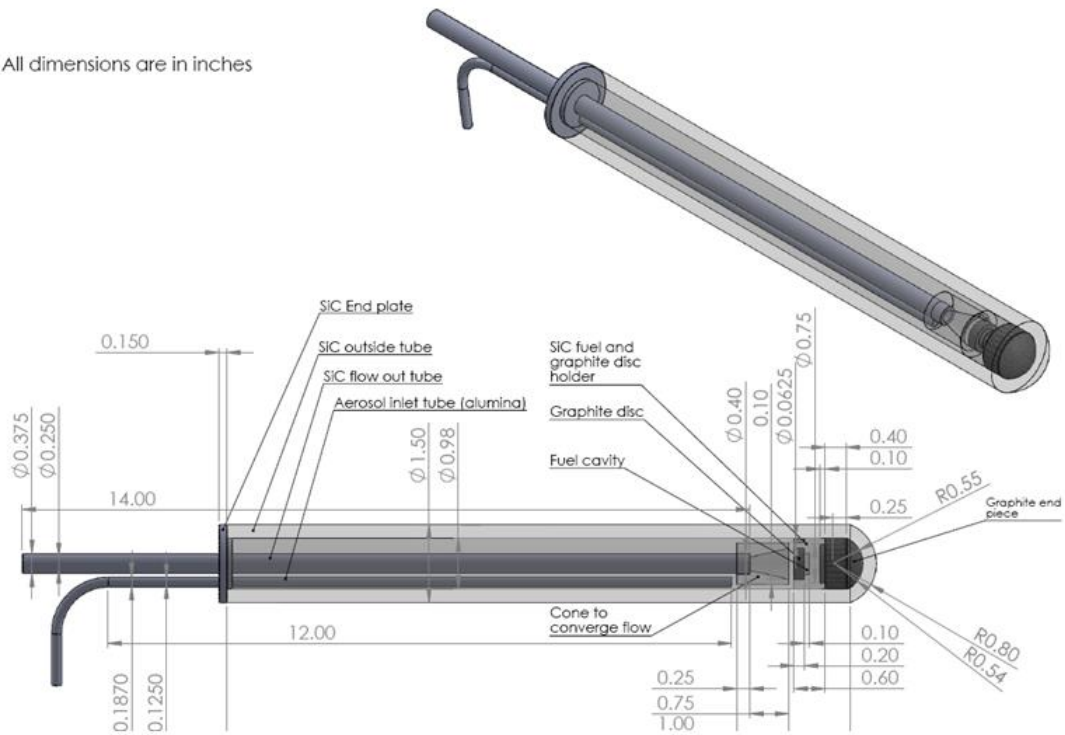


Figure 4.3: SiC diffusion cell schematic

4.1.1. Overview

The diffusion cell houses some combination of fission product diffusant(s) and graphitic medium, and fission products diffusing through the downstream (low concentration) surface of the medium will be swept away from the cell for analysis.

4.1.2. Design features

4.1.2.1. Aerosol inlet/outlet tubes

The aerosol inlet routes a helium stream containing a graphite aerosol toward the sample. Diffusing fission products adsorb onto aerosol particles at the sample/aerosol interface and are swept through the outlet tube toward an ICP-MS instrument.

4.1.2.2. Sample chamber

The cell's sample chamber design is such that measurement of diffusion is possible using permeation, release, or profile methods (described in 2.2-2.4), with real-time measurement restricted to permeation and release techniques.

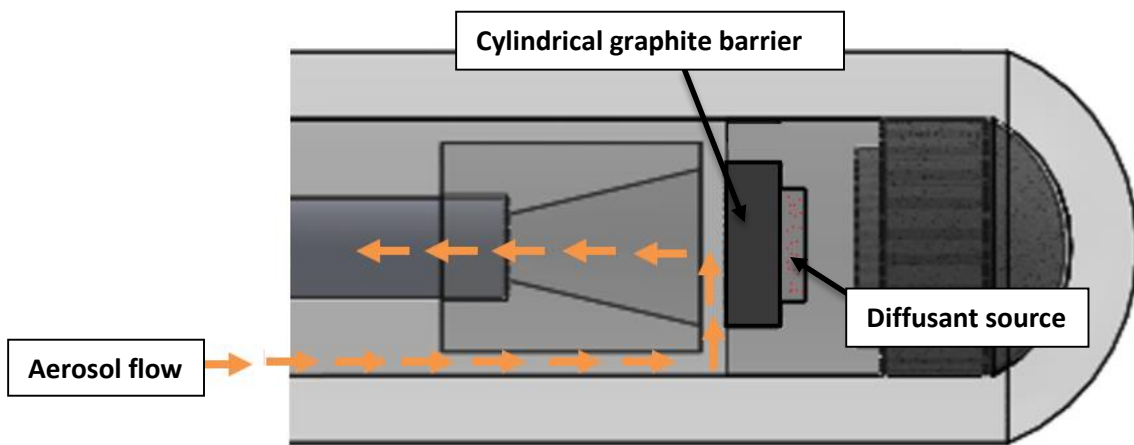


Figure 4.4: Close-up of sample holder region in permeation configuration

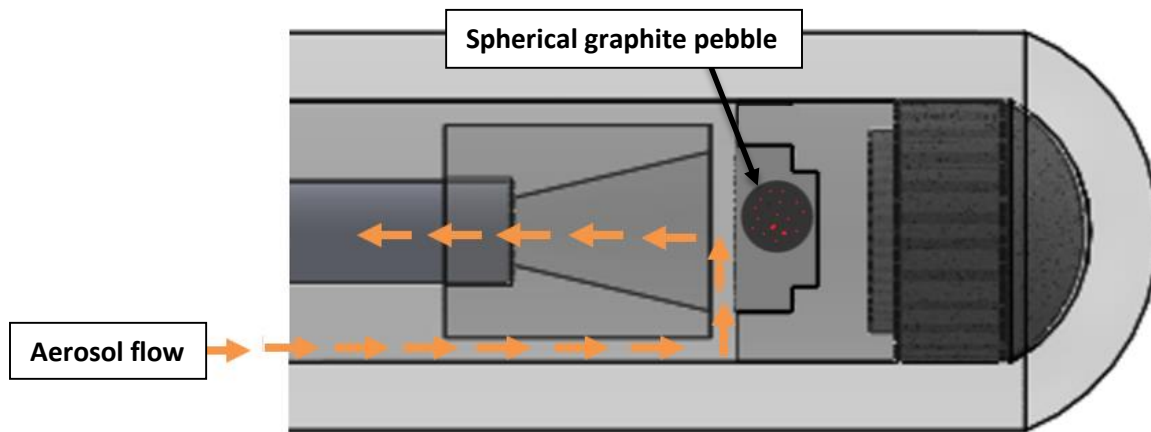


Figure 4.5: Close-up of sample holder region in release configuration. Dots in spherical pebble represent diffusant particles dispersed within the pebble.

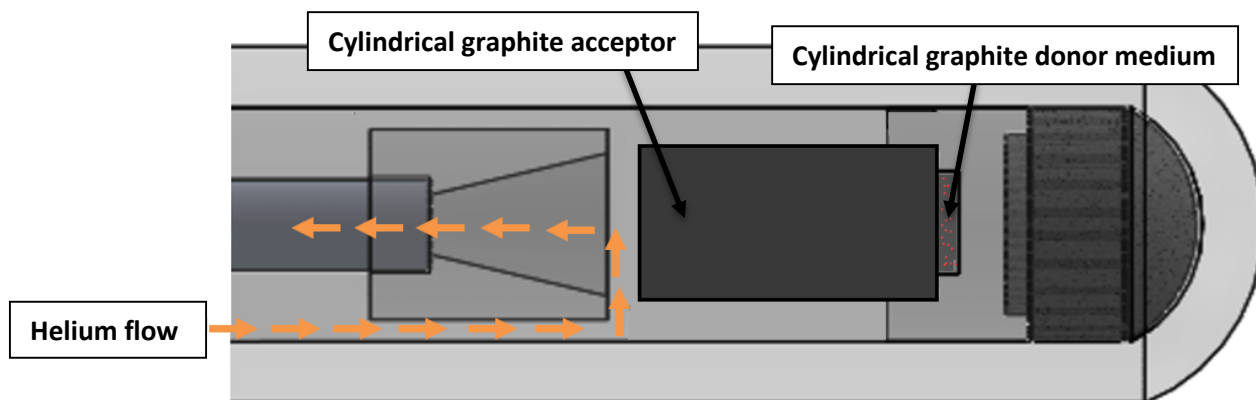


Figure 4.6: Close-up of sample holder region in profile configuration. The helium flow is present to prevent oxidation of the graphite donor and acceptor specimens; no aerosol is present as transport is not monitored in real time. In this scheme, the diffusant concentration profile in the acceptor specimen would be analyzed by a sectioning technique.

4.1.2.3. Tube furnace

A Lindberg Blue M-Series HTF55332C tube furnace maintains the sample end of the diffusion cell at temperatures up to 1200°C, sufficient for replicating temperature extremes present in HTGRs.

4.1.2.4. Aremco 890 cement

Aremco 890 is formulated for making graphitic and ceramic junctions. Aremco 890 is used for hermetic seals between SiC components of the diffusion cell.

4.1.2.4.1. Graphite bonding experiments

Experiments were conducted to determine the suitability of the Aremco 890 cement for bonding graphite and SiC. It was necessary to show that the seal material was less permeable to diffusants than graphite in order to ensure that diffusion was indeed proceeding primarily through the graphite.

To verify that Aremco 890 meets the system requirements, graphite bonding tests were performed. A hollow cylindrical section of SiC of 1.50" OD and 0.98" ID and a solid cylindrical disc of nuclear-grade graphite of 0.98" diameter and 0.25" thickness were bonded together using Aremco 890, and step cured in a box furnace to form a seal representative of those needed for assembly of the diffusion cell.

The seal was tested by subjecting the assembly to the temperatures and duration expected for a typical experimental run. Specifically, this amounted to a 10 hour heating cycle at 900°C under a flowing inert atmosphere.

Upon removal and cooling of the assembly after the heating, the seal was visually devoid of cracks and structural defects. It was apparent that the environment

inside the furnace was not completely oxygen-free, as mild oxidation (loss of graphite) was visually observed at the surface of the graphite disc. The Aremco 890 seal showed no evidence of oxidation, which illustrates the cement seal's resistance to oxidizing environments, and suggests that its integrity should be maintained when implemented in the diffusion cell.



Figure 4.7: Aremco 890 SiC-Graphite seal at start (top) and end (bottom) of 900° C, 10 hr heating cycle under argon atmosphere

An additional experiment was conducted to prove the seal was free of microscopic defects which would allow material to escape from the diffusion cell. The assembly used in the previous high-temperature exposure was stoppered, and pressurized helium gas was introduced into the resulting chamber. The assembly was submerged in a beaker of water, and helium bubbles (helium diffusion) were observed emanating only from the surface of the graphite. The absence of helium permeating the cement or around the edges of the seal further demonstrates the seal's integrity. The experiment also shows that the cement is impermeable relative to graphite, which should ensure diffusion observed in the operational diffusion cell is the result of permeation through the graphite barrier, rather than diffusion along the surface (edges) of the graphite disc between the graphite disc and the walls of the fuel/disc holder.



Figure 4.8: Aremco 890 graphite-SiC seal during helium permeation experiment.

In subsequent diffusion experiments (described in detail in Chapter 5), the cement was shown to be inadequate for preventing cesium escape from the sample chamber of the diffusion cell when testing certain graphites.

4.1.2.5. SiC construction

SiC was desirable for critical components of the diffusion cell due to its strength, impermeability, and resistance to damage from radiation, temperature extremes, and reactive chemical environments.

4.1.3. Diffusion cell temperature testing

The diffusion cell, cement, and related components were subject to temperature testing for safety and compatibility before the cell was used in diffusion analysis. After exposure to temperatures up to 1200°C (maximum temperature of the furnace), no

damage or degradation of the diffusion cell or any of the components was evident, and all external seals remained intact.



Figure 4.9: Interior of tube furnace at 1200K. The diffusion cell is at center.

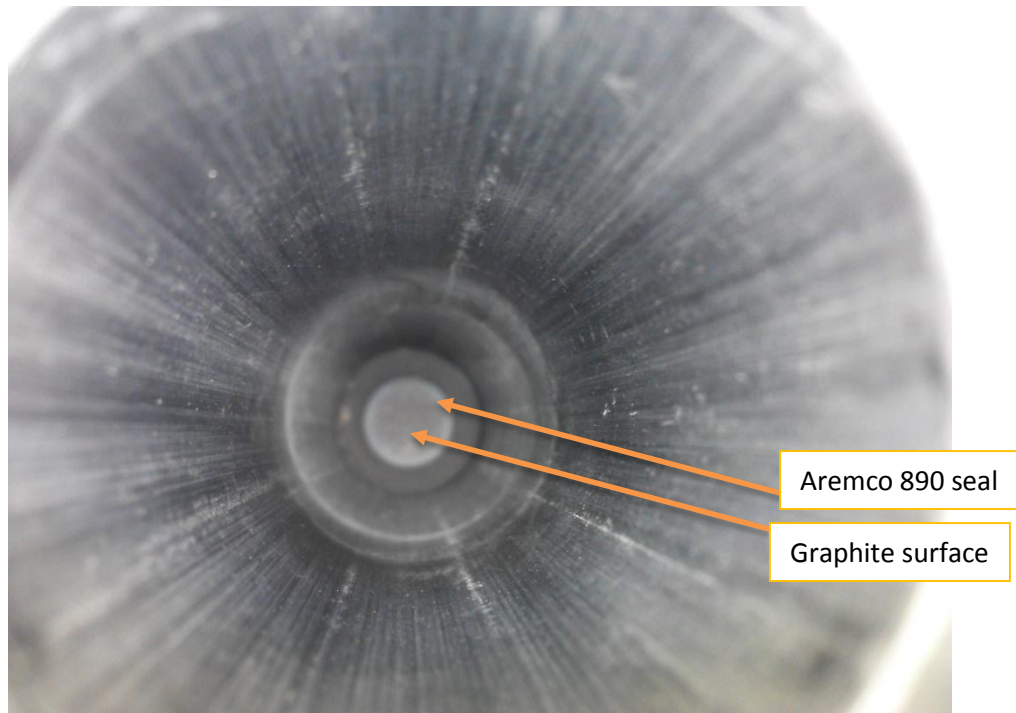


Figure 4.10: Interior of diffusion cell post-temperature test. The vertical marks spanning the length of the SiC outside tube are friction marks from insertion of the interior components. Note the Aremco 890 seal appears intact and the graphite surface shows minimal signs of oxidation.

4.1.4. Diffusion cell assembly, disassembly, and maintenance

Cell assembly is straightforward and involves cementing the connections into the top cap and cementing the cap onto the main SiC outside tube. All exterior seals will self-cure to an adequate extent during the furnace warmup procedure prior to a run.

Disassembly is most easily completed several days after a run. The cured cement seems to be hygroscopic at room temperature, and softens to the point that sealed components may be separated by simply wiggling them apart, or by gently prying with a thin flathead screwdriver.

The components should be cleaned after use to remove material which adsorbs onto component surfaces during a run. After disassembly, the components are cleaned with brushes and rinsed thoroughly with purified water and 2% nitric acid.

4.1.5. Diffusion cell development history

Previous design efforts are presented in this section to provide insight should modifications of the current cell design be required in the future.

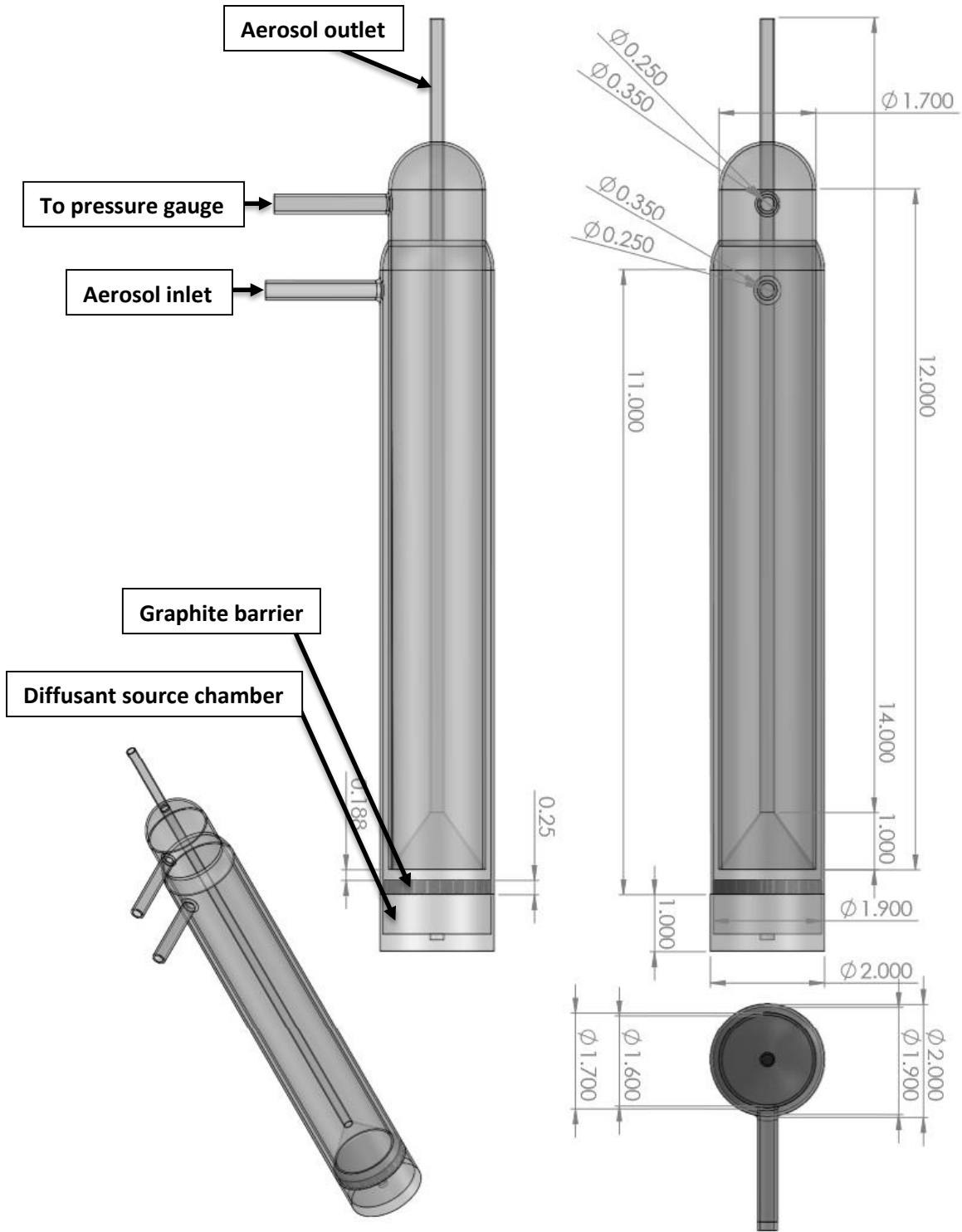


Figure 4.11: Quartz cell design which was to be fabricated by Technical Glass. The base of the cell is designed to be removable

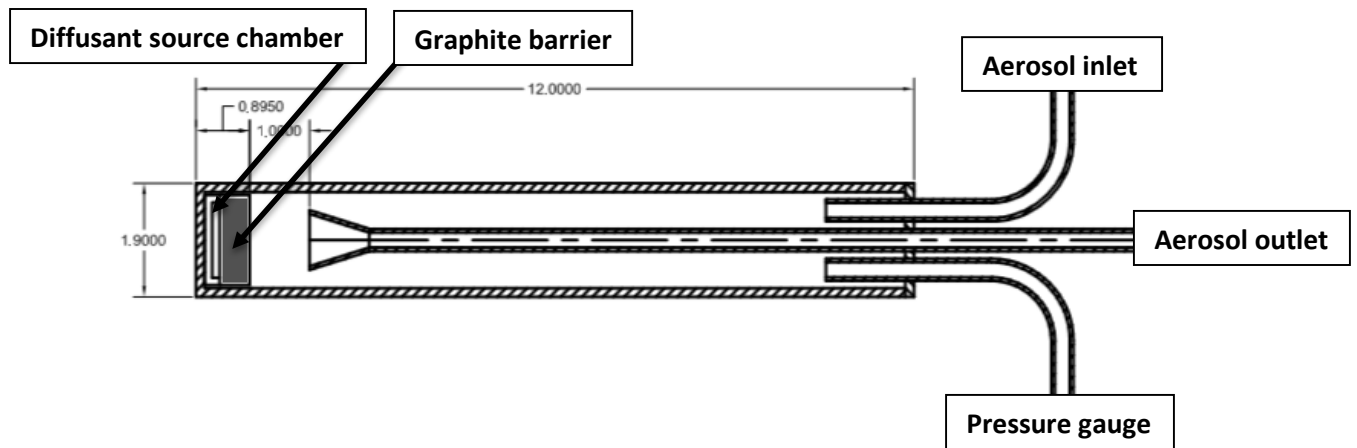


Figure 4.12: Quartz cell designed at MURR

The quartz designs were conceptually sound but were abandoned in favor of the current SiC design due in part to SiC's superior resistance to cracking during cooling, and in part due to the inability to form adequate seals between graphite and quartz.

Graphite bonding experiments similar to those described in Section 4.1.2.4.1 were conducted, mating quartz tubes to graphite discs using Aremco Graphi-bond cement. After baking the assemblies for 15 hours at 900°C under argon atmosphere, failure of the cement junctions was evident. Primary mechanisms for seal failure included formation of air bubbles in the cement during curing procedures and cracking of the quartz material.



Figure 4.13: Graphite disc bonded to quartz tube using Aremco Graphi-bond, after curing procedure. Note cracking in quartz tube at 2 o'clock position and air bubbles distributed around the edges of the barrier.

4.2. Gas-jet system

4.2.1. Overview

Transport of fission products to the ICP-MS will be accomplished using a carbon aerosol-laden helium gas-jet system consisting of a helium tank and regulator, carbon aerosol generator, valve for flow calibration, tubing, and connectors.

The fission products of primary interest are metals or metal ions, which quickly condense out of the gas phase in stationary or flowing systems to form salts or adsorb onto solid surfaces. The maximum range of transport of ions or metals in a flowing helium system has been shown to be only a few centimeters; this presents a problem as the length of the diffusion cell outlet tube is approximately 30 cm [1].

Aerosol assisted transport is a common solution to this issue [1,2]. The presence of aerosol particles in a flowing gas system provides a mobile surface for gas-phase ions, molecules, or atoms to adsorb onto, in our case providing a mechanism for transport of fission products from the diffusion cell to the ICP-MS. Eibach, et. al. [1] have proven the concept of fission product transport using carbon aerosols at the TRIGA-SPEC facility in Mainz, Germany, where a gas-jet is used to transport fission products from a source near the reactor core to the on-site spectroscopy facility. However, only a fraction of the material is successfully transported. Eibach et. al. reported transport efficiencies between 50% and 75% for most fission products over a 7 m distance.

The transport efficiency of the gas jet system is a function of aerosol particle size and concentration, temperature, carrier gas flow rate, and path geometry. Keeping these factors constant will ensure a constant transport efficiency necessary for accurate and consistent measurements. Tubing lengths and diffusion cell geometry remain unchanged during an experimental run, and temperature and carrier gas flow rate are held at constant values.

4.2.2. PALAS GFG 1000 aerosol generator

A special version of the commercial PALAS GFG 1000 aerosol generator was modified by PALAS for use with helium carrier gas. Helium was desirable due to its compatibility with ICP-MS techniques, and additionally, simulates flowing helium coolant in an HTGR.

The GFG 1000 produces a carbon aerosol via spark discharge between graphite electrodes in flowing helium. The instrument continuously charges a capacitor connected to two graphite electrodes. When the breakdown voltage of the helium sweep gas is reached, the capacitor discharges, producing a spark which evaporates a small quantity of the electrode material. The vaporized carbon subsequently condenses into aerosol particles which are routed out of the instrument.

In addition to transport properties desirable for fission product transport from the diffusion cell, a carbon aerosol may closely simulate fission product interactions with graphite dust present in HTGR cooling circuits and graphite dust generated in an accident scenario.

4.2.3. Aerosol characterization experiments

Experiments were conducted NSEI at the University of Missouri to investigate the stability of aerosol production and characterize the aerosol using an equivalent mobility diameter particle size distribution.

The parameters which affect aerosol production in the GFG 1000 are set at minimum to avoid unnecessary waste of helium and to avoid aerosol particle buildup in

the tubing and connectors. The aerosol concentration and size distribution were shown to be constant at the minimum flow values; specifically, at a spark frequency of 100 Hz and carrier helium flow rate of ≈ 4 L/min. Measurements were conducted at regular intervals over three consecutive days to examine both the short-term and long-term stability of aerosol production.

Aerosol data was acquired using a TSI 3936 Scanning Mobility Particle Sizer, a spectrometer which analyzes aerosol particles based on particle mobility. 51 samples were acquired and averaged to form a two-hour timescale stability curve; three two-hour replicates were acquired per day, and repeated for three consecutive days, for nine measurements total.

At 0.7 bar helium pressure and 100 Hz spark frequency, the aerosol generator was shown to produce carbon nanoparticles with an equivalent mobility diameter lognormally distributed around approximately 50nm. The size distribution was shown to be effectively invariant; the day-to-day and hour-to-hour stability of aerosol production under the conditions that will be used in the diffusion remained effectively constant, as evidenced by a superposition of the experimentally acquired curves.

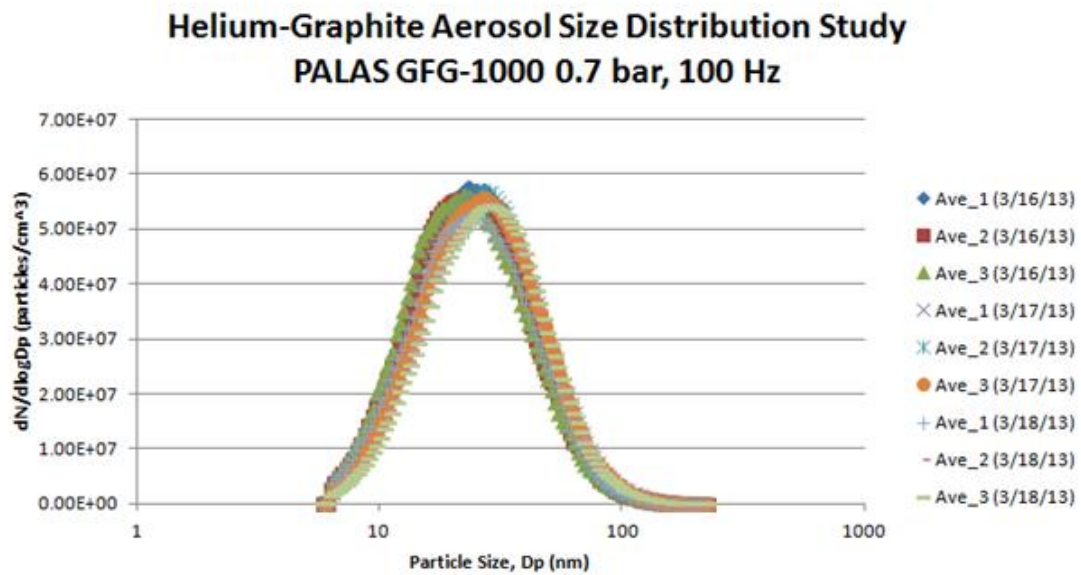


Figure 4.14: Stability of aerosol production over experimental timescale

The ICP-MS is compatible with a gas-phase sample introduction rate of ≤ 2 L/min. Excess aerosol flow is diverted through a HEPA filtration device to remove particulates and resulting helium is vented to atmosphere.

4.3. Inductively coupled plasma-mass spectrometry (ICP-MS)

4.3.1. Overview

ICP-MS is a powerful technique for trace metal analysis and analysis of radiochemical samples. ICP-MS is a highly sensitive technique and capable of detection

of many trace metals at the parts-per-trillion (ppt) level or below. Additionally, ICP-MS provides multi-element capabilities required by this analysis.

A typical ICP-MS operates by atomizing and ionizing a sample via RF plasma discharge. Ions are subsequently separated and analyzed according to their mass-to-charge ratios by the mass analyzer.

4.3.2. Nexion 300X ICP-MS

The specific instrument used in the present work is a Perkin Elmer Nexion 300X ICP-MS. This ICP-MS utilizes three quadrupoles and collision/reaction cell technology for unparalleled sensitivity and interference removal, and is well suited to quantitative multi-element analyses.

4.3.3. Dual-inlet spray chamber

The spray chamber is a primary component of the ICP-MS sample introduction system. In the present work, a dual-inlet variety is used which is compatible with the incoming fission product aerosol from the diffusion cell, and additionally allows for the introduction of a liquid internal standard via a nebulizer and peristaltic pump system. The internal standard used is 1.00 ppb indium in 2% aqueous HNO₃.

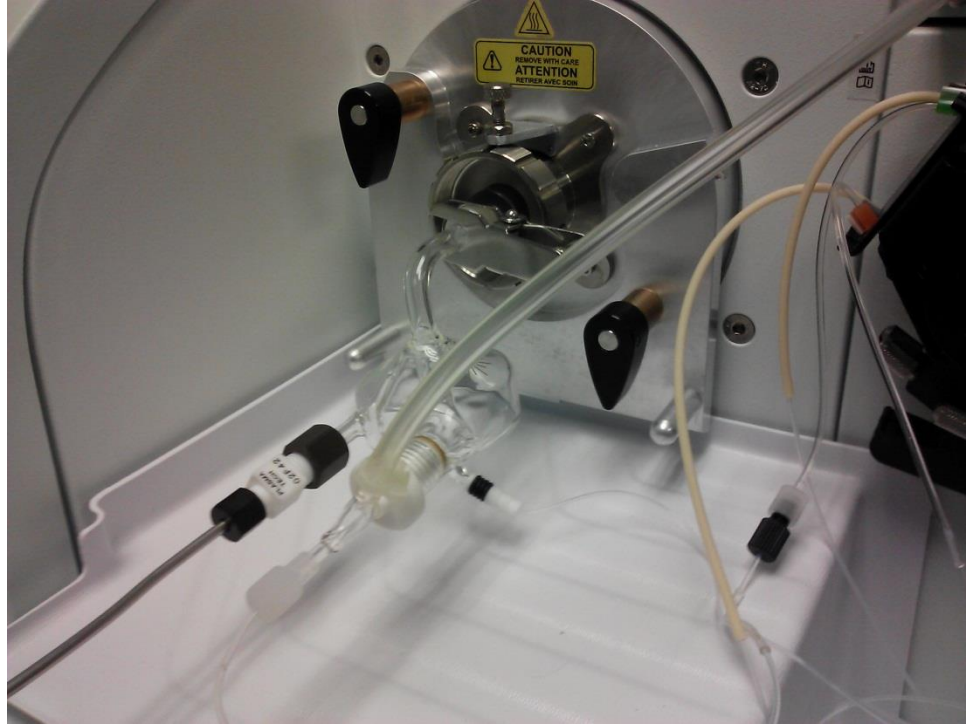


Figure 4.15: Dual-inlet spray chamber with connections to diffusion cell (left) and 1ppb indium standard (right)

4.3.4. Photon Machines Analyte Laser Ablation System

A Photon Machines Analyte excimer system was used for Cs concentration profile measurements in graphite samples where necessary. The instrument ablates material using a 192 nm argon/fluoride/trace neon pulsed laser. The laser was operated at a power density of 2 mJ/cm² and a pulse frequency of 10 Hz for measurements of Cs concentration in graphite in the present work.

4.4. Neutron activation analysis (INAA)

4.4.1. Overview

Neutron activation analysis is a sensitive technique for qualitative and quantitative determination of elemental sample composition. Elements in a sample form radioactive isotopes upon exposure to neutrons, and the resulting radiation spectrum is analyzed (typically via γ -spectroscopy) to determine elemental identity, quantity, or concentration. The relevant activation equation is:

$$A = \sigma\Phi N_T(1 - e^{-\lambda\tau})e^{-\lambda t} \quad (4.1)$$

Where:

A = activity after irradiation (Bq)

σ = neutron cross section (cm^2)

Φ = neutron flux ($1/\text{cm}^2$)

N_T = number of atoms in target

λ = decay constant ($1/\text{s}$)

τ = irradiation time (s)

t = decay time (s)

NAA experiments for the present work were conducted at the University of Missouri Research Reactor (MURR).

4.4.2. ICP-MS calibration

NAA experiments were conducted to calibrate the ICP-MS for measurement of fission product diffusion.

Over the course of a diffusion measurement, a quantity of a given fission product is lost from the sample and swept by the gas-jet system toward the ICP-MS. A small

fraction of the material which has diffused eventually interacts with the detectors in the ICP-MS and registers an instrument response in the form of a count rate (counts/s) or running count (counts). The following proportionality relationship exists between the mass of element diffused and the total number of counts produced on the ICP-MS detectors:

$$m_{diffused} = K_{measured} \cdot \left(\frac{\mathcal{M}}{\varepsilon_{measurement} \cdot N_A} \right) \quad (4.2)$$

Where:

$m_{diffused}$ = mass of fission product diffused (g)

$K_{measured}$ = total detector count (counts)

\mathcal{M} = molar mass of fission product (g/mol)

$N_A = 6.022 \times 10^{23}$ (mol⁻¹)

$\varepsilon_{measurement}$ = overall efficiency of measurement

Here $\varepsilon_{measurement}$ represents a product of individual efficiencies for each component of the transport and analysis systems. For a given run, the transport efficiency of the gas-jet system remains constant, and variation of the efficiencies in the ICP-MS system are corrected for via the internal standard response. Thus, the quantity in parentheses remains constant, and is the calibration factor for the measurement.

i.e.:

$$\left(\frac{\mathcal{M}}{\varepsilon_{measurement} \cdot N_A} \right) = F_{calibration} \quad (4.3)$$

Where:

$F_{calibration}$ = calibration factor (g/count)

In the present work, the total mass of element diffused during a run was determined via NAA determination of the initial and post diffusion quantities of a given diffusant. Before a diffusion run, the given sample of unknown diffusant concentration was irradiated at the MURR facility along with standards of known concentration. The sample and standards were counted via γ -spectrometry post irradiation to determine diffusant content. The procedure was repeated after the diffusion run to determine the total diffusant loss over the course of the measurement.

Each run produced data in the form of a plot of count rate vs. time. After normalization based on the internal standard response, the curves were integrated over the analysis time to give the total number of counts accrued over the measurement.

The ratio of these quantities is the calibration factor, which is then used to scale the original count rate data from the ICP-MS into units of diffusion rate ($\text{g}\cdot\text{s}^{-1}$) vs time, diffusion flux ($\text{g}\cdot\text{cm}^{-2}\cdot\text{s}^{-1}$) vs. time, or other units useful for determination of diffusion coefficients.

4.5. References

[1] Eibach, M., et al. "Transport of Fission Products with a Helium Gas-Jet at TRIGA-SPEC". *Nuclear Instruments and Methods in Physics Research A* 613 (2010) 226-231.

[2] Talbert, W. L. *Optimization of a He-Jet Activity Transport System to Use at LAMPF*. Los Alamos National Laboratory.

CHAPTER 5:

TIME-LAG MEASUREMENTS OF CESIUM DIFFUSION IN GRAPHITE

5.1. Overview

Graphitic materials are present in many core structures in HTGRs and these materials are expected to present a barrier to fission product release. Cesium-137 has been shown to be a main source of γ -activity present in the cooling circuits of such reactors and is a fission product of primary concern [1]. Diffusion behavior of cesium is investigated here in two types of nuclear grade graphite as well as a grade of commercial graphite. The primary objective during this portion of the present work was to develop a straightforward method for determination of diffusion coefficients in graphite using a time-lag measurement along with the diffusion cell described in Section 4.1.

5.2. Theoretical section

Experimental design follows the finite barrier model discussed in (2.4.1).

5.3. Sample preparation

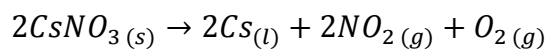
Cylindrical barriers of varying thickness were machined from stock samples of Toyo Tanso IG-110, Toyo Tanso IG-11, and a commercial grade of graphite. Dimensions and material identity for each sample are summarized in the Table 5.1 in the results section.

In each analysis, a 10 μ L aliquot containing a 1.0 μ g quantity of cesium in the form of CsNO_{3(aq)} was introduced into the diffusion cell sample chamber using a micropipette. The aliquot was evaporated to dryness, leaving the nitrate salt in the cavity of the sample chamber. A graphite specimen was then cemented into place with Aremco 890 on the stepped region of the sample chamber to hermetically seal the cesium source. The sample chamber was placed into the diffusion cell and the system seals and related connections were made.



Figure 5.1: Sealed sample chamber containing 1.0 μg cesium behind 1.0 mm IG-110 graphite barrier (uncured cement)

The cement used to seal the cesium source in the sample chamber required a stepped-temperature curing procedure (one hour at room temperature followed by two hours each at 200, 500, and 700°F) which was incorporated into the temperature ramp for each run, along with a one hour hold above the decomposition temperature of cesium nitrate (450°C) to produce elemental cesium via the reaction:



It was assumed that negligible diffusion occurred during the curing and decomposition stages of the experiments.

Following the decomposition stage, the temperature was quickly ramped to the desired diffusion temperature, with initial time defined as the ramp start time.

5.4. Diffusion measurements

Diffusion was monitored continuously by ICP-MS from the start of the temperature ramp until furnace shutdown. The ICP-MS standard used to monitor instrument stability was 1.00 ppb indium in 2% nitric acid.

5.5. Data analysis

The instrument signal was plotted as count rate vs. time to allow correction for instrument signal drift and cesium background corrections, and cumulative material diffused vs. time to determine the lag times and diffusion coefficients. The pseudo-steady state regions of the latter curves were extrapolated to the t-axis to determine the lag time as described in (2.4.1).

5.6. Results

Critical run data are summarized in the table below:

Run Number	Barrier	Temperature	Diffusion Coefficient (cm ² /s)
1	Commercial, 1.0mm	1150K	Not obtained
2	Commercial, 1.0mm	1200K	2.9×10 ⁻⁷

3	Commercial 1.0mm	1300K	2.8×10^{-6}
4	IG-110, 1.0mm	1200K	Not obtained
5	IG-110, 1.0mm	1200K	Not obtained
6	IG-110, 0.5mm	1100-1500K	Not obtained
7	IG-11, 1.0mm	1200K	Not obtained

Table 5.1: Diffusion data for time-lag measurements

Diffusion curves for two selected analyses of diffusion in commercial graphite (runs 2 and 3) are presented below, along with the linear extrapolation of the pseudo-steady state region used to determine the lag time and diffusion coefficient. The data curves for the IG-110 and IG-11 graphites deviated greatly from what would be considered physical behavior, and was attributed to failure of the cement used to seal the sample chamber.

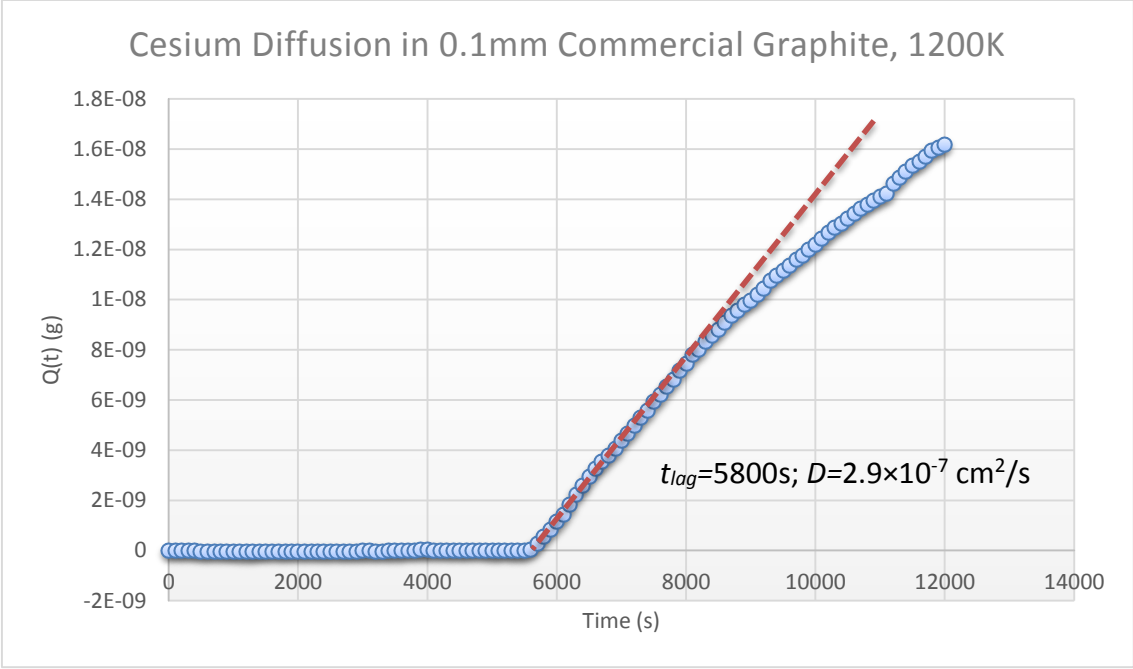


Figure 5.2: Time-lag analysis of cesium diffusion in 0.1cm commercial graphite at 1200K

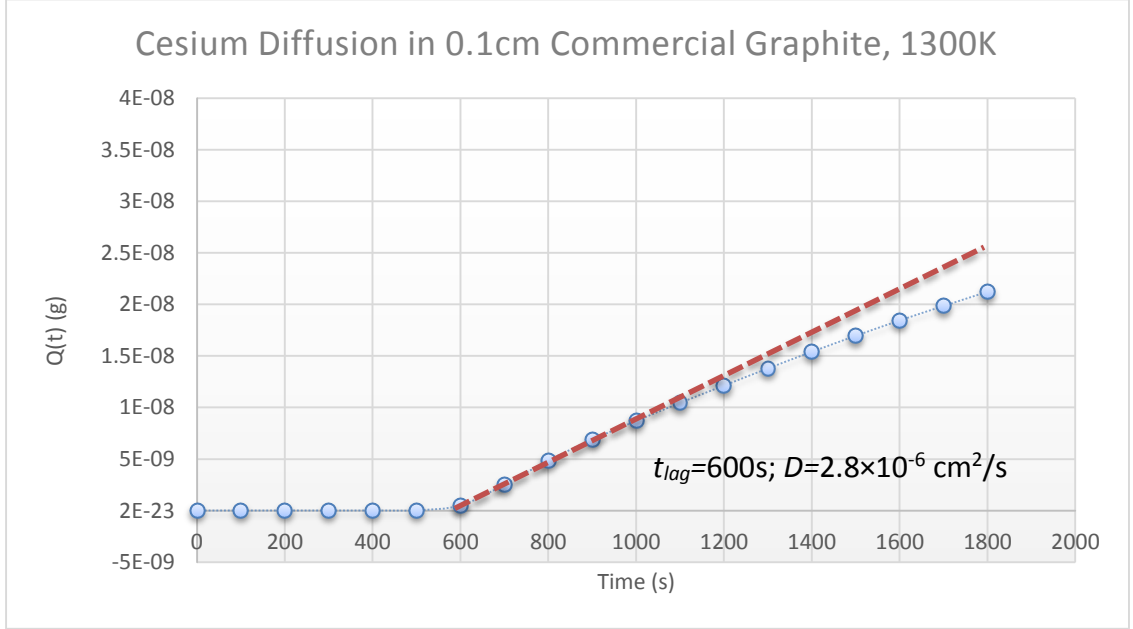


Figure 5.3: Time-lag analysis of cesium diffusion in 0.1cm commercial graphite at 1300K

The temperature dependence of the diffusion coefficient for cesium in the commercial grade graphite from these measurements is:

$$D_{Cs,Commercial} = \left(1.8 \times 10^{-6} \text{ cm}^2/\text{s}\right) e^{-\left(\frac{2.9 \times 10^5 \text{ J/mol}}{RT}\right)} \quad (5.1)$$

in the range of 1200-1300K.

5.7. Discussion of experimental error

The data for diffusion in the IG-110 and IG-11 grades of graphite are unsuitable for determination of a diffusion coefficient using the finite barrier approach. The primary source of error was suspected to be failure of the barrier seals resulting in bulk cesium release. This was confirmed in many of the trials upon disassembly of the diffusion cell, as relatively large cracks or voids in the cement seals were often visible to the naked eye.

This decreases confidence in the results obtained from the commercial graphite, as the same cement and similar curing procedures were used. Though the values of the diffusion coefficients and related activation energy for the commercial graphite are in reasonable agreement with literature values, the shape of the curves in Figures 5.2 and 5.3 (specifically the curvature in the non-steady state diffusion region) deviates from what would be considered physical behavior for a diffusion process. This becomes evident when attempting to determine the diffusion coefficients using a least squares fit

of solutions of the diffusion equation to the present data. The deviations may be attributable to anomalous diffusion behavior, but considering the known errors present from the IG-110 and IG-11 graphite trials, it seems much more likely to be due to failure of the cement seals. The consequence could be a fast diffusion process or an effusive process which would be more consistent with the observed data.

Additional error is present in all runs due to variable temperature at the start of the experiment, as the cell must heat up to the desired temperature. This contributes to overestimation of the lag time, while any diffusion that occurs during the curing process contributes to underestimation. These errors will partially offset one another, but it is unknown to what extent.

5.8. Conclusion

The time lag method appears to be incapable of accurate determination of diffusion coefficients in graphite given the current experimental design. However, the results did show proof of concept for the measurement, as cesium transport via carbon aerosols in helium (whether via diffusive, effusive, or bulk flow processes) was successfully observed and analyzed by ICP-MS.

In the present work, the time-lag method was abandoned at this stage in order to attempt release-type measurements. The release method, by design, eliminates the need for hermetic sealing of the sample chamber of the diffusion cell. Another driving factor in the decision to switch to release measurements was the potential to greatly

reduce the prohibitively long analysis times that would likely be required to study multi-component diffusion of species with largely different diffusion coefficients, or graphites with macroscopically inhomogeneous structure. Analysis times may be minimized by using a thin barrier; however, in the case of graphite this comes at the price of increased sample dependence and exacerbates the errors discussed in Section 5.1.7.

The knowledge gained from the time-lag experiments provided an excellent starting point for designing the first release measurements.

5.9. Proposed design modifications for time-lag measurement

In the event the time-lag measurement scheme should be revisited, the following design modifications are recommended to eliminate the effect of transport through seal materials observed in the initial trials.

The primary issue with leakage of diffusant through the seal material is not nearly as much of an issue with source material loss (a deviation from the specified boundary conditions in the finite barrier model) as it is with the lost material introducing a changing background in which it is impossible to detect changes in the rate of material transported due to diffusion. The following design borrows much from the design tested here, but differs mainly in the way the cell is sealed:

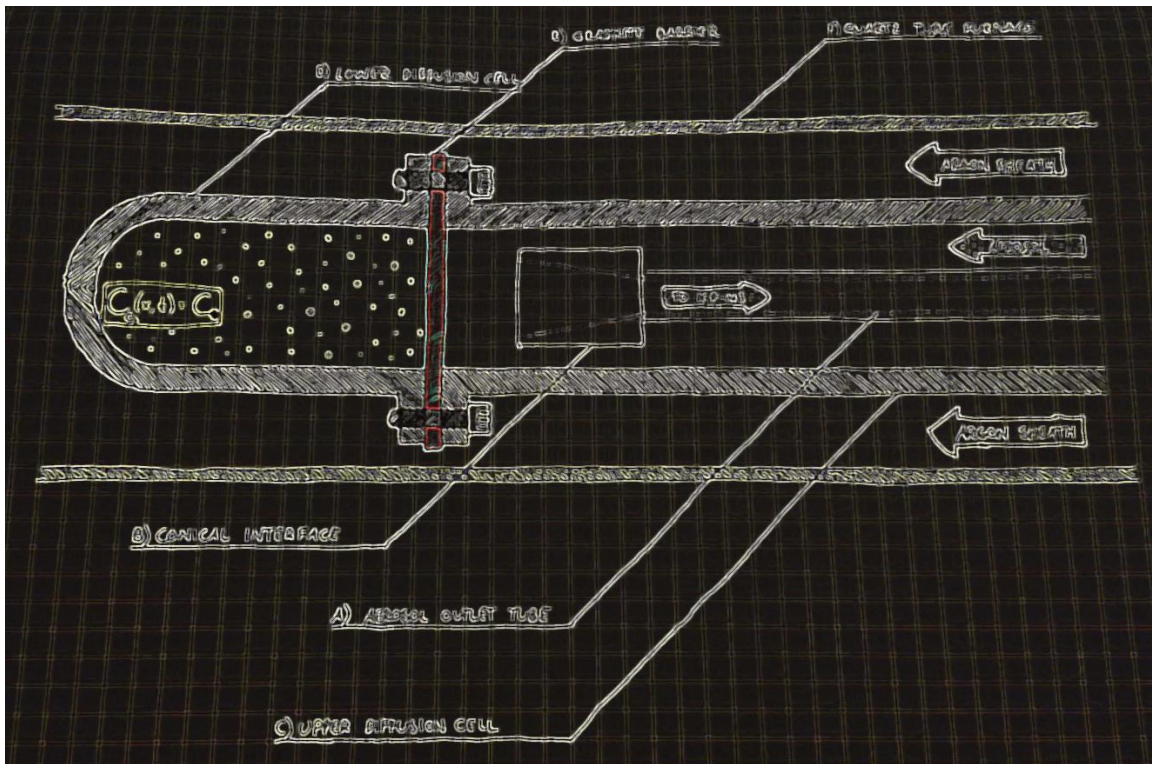


Figure 5.4: Proposed time-lag design modifications

The design modification involves separating the diffusion cell into an upper component C) and lower component D) as seen in Figure 5.4. Any diffusant escaping the high concentration chamber through the C)/D) interface should be largely displaced to the left and should not contribute to the ICP-MS signal. The material for the screws that form the compression fit between C), D), and the graphite barrier should be chosen such that their coefficient of linear expansion is less than that of graphite. This should guarantee the compressive forces sealing the source will increase as a function of temperature. Housing the assembly in a quartz tube furnace provides additional safeguards in the event of a cell component breakage.

5.10. References

- [1] Evans, R. B. III. *Cesium Diffusion in Graphite*. Oak Ridge National Laboratory. ORNL-5648

CHAPTER 6:

MEASUREMENT OF CESIUM DIFFUSION COEFFICIENTS IN GRAPHITE IG-110

6.1. Highlights

- A method was developed for real time analysis of fission product diffusion in graphite by ICP-MS
- The design simulates HTGR conditions
- Diffusion coefficients for cesium in IG-110 graphite were obtained

6.2. Abstract

An understanding of the transport of fission products in High Temperature Gas-Cooled Reactors (HTGRs) is needed for operational safety as well as source term estimations. We have measured diffusion coefficients of Cs in IG-110 by using the release method, wherein we infused small graphite spheres with Cs and measured the release rates using ICP-MS. Diffusion behavior was investigated in the temperature range of 1100-1300K. We have obtained:

$$D_{Cs} = \left(1.0 \times 10^{-7} \text{ m}^2/\text{s}\right) \exp\left(\frac{-1.1 \times 10^5 \text{ J/mol}}{RT}\right)$$

and, compared our results with those available in the literature.

6.3. Introduction

High Temperature Gas-Cooled Reactors (HTGRs) have five barriers to fission product (FP) release (the TRISO fuel coating, the fuel elements, core graphite, primary coolant system, and the reactor building). While very substantial understandings and data already exist [1-3], there is a need for new data and computational tools as new types of nuclear graphite are being used, or will be used than in the past. Our purpose in this paper is to describe a method we have developed to obtain diffusion coefficients of Cs in IG-110 graphite at HTGR temperatures. The method uses inductively coupled plasma-mass spectrometry (ICP-MS) to measure Cs release rates from graphite spheres infused with Cs. The method is general, and can be applied to measurements of diffusion coefficients of other substances or mixtures of substances as well.

We note that the release and profile methods were used previously for measurements of diffusion coefficients of Cs and other FP diffusants in graphite [4-11]. In these works graphite samples were impregnated with the FP material, and then annealed at specified temperatures and for certain time periods to effect release of FP. These techniques involved radioanalytical measurements of initial and final FP concentration in the graphite sample (release method), or the concentration profile by sectioning of the sample (profile method). The diffusion coefficients were then extracted from the data by comparison with theoretical results as given by the diffusion equation.

Additionally, in one case [7] the release rates of Cs-134 from a sphere were measured

using gamma spectrometry, and the diffusion coefficient was extracted by comparing this rate to the theoretical expression for the release rate. Typical results for H-451, matrix graphite A-3, HS-1-1, and IG-110 that have been reported are:

Table 6.1: Selected previous measurements of Cs diffusion in various graphites

Investigators	Graphite	Method	$D = D_0 \exp(-E/RT)$		$D \text{ (m}^2\text{s}^{-1}\text{)}$
			$D_0 \text{ (m}^2 \text{ s}^{-1}\text{)}$	$E \text{ (J}\cdot\text{mole}^{-1}\text{)}$	
Meyers [6]	H-451, cylindrical samples	Used sectioning technique. Diffusion trapping included; data obtained between ≈ 850 to 950°C			2.20×10^{-10} to 1.31×10^{-9}
Leyers [7]	Matrix A3, spherical samples	Helium flow over 1 cm sphere infused with Cs-134; gamma activity measurement for release rate	2.01×10^{-4}	1.98×10^5	
Hoinkis [8]	Matrix A3-3	Doping with Cs-137 and release	1.99×10^{-4}	1.81×10^5	
Evans [9]	HS-1-1	Sectioning technique	4.44×10^{-2}	1.27×10^5	
Hayashi and Fukuda [10]	IG-110 graphite	Sectioning of diffusion couple acceptor specimen	1.2×10^{-4} (Series A) 1.7×10^{-4} (Series B)	1.12×10^5 9.5×10^4	
Hayashi [11]	Irradiated IG-110 graphite	Sectioning of IG-110 specimen from OGL-1 fuel irradiation experiments	9.0×10^{-6}	1.57×10^5	

6.4. Materials and Methods

6.4.1. The release model and method

One considers a sample impregnated with a FP or any other volatile. As the sample is heated to a higher temperature, the FP is released from the sample at a time dependent rate. This release rate is dependent on many parameters as the sample may be porous, fractured, contain trapping contaminants, and the initial distribution of the FP itself may not be uniform or precisely known. The sample shape may deviate from an ideal geometry, and because of flow of helium or some other gas over the sample, surface mass transfer may not be easily estimated. While all these factors need to be eventually considered, ideally, one assumes that the release rate is dominated by the diffusion equation, and in this instance the effect of other factors is small. If a mathematical expression for the release rate, (dependent on the diffusion coefficient and known sample dimensions) and hence the cumulative release over a certain time period, are obtained, then by comparing the expressions for rate or cumulative release with the data, one can obtain the diffusion coefficient. The case of the spherical geometry is especially simple, where:

$$\frac{\partial C(r,t)}{\partial t} = \frac{1}{r^2} \frac{\partial}{\partial r} \left(D r^2 \frac{\partial C(r,t)}{\partial r} \right) \quad (6.1)$$

With the initial and boundary conditions:

$$C(r, 0) = C_0 \quad (6.2)$$

$$C(0, t) = \text{finite} \quad (6.3)$$

$$C(R, t) = 0 \quad (6.4)$$

Here, $C(r,t)$ is the concentration of the FP (g/m^3), D is the diffusion coefficient (m^2/s), r is the radial coordinate (m), R is the radius of the sphere (m), and t is the time (s). C_0 is a constant; the initial uniform concentration.

This is a well-known equation of mass transfer, and can be solved by series expansion or transform techniques [12]. In particular, the cumulative fractional release (defined as the ratio of total mass release of FP from the sphere at time t to the initial total mass of FP in the sphere), can be expressed as:

$$F(t) = 1 - \frac{6}{\pi^2} \sum_{n=1}^{\infty} \frac{1}{n^2} e^{-\left(\frac{n\pi}{R}\right)^2 Dt} \quad (6.5)$$

This series converges slowly, especially for short times. For extraction of the diffusion coefficient, a short time solution (obtained through the Laplace Transformation) is more convenient. This solution is known to be:

$$F(t) = 6 \sqrt{\frac{Dt}{\pi R^2}} - 3 \frac{Dt}{R^2} \quad (6.6)$$

This solution is considered to be valid for a fairly long range of time (up to and exceeding 90% release), and generally for short times (up to 30% release) one can use just the first term only [12]. The diffusion coefficient is calculated by fitting solutions of the fractional release equation above to fractional release data. We can also use the theoretical rate equation, which is the product of the derivative of the above and the initial FP mass, for comparisons with the corresponding measurements. The short time theoretical release rate $Z_R(t)$ (g/s) is:

$$Z_R(t) = 3m_0 \left(\sqrt{\frac{D}{\pi R^2 t}} - \frac{D}{R^2} \right) \quad (6.7)$$

where m_0 is the total initial mass (g) of FP in the sphere. We have used both the cumulative release and the release rate data and expressions for calculation of diffusion coefficients and have observed agreement among the obtained values.

6.4.2. Materials and sample preparation

The graphite used in this study was IG-110 manufactured by Toyo Tanso. It is produced using an isostatic rubber press process and is semi-isotropic. Spherical samples were milled to a radius of 0.2 cm. The spheres were infused (impregnated) with cesium using a modified procedure that was adapted from Hayashi and Fukuda [10]. Ten graphite spheres were loaded into a quartz vial (0.6 cm diameter, 4 cm length) with 600 μg of Cs in the form of CsNO_3 . The vial was then sealed under vacuum with a measured pressure of 40 mTorr. The sealed quartz vial was heated to 500°C to convert the nitrate salt to elemental Cs by the following reaction:



After 1 hour, the temperature was increased to 1100°C and maintained for 99 additional hours to uniformly distribute cesium within the graphite spheres. The temperature was reduced at a rate of 1°C/min until the oven temperature was 200°C. The spheres were removed from the vial and reduced to a final radius of 0.15 cm using SiC sandpaper. The purpose of reducing the radius from 0.2 cm to 0.15 cm was to remove any Cs which may have condensed onto the spheres during the cooling period in the oven.

The initial mass of Cs in each sphere was measured using instrumental neutron activation analysis (INAA). Comparator standards were prepared from a certified solution of CsNO₃ purchased from High Purity standards. A 50 μL aliquot of the standard solution was pipetted onto filter placed paper in a high density polyethylene vial with a volume of 200 μL. The standards were dried and capped with friction fit caps. The graphite spheres and comparator Cs standards were irradiated in the row 2 pneumatic tube irradiation position for 30 seconds in a neutron flux of 5.0×10^{13} n/cm²/s. The 127.5 keV gamma ray from decay of ^{134m}Cs produced by the reaction ¹³³Cs(n,g)^{134m}Cs was measured by counting the sample 2.5 cm from the face of a HPGe detector. The samples were counted until at least 10,000 counts were measured in the 127.5 keV photopeak. The initial mass of Cs in the 10 graphite spheres ranged from 12.2 μg to 16.1 μg.

6.5. Experimental

The release experiment is carried out inside of a SiC tube mounted in a Lindberg tube furnace. A diagram of the experimental apparatus is shown in Figures 6.1 and 6.2.

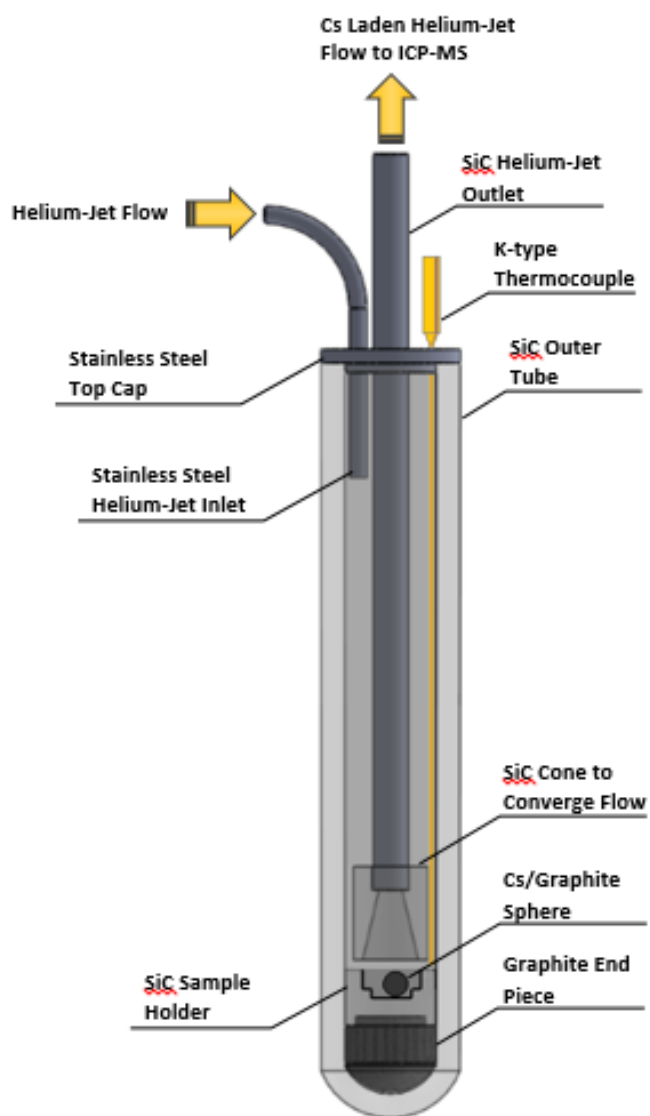


Figure 6.1: The release experiment takes place inside SiC tube that is closed at one end and mounted vertically in a Lindberg tube furnace. The arrows show the helium jet path.

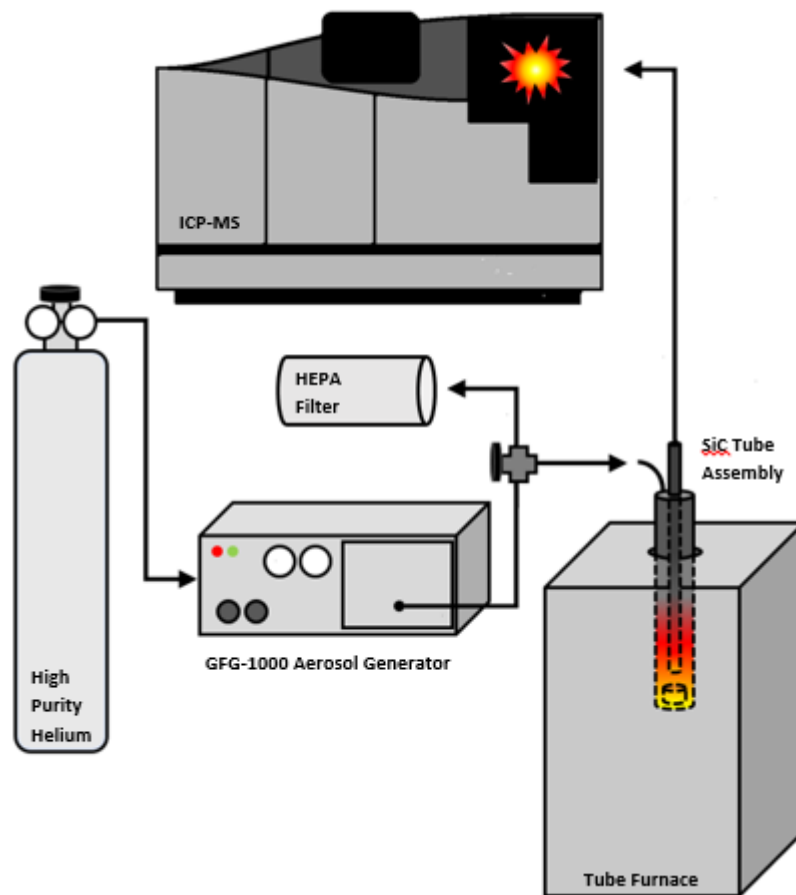


Figure 6.2: Schematic of the release experiment setup. The graphite sphere is located inside the SiC tube. Cs that is released is transported to the ICP-MS by a He-jet system.

The tube furnace heats the sample region of the SiC tube assembly to the target temperature. The top 10 cm of the SiC tube extends out of the tube furnace and is accessible. The temperature at the SiC holder is monitored using a K-type thermocouple. At the start of an experiment a room temperature graphite sphere containing a known mass of Cs is dropped into the heated sample holder. A sample holder constructed of SiC sits at the bottom of the assembly and holds the graphite

sphere. The Cs released from the graphite sphere is transported from the diffusion chamber to an online ICP-MS for real time analysis using a carbon aerosol helium gas jet system.

A gas jet uses particles entrained in flowing gas to transport elements over long distances at room temperature [13]. The helium jet built for this experiment was modeled after the system used at the TRIGA reactor in Mainz, Germany which uses carbon nanocrystals [14]. A modified Palas GFG 1000 carbon aerosol generator was used to produce carbon particles with diameter lognormally distributed around 50 nm. The aerosol generator functions by creating a spark discharge between two graphite electrodes which vaporizes carbon at the electrode surfaces. The vaporized carbon condenses into carbon particles entrained in helium that flows between the graphite electrodes at 4 L/min. The carbon aerosol laden helium is introduced into the SiC tube assembly using the He-jet inlet tube shown in Figure 6.2. The path of the helium jet inside the SiC tube assembly is illustrated in Figure 6.2 by the orange arrows. The helium jet flows around the graphite sphere where released Cs sorbs onto the carbon particles. The Cs laden helium jet exits the SiC tube and travels through a 3 m stainless steel tube that connects to a Perkin Elmer Nexion 300X ICP-MS via a two port quartz spray chamber, shown in Figure 6.3. The other port of the spray chamber contains a liquid nebulizer which continuously introduces a standard solution of 1.00 ng/g indium. The indium is used as an internal standard to monitor and correct for instrument drift

over the course of the experiment. The helium jet operates for up to 6 hours during the experiment.



Figure 6.3: Dual inlet spray chamber. Inlet 1 (left) from He-jet with He flow rate of 1 L/min. Inlet 2 (right) from nebulizer that injects 200 $\mu\text{L}/\text{min}$ of 1.00 ng/g In as an internal standard.

At the start of an experiment, the SiC tube assembly is heated to the target temperature. The helium-jet system is turned on and the ICP-MS is started, tuned, and set to collect data for 30-60 minutes prior to introduction of the graphite sphere. Prior to sample introduction residual Cs on the SiC tube assembly surfaces is released and transported by the helium-jet to the ICP-MS detector. This constitutes a detector

background of Cs. The background is monitored until it represents less than 1% of the expected Cs count rate. The He-jet outlet tube is disconnected while the SiC tube assembly is at the target temperature and the graphite sphere is dropped inside and, by gravity, descends into the SiC tube sample holder. The sphere is positioned as shown in the cutout section of Figure 6.1.

6.6. Data and Analysis

Diffusion coefficients are computed by measuring cumulative mass release or release rate from the graphite sphere as a function of time using ICP-MS. The value of the diffusion coefficient follows via a regression analysis.

The ICP-MS output is the count rate of Cs and the internal standard indium measured at the detector. It must be calibrated to produce a signal in units of an actual mass transport rate or quantity. The Cs count rate is scaled to the Cs mass transport rate by multiplication with the calibration factor, $F_{calibration}$ (g/count) which is a ratio of the total mass of Cs which has diffused $m_{diffused}$ (g) in an experiment and the total number of detector counts acquired by the ICP-MS $K_{measured}$ (counts) in the same time interval:

$$F_{calibration} = \frac{m_{diffused}}{K_{measured}} \quad (6.9)$$

The $m_{diffused}$ was calculated as the Cs mass difference of the graphite sphere before and after the diffusion experiment measured by INAA. The calibration factor is

used to calculate the release rate Z_R (g/s), using the detector count rate $k_{measured}$ (counts/s) the calibration factor $F_{calibration}$ (g/count). The experimental release rate is:

$$Z_R = k_{measured} \cdot F_{calibration} \quad (6.10)$$

Integration of the experimental release rate with respect to time yields the Cs mass diffused, and the experimental fractional release $F(t)_{exp}$ is the ratio of the mass diffused to the mass initially present in the sphere. For a given experiment, a plot of the $F(t)_{exp}$ vs. t is fitted with solutions of eqn. 6.6 via a regression analysis to determine the diffusion coefficient.

Diffusion coefficients for Cs in IG-110 graphite at 1100, 1200, and 1300K are summarized in Table 6.2. Release rate and fractional release ICP-MS data for the analysis of Trial 10 are presented in Figure 6.4.

Table 6.2: The table lists the diffusion coefficients calculated by fitting solutions of eqn. 6 to the experimental data using a regression algorithm. The initial and final Cs content was measured using INAA.

Trial	Initial Cs Content (μg)	Final Cs Content (μg)	Temperature (K)	D (m^2/s) [Eqn. 6 Regression]	D (m^2/s) [Eqn. 7 Regression]	D (m^2/s) [INAA Mass Difference]
1	14.5	11.7	1100	9.5E-13	8.5E-13	1.3E-12
6	12.2	10.3	1100	6.3E-13	5.9E-13	8.5E-13
7	16.1	13.8	1100	1.4E-13	7.1E-14	1.8E-13
8	13.9	11.3	1100	1.0E-12	8.0E-13	1.1E-12
2	12.7	11.1	1200	8.0E-13	8.5E-13	7.8E-13
4	14.3	11.8	1200	1.2E-12	1.5E-12	1.1E-12
10	15.3	12.4	1200	1.3E-12	1.5E-12	1.4E-12
3	12.9	8.56	1300	4.9E-12	1.1E-11	4.2E-12
5	12.6	8.83	1300	4.3E-12	8.3E-12	3.6E-12
9	14.7	10.6	1300	2.5E-12	3.7E-12	2.7E-12

The sphere introduction time is defined as $t=0$. Because the time required for transport to the ICP-MS and the time required for the sphere to come to thermal equilibrium with the cell are both non-zero and not precisely known, there is a slight delay in data acquisition. Additionally, small deviations from ideal transport behavior of the FP laden aerosol stream (e.g. diffusional broadening, interactions with component surfaces) result in broadening of the signal, which would ideally be represented as proportional to a delta function. These effects are obvious from the release rate plot in figure 4, below, as initially the release rate is zero and is increasing, which does not reflect physical diffusion behavior based on the assumptions of the release model. Conversely, when fractional release data is considered, the initial data points correspond more closely to physical behavior (zero cumulative release at $t=0$, and increasing thereafter). The accuracy of diffusion coefficients computed from the rate data may be improved by excluding some initial data points or by redefining the initial time. This would require additional assumptions and/or measurements, as the regression analysis would be affected significantly. These manipulations would have a much smaller effect on the fractional release data series (i.e. the fractional release regression is less sensitive to redefining the initial time or excluding the corresponding data points), and therefore it is believed that the fractional release regression gives the best estimate of the diffusion coefficient. For comparison, we have also calculated

diffusion coefficients via regression analysis using the rate equation (eqn. 6.7), with similar results.

Data obtained during the time interval from sphere introduction ($t=0$) to the moment the furnace is turned off ($t=t_{end}$) has been considered during fitting procedures. It is important to note that a small amount of additional diffusion occurs after t_{end} , as the furnace cools down from the experimental temperature. This additional transport is monitored by the ICP-MS, and incorporated into the calibration factor. However, it is excluded in all regression analyses as we wish to consider diffusion at constant temperature.

We also note that the INAA mass difference measurement and the width of the annealing time interval (t_{end}) gives an indication of the diffusion coefficient in itself, which is an exact solution from eqn. 6.6. However, there is no way to exclude diffusion which occurs after furnace shutdown when computing diffusion coefficients in this way, and as the ICP-MS data gives the cumulative release (or rate) at many time points, the system is overdetermined and a regression analysis should give the best estimate of the effective diffusion coefficient. We present the values corresponding simply to the INAA mass difference measurement for comparison in Table 6.2.

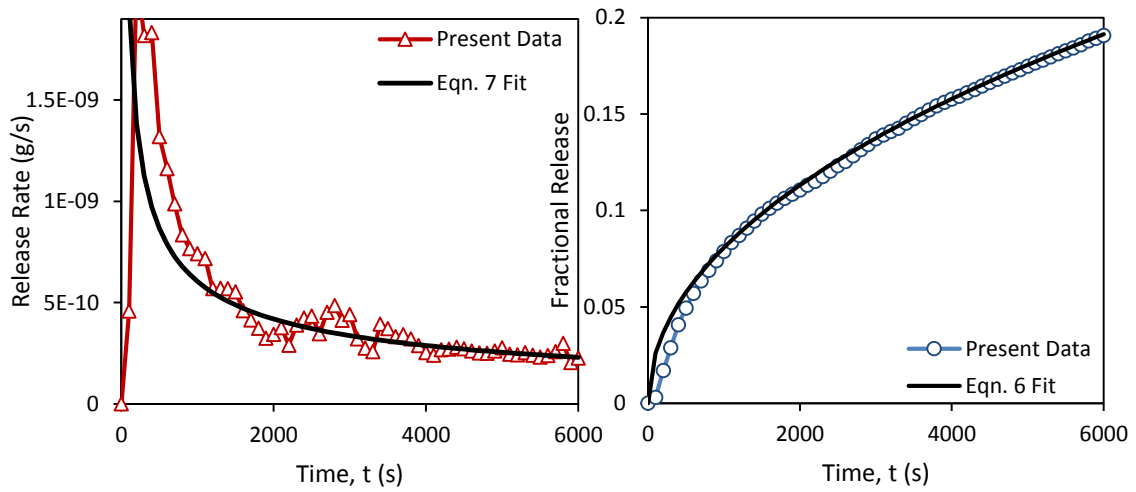


Figure 6.4: Sphere 10 release flux plot (left) and fractional release plot (right) with best fit theoretical curve corresponding to $D=1.3 \times 10^{-12} \text{ m}^2/\text{s}$.

The Arrhenius equation is used to describe the temperature dependence of the diffusion coefficient in terms of the pre-exponential factor D_0 (m^2/s) and corresponding activation energy E (J/mol). We have obtained D_0 and E in the temperature range of 1100-1300K from an Arrhenius plot of the data in columns 4 and 5 of Table 6.2. These values and uncertainties are given in Table 6.3.

Table 6.3: Pre-exponential and activation parameters for diffusion of Cs in IG-110 graphite between 1100K and 1300K.

Material	FP	D_0 (m^2/s)	$\pm \Delta \ln D_0$	E (J/mol)	$\pm \Delta E$ (J/mol)
IG-110	Cs	1.0×10^{-7}	2.90	1.1×10^5	2.8×10^4

contains other FPs, adsorbents, or is subjected to irradiation or oxidative stresses. In modeling, we have assumed that the graphite spheres are perfectly spherical, FP is initially uniformly distributed in them, the spheres are in infinite space (not touching any surface), and that the surface concentration of FP is zero. Sensitivity of results to deviations from these assumptions is likely small (our preliminary investigations of small deviations from non-uniform concentration confirm this), but should be investigated in the future.

It is evident from Figure 6.5 that there are differences in results, which is typical of measurements of this type. Some variation is due to differences in the properties of the materials tested, while the nature of the measurement technique likely plays a role as well.

Myers [5] and Hayashi [10] have reported that effect of fast neutron damage causes a decrease in the diffusivity by orders of magnitude. In contrast, Hoinkis [8] reported no change in measured diffusion coefficients when comparing irradiated and as-received graphite. Interestingly, diffusion coefficients obtained by Hayashi [11] from in-pile irradiated IG-110 graphite correlate well with those obtained in the present work. This suggests that Cs diffusion coefficients in IG-110 may not be strongly dependent on fast neutron fluence. Hayashi observed wide variation in the results when testing unirradiated IG-110 graphite in separate experiments [10] and suggested material inhomogeneity among different production lots was responsible for the variation. It

may therefore be important to test representative samples from each lot of IG-110 to determine if the measured diffusion coefficient is within a tolerable range.

6.8. Conclusions

We have measured diffusion coefficients of Cs in IG-110 in the temperature range of 1100-1300K by using the release method and ICP-MS. We have used a carbon aerosol laden helium-jet system to transport Cs diffusing from a heated graphite sphere to an online ICP-MS to determine release rates and cumulative release in real time. We have obtained:

$$D_{Cs} = \left(1.0 \times 10^{-7} \text{ m}^2/\text{s}\right) \exp\left(\frac{-1.1 \times 10^5 \text{ J/mol}}{RT}\right) \quad (6.11)$$

The method we have developed is easily adaptable to measure diffusion of other fission products or of multiple fission products, diffusion in other types of graphite or other materials of interest, and the effects of oxidation and other chemical or physical stresses on diffusion behavior. We have observed that Cs diffusion in IG-110 graphite in the temperature range of 1100-1300K may be adequately described by the classical diffusion equations.

6.9. Acknowledgements

This research was supported by a NEUP-2982 grant, "A Research Program for Fission Product/Dust Transport in HTGRs" by the U. S. Department of Energy. The

spheres were machined at the MURR Science Instrument shop, and the measurements, including NAA, were conducted at MURR facilities. We acknowledge support of several colleagues including Drs. Rajesh Gutti and Matt Simones regarding use of the Palas particle generator, and Professor Tushar Ghosh for information on the existing literature.

6.10. References

- [1] “Mechanistic source terms white paper”. INL/EXT-10-17997. Idaho National Laboratory, Idaho, US. (2010).
- [2] IAEA Tech Doc 978. Fuel performance and fission product behavior in gas cooled reactors. IAEA (1997). p 461.
- [3] Becker Technologies GmbH. Fission product retention in HTGR confinement buildings. Summary of final report BF-R-40.039-1.0 (2010. original in German, 1988).
- [4] E. Hoinkis, Editor. Transport of fission products in matrix and graphite. HMI-B372. Proceedings of a colloquium held at Hahn-Meitner-Institut, Berlin, 1981 (published, June 1983). These proceedings contain many papers of interest, we cite relating to the release method below.
- [5] B. F. Meyers. A Review of the diffusion of selected fission product metals in polycrystalline graphite. *ibid*, p. 56.
- [6] B. F. Meyers and D. W. Hill. Cesium diffusion in H-451 graphite. *ibid* p. 68.
- [7] H. J. Leyers. Cesium release out of graphite matrix A3 in flowing helium. *ibid* p. 103.
- [8] E. Hoinkis. The determination of diffusion coefficients of cesium and silver by the release method in as received, oxidized and neutron irradiated graphite-matrix. *ibid* p. 77.
- [9] R. B. Evans, W. Davis, A.L. Sutton. “Cesium diffusion in graphite”. ORNL-5648, Oak Ridge National Laboratory, Tennessee, US. (1980)

[10] K. Hayashi and K. Fukuda. Diffusion coefficients of cesium in un-irradiated graphite and comparison with those obtained from in-pile experiments. *J. Nuc. Materials* 168 (1989) 328-336.

[11] K. Hayashi, T. Kikuchi, F. Kobayashi, K. Minato, K. Fukuda, K. Ikawa, K. Iwamoto. Distribution of fission products in irradiated graphite materials of HTGR fuel assemblies: Third and fourth OGL-1 fuels. *J. Nuc. Materials* 136 (1985) 207-217.

[12] D. R. Olander, *Fundamental Aspects of Nuclear fuel Elements*. Energy Research and Development Administration. 1976.

[13] Rengan K., and Meyer R.A. *Ultrafast Chemical Separations*. National Academy Press, Washington D.C. 49-58 (1993).

[14] Eibach M., Beyer, T., Blaum K., Block M., Eberhardt K., Herfurth F., Geppar C., Ketalaer J., Ketter J., Kramer J., Krieger A., Knuth K., Nagy S., Narthershauser W., and Smorra C. "Transport of fission products with a helium gas-jet at TRIGA-SPEC". *Nucl. Instrum. Methods Phys. Res., Sect. A*, 613:226-231 (2010).

CHAPTER 7:

CALIBRATION OF A SYSTEM FOR MEASUREMENTS OF DIFFUSION COEFFICIENTS OF FISSION PRODUCTS IN HTGR/VHTR CORE MATERIALS

7.1. Abstract

High Temperature Gas-Cooled Reactors (HTGRs) are designed to operate 1100 K and use He as a primary coolant gas. The HTGRs use TRISO fuel kernels which are 0.9 mm in diameter and coated with layers of graphite and silicon carbide that prevent fission product release. Measurements of the diffusion coefficients of fission products in graphitic materials used in the TRISO fuel and other core components are needed for transport and release modeling. In this work, we present a novel method to measure the diffusion coefficient of fission products in graphite and demonstrate calibration of the system for quantification of Cs release rates from graphite. Spheres of graphite were loaded with Cs metal. The Cs released from the graphite spheres was transported directly to an inductively coupled plasma mass spectrometer (ICP-MS) for release measurements using a carbon particle helium jet. Cs calibration factors were determined using neutron activation analysis.

7.2. Introduction

High-Temperature Gas-Cooled Reactors (HTGRs or VHTRs) remain one of the most promising candidates for the next generation of nuclear power reactors. Existing knowledge gaps specific to HTGR technology include an incomplete understanding of fission product transport in core materials under operational and off normal conditions. In particular, diffusion coefficients for fission products in HTGR core materials are required to develop accurate models for estimation of fission product release rates. Graphite comprises several permanent and replaceable structures in an HTGR core, and serves as a moderator and barrier to fission product release.

The HGTR/VHTR is expected to operate at temperatures in excess of 1100 K, and in accident scenarios may reach temperatures exceeding 2000 K. In this temperature range, diffusion is known to be an important mode of fission product transport in graphite, and therefore the current work focuses on the determination of diffusion coefficients for fission products in graphite. The isotopes ^{137}Cs , ^{134}Cs , ^{90}Sr , and $^{110\text{m}}\text{Ag}$ are of interest due to the radiological hazard they present in the event of release.

Several types of graphite are utilized for permanent and replaceable core components in the High Temperature Test Reactor and HTR-10, contemporary experimental HTGRs. Substantial data for diffusion of key fission products exist for historical nuclear graphite grades; however, newer grades of nuclear graphite will be or are currently being used due to the unavailability of historical grades and the superior thermal, mechanical, and

physical properties of contemporary graphites [1-13]. Previous research has shown that fission product diffusion behavior may vary depending on graphite properties including binder and pitch composition, pore structure, impurity identity and concentration, manufacturing techniques, irradiation history, oxidation, and presence of other diffusants [5-12]. The diffusion of fission products in contemporary nuclear graphites at the temperatures present in HTGRs must be thoroughly investigated before they can be implemented on a large scale.

In this paper, we report on a versatile method for quantifying diffusion coefficients of multiple fission products in graphite using a release method. The system implements a silicon carbide (SiC) cell which houses a graphite sample in a simulated HTGR environment. The SiC cell is coupled to an ICP-MS to quantify the release of material from a graphite sample. The system may be configured to analyze diffusion in graphite under a variety of simulated HTGR operational or accident scenarios, and may be applied to measurements of diffusion in other materials as well as graphite. The capability of the method is demonstrated in the present work through measurement of Cs release rates from spherical graphite samples previously impregnated with Cs.

7.3. Theory

The diffusion coefficient is a primary parameter which characterizes transport of a material (here, fission product) in a particular medium (graphite) in the absence of convection or advection. Diffusion is classically described by Fick's laws:

$$J_j = -D_j \nabla C_j \quad (7.1)$$

and

$$\frac{\partial C_j}{\partial t} = D_j \nabla^2 C_j \quad (7.2)$$

where J_j is the flux of the j th material ($\text{kg}\cdot\text{m}^{-2}\cdot\text{s}^{-1}$), C_j is its concentration ($\text{kg}\cdot\text{m}^{-3}$), t is the time (s), and D_j is the diffusion coefficient ($\text{m}^2\cdot\text{s}^{-1}$). The temperature dependence of the diffusion coefficient is expressed by the Arrhenius parameters $E_{a,j}$ ($\text{J}\cdot\text{mol}^{-1}$) and $D_{j,0}$ ($\text{m}^2\cdot\text{s}^{-1}$), viz.:

$$D_j = D_{j,0} \exp(-E_{a,j}/RT) \quad (7.3)$$

where R ($\text{J}\cdot\text{mol}^{-1}\cdot\text{K}^{-1}$) is the universal gas constant and T (K) is the absolute temperature. Diffusion coefficients can be calculated from experimental release data if the sample dimensions and initial distribution of diffusant are known by fitting solutions of (7.2) to the experimental release data.

Determination of diffusion coefficients in graphite is often performed using the release method, wherein it is common to load a graphite sphere with a uniform concentration of fission product surrogate and then measure the release rate [8,13,14].

When heated, material is released from the graphite sphere at a rate determined by the diffusion equation and corresponding boundary conditions. It can be shown that for a sphere of radius R (m) containing an initial mass $m_{j,i}$ (g) of the j th material, the release rate $Z_j(t)$ is given by:

$$Z_j(t) = 3m_{j,i} \left(\sqrt{\frac{D_j}{\pi R^2 t}} - \frac{D_j}{R^2} \right) \quad (7.4)$$

and the fractional release $\Phi_j(t)$, defined as the ratio of the cumulative mass of material released to the total initial mass of material present in the sphere, given by:

$$\Phi_j(t) = 6 \sqrt{\frac{D_j t}{\pi R^2}} - 3 \frac{D_j t}{R^2} \quad (7.5)$$

when diffusing material is continually removed from the sphere surface (the theoretical boundary condition present for a sample in the SiC cell). The diffusion coefficient may be determined by fitting solutions of (7.4) or (7.5) to experimental release data. One of the most important advantages to using ICP-MS is that the high sensitivity of the instrument allows measurement of the instantaneous release rate of material from the cell even when the absolute mass of material released from the graphite sample is very small. An additional advantage is the fast scan rate of the quadruple ICP-MS allows for measurement of single- and multi-element mixtures of material released from the sample.

7.4. Experimental

7.4.1. Overview

Spherical graphite samples are placed in a SiC tube assembly that is housed vertically in a Thermo Lindberg HTF55322C tube furnace to replicate temperature extremes to 1200°C. The SiC cell accommodates a dedicated K-type chromel/alumel thermocouple to accurately measure temperatures at the sample region. He flows through the cell at 2 L·min⁻¹ to displace oxygen and prevent oxidation of the graphite. The graphite spheres are loaded with a fission product surrogate(s); in the present case, with Cs. A prepared graphite sphere is placed inside the preheated SiC release chamber to effect fission product release. The Cs that is released out of the graphite sphere is transported to an ICP-MS for measurement using a helium jet aerosol transport system. The helium jet aerosol is produced using a PALAS GFG-1000 spark discharge aerosol generator modified to operate with He instead of Ar. The helium jet system is modeled based on a system developed for the TRIGA-SPEC facility, and increases the transport range of the fission products by several orders of magnitude relative to their range in pure flowing helium [15]. A schematic drawing of the experimental components is given in Figure 7.1.

The transport efficiency of the gas jet system is a function of aerosol particle size and concentration, temperature, carrier gas flow rate, and path geometry. Using aerosol production parameters of 0.7 bar He and 100 Hz spark frequency, the graphite

particle size was characterized over 6 hours of continuous operation of the GFG-1000 using a TSI 3936 scanning mobility particle sizer on 3 consecutive days. The particle equivalent mobility diameter is lognormally distributed around a most probable diameter of 25(2) nm. The relative standard deviation of the total particle concentration was 3%.

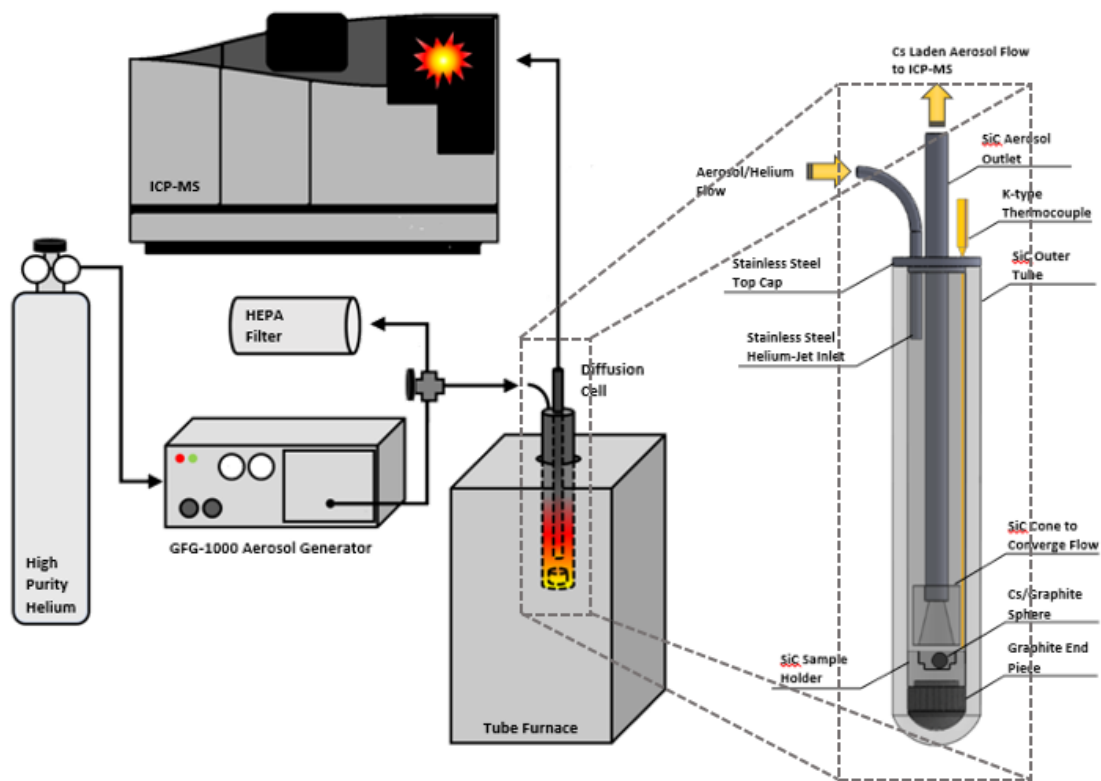


Figure 7.1: Experimental setup

The helium jet is coupled to the ICP-MS using a Glass Expansion dual-port quartz spray chamber. One port receives the aerosol from the SiC cell. The other port houses a nebulizer which introduces a 1.00 ppb indium standard at $200 \mu\text{L}\cdot\text{min}^{-1}$ in order to

correct for variations in instrument sensitivity over the course of an experiment. The instrument produces a signal in default units of counts/s at the detector, and must be externally calibrated to produce a signal in units of the actual mass transport rate ($\text{g}\cdot\text{s}^{-1}$).

The mass transport rate may be expressed as:

$$Z_j(t) = k_j(t)F_j \quad (7.6)$$

where t is the time, Z_j is the mass transport rate of the j th material ($\text{g}\cdot\text{s}^{-1}$), k_j is the detector count rate ($\text{counts}\cdot\text{s}^{-1}$), and F_j is the calibration factor ($\text{g}\cdot\text{count}^{-1}$) which is a ratio of the total mass of material released by a sample to the total number of counts produced at the detector. The detector count rate is computed by normalizing the internal standard count rate to a constant value of 2000 counts $\text{In}\cdot\text{s}^{-1}$ and proportional multiplication of the detector signal for the j th material by the normalization factor.

The calibration factor is measured for a material using instrumental neutron activation analysis (INAA). The mass of a particular fission product surrogate, in this case Cs, initially present in the graphite sample $m_{j,i}$ is measured using INAA via the standard comparator method. The graphite sample is introduced into the SiC cell at a set temperature and time t_i , and the fission product release rate is measured in $\text{counts}\cdot\text{s}^{-1}$ by the ICP-MS. The sample remains in the SiC cell for a time that is sufficient for a significant fraction of the material to be released. At the end of the experiment, the furnace is turned off to stop release of material from the graphite sample. The sample is removed and the remaining mass of material $m_{j,f}$ is measured by INAA, at the end of

the experiment t_f . The calibration factor F_j is calculated as the quotient of the mass of material released and the total number of counts during the experiment.

$$F_j = \frac{m_{j,t} - m_{j,f}}{\int_{t_i}^{t_f} k_j(t) dt} \quad (7.7)$$

7.4.2. Specific methods

Reagents: 0.62 cm diameter spheres of nuclear grade NBG-18 graphite were machined from stock. Solid cesium nitrate was used as-received from Alfa Aesar. 1000 $\mu\text{g}\cdot\text{mL}^{-1}$ Cs and In ICP-MS standards were purchased from High Purity Standards. Ultrapure helium was purchased from Airgas.

Calibration of the system to measure Cs release rates is demonstrated in the present work. Ten 0.62 cm diameter NBG-18 graphite spheres and approximately 0.5 mg of solid CsNO_3 were sealed together in a quartz vial under 100 mtorr vacuum. The vial and contents were heated to 1100 °C for 6 days to decompose the nitrate and allow elemental Cs to diffuse into the spheres [10]. The spheres were then removed from the vial and machined down to a final diameter of 0.60 cm.

The spheres were analyzed using standard comparator INAA at the MURR facility to determine the mass of Cs present within each sphere. Comparator standards were prepared by transferring 25 μL aliquots of 1000 $\mu\text{g}\cdot\text{mL}^{-1}$ CsNO_3 in 2% HNO_3 onto stacked filter paper in polyethylene vials. The additions were measured gravimetrically; the

three standards contained 24.3(1), 24.4(1), and 24.6(1) μg Cs. The graphite spheres were added to similar vials. The samples and standards were irradiated for 7 s at a neutron flux of $6.5 \times 10^{13} \text{ n}_{\text{th}} \cdot \text{cm}^{-2} \cdot \text{s}^{-1}$ in row 2 of the pneumatic tube irradiation system of the MURR facility, producing trace $^{134\text{m}}\text{Cs}$ via the reaction:



Following a decay time of 5 min, the samples and standards were counted for seven minutes at a distance 5 cm from the face of a 20% relative efficiency HPGe detector; the FWHM resolution of the detector is 1.70 keV at 1332 keV. The analysis measured counts from the 128 keV photopeak from decay of Cs-134m and was corrected for background contribution. Detector dead time was handled using the loss-free counting technique.

Each sphere was introduced into the preheated SiC cell and Cs loss from the graphite was monitored by ICP-MS for five hours. After normalization for instrument drift via the In internal standard response, the cumulative Cs counts was determined by computing the time integral of the Cs count rate. This process was repeated at different temperatures for the remaining spheres.

The spheres were analyzed again by INAA to determine the mass of Cs remaining in each sphere, using the same standards and procedure described previously. Calibration factors were determined using equation (7.7).

7.5. Results and Discussion

Table 7.1: Cs release calibration factors obtained using 50 Hz spark generation frequency and 0.7 bar He aerosol generation parameters. ICP-MS Cs counts were normalized relative to 2000 cps In

Temperature (K)	Initial Cs mass, m_i (μg)	Final Cs mass, m_f (μg)	Cumulative ICP-MS Counts	Calibration factor, F_j (g/count)
1090	14.3(1)	13.45(9)	2.23×10^7	$3.6(7) \times 10^{-14}$
1140	15.1(1)	13.94(9)	4.13×10^7	$2.8(4) \times 10^{-14}$
1185	15.1(1)	13.8(1)	7.30×10^7	$1.8(2) \times 10^{-14}$
1238	14.3(1)	13.20(9)	9.37×10^7	$1.2(2) \times 10^{-14}$
1290	15.7(2)	12.97(9)	1.14×10^8	$2.4(2) \times 10^{-14}$
1340	15.3(2)	13.3(1)	1.93×10^9	$1.10(9) \times 10^{-15}$
1395	14.6(1)	11.54(9)	6.00×10^8	$5.0(2) \times 10^{-15}$

The ICP-MS calibration factors for release measurements at different temperatures for Cs transport are given in Table 7.1. The calibration factor is expected to be different for each material and may vary with SiC cell temperature, instrument component geometry, aerosol concentration and size distribution, and carrier gas flow rate. Physically the calibration factor represents a product of transport efficiencies through each inline component in series from the diffusion cell sample chamber to the ICP-MS detector. The Cs calibration factor reported in table 1 does not follow a smooth trend as a function of SiC cell temperature, and therefore it is necessary to determine the calibration factor for the measurement of Cs release for each individual sample by measuring the initial and final quantities of Cs by INAA. The error in the calibration

factor may be minimized by allowing sufficient time for a large fraction of the initial mass of material to be released, which minimizes the error in the measured mass difference.

Initial measurements of the concentration profile in the Cs impregnated NBG-18 spheres suggests the radial distribution of Cs was non-uniform after the 6 day loading procedure. We have measured the average concentration of Cs in one of the 0.62 cm diameter spheres and determined the Cs concentration to be $184 \mu\text{g}\cdot\text{cm}^{-3}$. The same sphere contained $135 \mu\text{g}\cdot\text{cm}^{-3}$ Cs when machined down to its final diameter of 0.60 cm. This implies that Cs is concentrated at the surface and invalidates the assumption of uniformity required for determination of the diffusion coefficient from equation (7.5) or (7.6). Future work focuses on measurements to determine the initial concentration distribution of Cs in the spheres. The diffusion coefficients will be obtained by fitting solutions of the diffusion equation with initial condition corresponding to the measured initial Cs distribution.

7.6. Conclusion

We have designed and constructed a SiC cell for measurement of diffusion coefficients of fission products in graphitic materials under HTGR conditions of high temperature and flowing helium. The measurement technique has been calibrated to allow release rates of Cs to be determined continuously as a function of time.

Simultaneous analysis of multi-element diffusion may be made in a variety of HTGR core materials in addition to graphite by simple adaptations to the experimental procedure.

7.7. Acknowledgements

This research was funded by a United States Department of Energy NEUP-2982 grant, "A Research Program for Fission Product/Dust Transport in HTGRs". SiC cell components were manufactured by Saint-Gobain Hexaloy and graphite spheres were machined by the MURR Science Instrument Shop. ICP-MS and INAA measurements were conducted at the MURR facility.

7.8. References

- [1] "Mechanistic source terms white paper". INL/EXT-10-17997. Idaho National Laboratory, Idaho, US. (2010).
- [2] IAEA Tech Doc 978. Fuel performance and fission product behavior in gas cooled reactors. IAEA (1997). p 461.
- [3] Becker Technologies GmbH. Fission product retention in HTGR confinement buildings. Summary of final report BF-R-40.039-1.0 (2010. original in German, 1988).
- [4] C.I. Contescu, T. Guldan, P. Wang, and T.D. Burchell. The effect of microstructure on air oxidation resistance of nuclear graphite. Carbon 50 (2012) 3354-3366.
- [5] E. Hoinkis, Editor. Transport of fission products in matrix and graphite. HMI-B372. Proceedings of a colloquium held at Hahn-Meitner-Institut, Berlin, 1981 (published, June 1983). These proceedings contain many papers of interest, we cite relating to the release method below.

- [6] B. F. Meyers. A Review of the diffusion of selected fission product metals in polycrystalline graphite. *ibid*, p. 56.
- [7] B. F. Meyers and D. W. Hill. Cesium diffusion in H-451 graphite. *ibid* p. 68.
- [8] H. J. Leyers. Cesium release out of graphite matrix A3 in flowing helium. *ibid* p. 103.
- [9] E. Hoinkis. The determination of diffusion coefficients of cesium and silver by the release method in as received, oxidized and neutron irradiated graphite-matrix. *ibid* p. 77.
- [10] R. B. Evans, W. Davis, A.L. Sutton. "Cesium diffusion in graphite". ORNL-5648, Oak Ridge National Laboratory, Tennessee, US. (1980)
- [11] K. Hayashi and K. Fukuda. Diffusion coefficients of cesium in un-irradiated graphite and comparison with those obtained from in-pile experiments. *J. Nuc. Materials* 168 (1989) 328-336.
- [12] K. Hayashi, T. Kikuchi, F. Kobayashi, K. Minato, K. Fukuda, K. Ikawa, K. Iwamoto. Distribution of fission products in irradiated graphite materials of HTGR fuel assemblies: Third and fourth OGL-1 fuels. *J. Nuc. Materials* 136 (1985) 207-217.
- [13] L.M. Carter, J.D. Brockman, S.K. Loyalka, and J.D. Robertson. Measurement of cesium diffusion coefficients in graphite IG-110. *J. Nuc. Materials* 460 (2015) 30-36.
- [14] A.H. Booth. A method for calculating fission gas diffusion from UO₂ fuel and its application to the X-2-f loop test. Atomic Energy of Canada Ltd. Technical Report AECL-496, 1957.
- [15] Eibach M., Beyer, T., Blaum K., Block M., Eberhardt K., Herfurth F., Geppar C., Ketalaer J., Ketter J., Kramer J., Krieger A., Knuth K., Nagy S., Narthershauser W., and Smorra C. "Transport of fission products with a helium gas-jet at TRIGA-SPEC". *Nucl. Instrum. Methods Phys. Res., Sect. A*, 613:226-231 (2010).

CHAPTER 8:

ICP-MS MEASUREMENT OF DIFFUSION COEFFICIENTS OF CS IN NBG-18 GRAPHITE

8.1. Highlights

- A method for analysis of fission product diffusion in graphite by ICP-MS was applied to nuclear-grade graphite NBG-18
- The design simulates HTGR conditions
- Diffusion coefficients for cesium in NBG-18 graphite were obtained

8.2. Abstract

Graphite is used in the HGTR/VHTR as moderator and it also functions as a barrier to fission product release. Therefore, an elucidation of transport of fission products in reactor-grade graphite is required. We have measured diffusion coefficients of Cs in graphite NBG-18 using the release method, wherein we infused spheres of NBG-18 with Cs and measured the release rates in the temperature range of 1090-1395 K.

We have obtained:

$$D_{Cs,NBG-18} = (1.0 \times 10^{-7} \text{ m}^2/\text{s}) \exp\left(\frac{-1.23 \times 10^5 \text{ J/mol}}{RT}\right)$$

These seem to be the first reported values of Cs diffusion coefficients in NBG-18. The values are lower than those reported for other graphites in the literature.

8.3. Introduction

Release of fission products from nuclear reactors is a fundamental safety concern. The High Temperature Gas-Cooled Reactor (HTGR/VHTR) uses graphite as a moderator and as a barrier to fission product release in the reactor core. The VHTR is expected to operate with a core outlet temperature exceeding 1273K, and in an accident scenario may reach temperatures of 1873K. At these temperatures, diffusion becomes an important mechanism of fission product transport and release from the core. Improvements in manufacturing techniques coupled with unavailability of historical graphite grades (e.g. H-451) have led to the development of contemporary grades of nuclear graphite including IG-110, NBG-18, and PCEA, and these and other candidate graphites need to be well qualified [1]. Currently, material properties and diffusion/oxidation behavior of candidate graphites are being intensely investigated. Measurements of diffusion coefficients for fission products in graphite are required for source term estimations and reactor safety.

We have previously measured diffusion coefficients for Cs in IG-110 graphite using the release method, in which graphite spheres were infused with Cs and subsequent release of Cs measured by ICP-MS [2], and we have illustrated infusion

procedures and instrument calibration for Cs in NBG-18 graphite [3]. In this paper we apply the technique to diffusion of Cs in NBG-18 graphite, and focus on the results for NBG-18 and comparisons with IG-110.

We note that IG-110 graphite is a very fine-grained petroleum coke filler-based graphite produced by Toyo Tanso in Japan using an isostatic rubber press process. NBG-18 is manufactured using a vibrational molding process by SGL Carbon GmbH in Germany, using a much larger grain size and coal coke filler. Differences in manufacturing techniques and materials impart wide variation among the properties of nuclear graphites, including pore size distribution, concentration of impurities, density, and grain sizes. These characteristics are expected to have an effect on fission product diffusion coefficients in graphite. A summary of relevant characteristics for IG-110 and NBG-18 is given in Ref. [5].

8.4. Theory

Transport of Cs in certain graphites has been shown to occur via a pore surface diffusion mechanism which consists of series of random “jumps” of Cs atoms between diffusion sites [6-11]. The permeability of a material to a particular diffusant is characterized by the diffusion coefficient. The diffusion coefficient generally follows an Arrhenius type dependence on temperature, specifically:

$$D = D_0 \exp\left(\frac{-E_a}{RT}\right) \quad (8.1)$$

where D is the diffusion coefficient (m^2/s), D_0 is the diffusion coefficient at infinite temperature, E_a is the activation energy (J/mol), R the gas constant ($\text{J/mol}\cdot\text{K}$), and T the temperature (K). In graphite, the diffusion coefficient may be a function of other factors in addition to temperature, including pore size distribution, oxidation, irradiation, and concentration of contaminants.

Here we consider a spherical graphite sample of radius $r=R$ which has been infused with a particular fission product (FP). As the sample is heated, the concentration of the FP changes at a time dependent rate governed by the diffusion equation, as the FP atoms diffuse through and out of the sphere through its surface. Under the assumption that the mass distribution of the FP is spherically symmetric, we have [2,9,12,13]:

$$\frac{\partial C(r,t)}{\partial t} = \frac{1}{r^2} \frac{\partial}{\partial r} \left(D r^2 \frac{\partial C(r,t)}{\partial r} \right) \quad (8.2)$$

With boundary condition:

$$C(R,t) = 0 \quad (8.3)$$

Here, $C(r,t)$ is the concentration of the FP (g/cm^3), and t is the time (s). Note that

$C(r,t)$ is non-negative and is finite everywhere. This mass transfer equation is well

known, and may be solved using separation of variables, transform techniques, or numerical methods.

The series solution of Eqns. (8.1-8.2) is known to be:

$$C(r,t) = \sum_{n=1}^{\infty} A_n \psi_n(r) \text{Exp}(-\lambda_n^2 Dt) \quad (8.4)$$

Where,

$$\begin{aligned} \lambda_n &= n\pi / R \\ \psi_n(r) &= \sin(\lambda_n r) / r \\ A_n &= \frac{2}{R} \int_0^R r^2 C(r,0) \psi_n(r) dr \end{aligned} \quad (8.5)$$

where $C(r,0)$ is the initial condition, the concentration profile in the sphere, at $t=0$.

The mass loss rate (g/s) of FP from the sphere is expressed as:

$$\dot{m}(t) = -4\pi R^2 D \frac{\partial}{\partial r} C(r,t) \Big|_{r=R} = 4\pi R D \sum_{n=1}^{\infty} A_n (-1)^{n-1} \lambda_n \text{Exp}(-\lambda_n^2 Dt) \quad (8.6)$$

And, the cumulative fractional release $F(t)$, defined as the ratio of mass of FP released from the sphere (up to time t) to the total initial FP mass, is thus:

$$F(t) = \frac{1}{m_0} \int_0^t \dot{m}(t') dt' = \frac{4\pi R D}{m_0} \sum_{n=1}^{\infty} A_n (-1)^{n-1} \frac{1}{\lambda_n D} [1 - \text{Exp}(-\lambda_n^2 Dt)] \quad (8.7)$$

Where m_0 is the total initial total mass of the FP in the sphere,

$$m_0 = 4\pi \int_0^R r^2 C(r,0) dr \quad (8.8)$$

If the initial distribution of FP, $C(r,0)$ is known, (8.6) or (8.7) may be fit to experimental release data to determine the diffusion coefficient. In particular, if we take,

$$C(r,0) = \alpha + \beta (r/R) \quad (8.9)$$

Where α and β are some constants, then we find:

$$A_n = -\frac{2R}{n^3 \pi^3} \left\{ 2\beta + (-1)^n \left[-2\beta + n^2 \pi^2 (\alpha + \beta) \right] \right\} \quad (8.10)$$

And, Eqn. (8.7) can be written as:

$$F(t) = \frac{8R^3}{m_0 \pi^3} \sum_{n=1}^{\infty} \frac{(-1)^n}{n^4} \left[1 - e^{-\left(\frac{n\pi}{R}\right)^2 Dt} \right] \left\{ 2\beta + (-1)^n \left[-2\beta + n^2 \pi^2 (\alpha + \beta) \right] \right\} \quad (8.11)$$

An alternative and more convenient expression for $F(t)$ corresponding to Eqn. (8.11), valid for short time, can be found using the Laplace Transform technique. We have found this solution, to order t , to be (we call it, $F_{short}(t)$ to distinguish it from the above series solution)

$$F_{short}(t) = \frac{4\pi R^3}{m_0} \left[\alpha (2\sqrt{\tau/\pi} - \tau) + 2\beta (\sqrt{\tau/\pi} - \tau) \right] \quad (8.12)$$

Where, the non-dimensional quantity τ is defined as (this combination appears in Eqn. (8.11) above also):

$$\tau = \frac{Dt}{R^2} \quad (8.13)$$

For the case of flat initial profile, $\beta = 0$, and Eqn. (8.12) is then the same as we had used in our previous work on IG-110. Also, as for the flat profile, we have found that Eqn. (8.12) is surprisingly accurate even for fairly large times (we have compared $F(t)$ and $F_{short}(t)$ for a range of parameter;, generally for good accuracy, it is necessary to retain about 100 or more terms in the series as it converges very slowly for short times).

We have explored use of both Eqns. (8.11) and (8.12) in our analysis, and have found that for the time periods (about 5 hours) of the release measurements in our experiments, results obtained from the two (we used 100 terms in the series) are indistinguishable.

8.5. Experimental

8.5.1. Instrumentation

A scanning quadrupole ICP-MS instrument (Perkin Elmer Nexion 300X) with a dual port quartz spray chamber was used for quantification. In order to correct for

instrument variation during the measurements, a nebulizer continuously introduced a 1.00 pbb In internal standard solution in 2% aqueous HNO₃ at 200 μL/min into one port of the spray chamber. A carbon aerosol helium jet system was used for transport of diffusing FPs to the other port of the dual port spray chamber. The gas jet system consisted of a helium source and a Palas GFG-1000 carbon aerosol generator specially fabricated by Palas for use with helium carrier gas. The gas jet was routed through a custom SiC cell designed to hold the graphite samples under simulated VHTR conditions (high temperature, flowing helium environment). The cell was housed in a Lindberg M Series hinged tube furnace and connected to the spray chamber with stainless steel capillary tubing, Swagelok stainless steel connectors, and Plasmatech polymer connectors. A complete description of the instrumentation and calibration procedures for release measurements is given in references [2] and [3].

We should note that transport of atoms and molecules in pure helium has been shown to occur only for distances on the order of centimeters [14] due to high diffusion rates of gas phase atoms and molecules, and subsequent deposition onto tubing walls. The addition of carbon aerosol particles to the flowing helium stream increases the transport efficiency of our measurement by greater than three orders of magnitude. The transport efficiency is also demonstrated to be sensitive to increased carbon particle density in the He stream which results from changes in the spark frequency in the aerosol generator (Fig. 8.1). This suggests that transport of FPs in VHTR cooling circuits may be greatly enhanced by the presence of graphite dust or other particulates

present, and may contribute to release of FPs especially in a cooling circuit breach accident scenario.

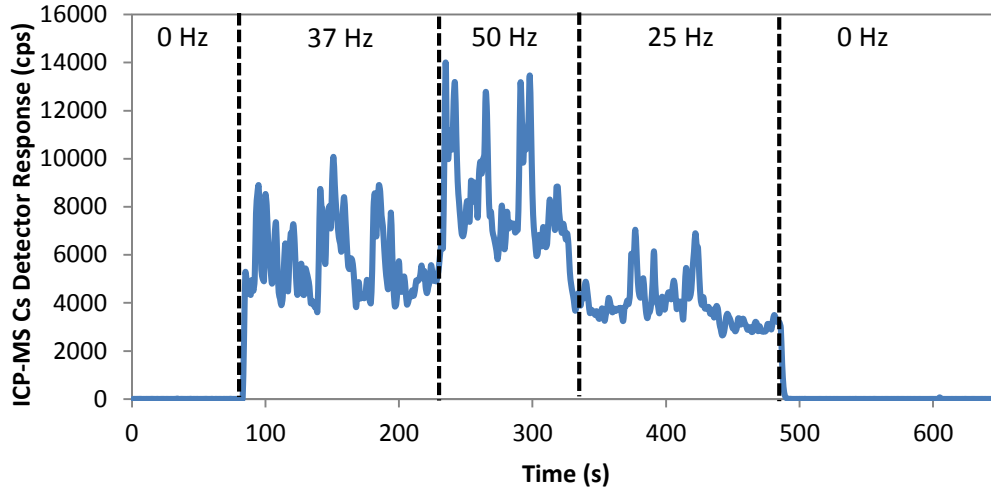


Figure 8.1: ICP-MS sensitivity as a function of carbon aerosol generator spark frequency (Hz) or carbon particle aerosol density in the He carrier gas.

Further, we used a Photon Machines Analyte excimer laser in combination with the Nexion 300X ICP-MS for measurements of the Cs concentration profile in the NBG-18 carbon sphere via laser ablation. The laser uses an argon/fluoride/trace neon cell and operates at 192 nm.

8.5.2. Specific Methods

8.5.2.1. Sample preparation

Spheres with 0.32 cm radii were milled from as-received NBG-18 stock material by the MURR Science Instrument shop. The spheres were added to a cylindrical quartz

vial along with solid CsNO₃ (as-received from Alfa Aesar). The vial was sealed under 90 mtorr vacuum with a flame sealing torch. The vial was heated to 500°C for one hour to convert the nitrate salt to elemental cesium [8-10, 15].

The vial was then heated to 1100°C and maintained at this temperature for 8 days in an attempt to uniformly distribute cesium within the spheres. The spheres were machined down to a diameter of 0.30 cm using SiC sandpaper. Contamination and dust was removed from the surfaces of the spheres using compressed air.

8.5.2.2. Initial Cs content analysis

The cesium content of each sphere was measured using standard comparator neutron activation analysis at the MURR facility. Comparator standards were prepared from a certified solution of CsNO₃ purchased from High Purity standards. The spheres and standards were irradiated in the row 2 pneumatic tube irradiation position for ten seconds at a thermal flux of 5.0×10^{13} n/cm²/s to produce trace ^{134m}Cs via the reaction ¹³³Cs(n,γ)^{134m}Cs. The 127.5 keV gamma ray from decay of ^{134m}Cs was measured using a HPGe detector; samples were counted until at least 10,000 counts were acquired in the 127.5 keV peak. The initial cesium mass present in each sphere ranged from 14.3 to 15.7 μg.

The distribution of Cs in the spheres was measured by laser ablation inductively coupled plasma mass spectrometry (LA-ICP-MS) using a Photon Machines Analyte 193 excimer laser and Nexion 300X ICP-MS. Two of the spheres prepared as described in

3.2.1 were sectioned into hemispheres with a razor blade. The Cs concentration profile was analyzed by making 40 μm line scans using a 40 μm laser spot size at distance intervals of 200 μm along the radii of the flat surface of the hemispheres. The laser was operated at a power density of 2 mJ/cm^2 and a pulse frequency of 10 Hz.

8.5.2.3. Diffusion measurements

Cs release from the graphite spheres was measured isothermally at temperatures in the range of 1090K to 1395K. Release was measured for a period of approximately five hours at all temperatures. At the start of the experiment, the SiC cell is heated to target temperature and the ICP-MS is tuned. The Cs signal is monitored for approximately one hour before a sphere is introduced into the cell to allow for correction due to instrument Cs background. A sphere is introduced into the cell by disconnection of the gas-jet system at the aerosol outlet of the SiC cell; the sphere is dropped in and descends into the heated sample holder of the cell. Due to the high thermal diffusivity of the graphite, small size, and small heat capacity, we assume the sphere heats instantaneously to the experimental temperature and that diffusion is measured isothermally. We have conducted thermal diffusivity calculations to investigate the rate of change of temperature of the spheres; these calculations indicate this is a valid approximation.

8.5.2.4. Final Cs content analysis

After release measurements, the Cs content of each sphere is quantified again using standard comparator INAA as described in Section 8.5.2.2. The difference in Cs mass from before and after release measurements is used to determine the ICP-MS calibration factor. The calibration factor scales the real time ICP-MS count rate or cumulative count total to actual mass transfer units (grams Cs/s or grams Cs, respectively).

8.6. Results

The initial distribution of Cs in the spheres after the loading procedure (infusion) was determined by LA-ICP-MS and is given in Fig. 8.2:

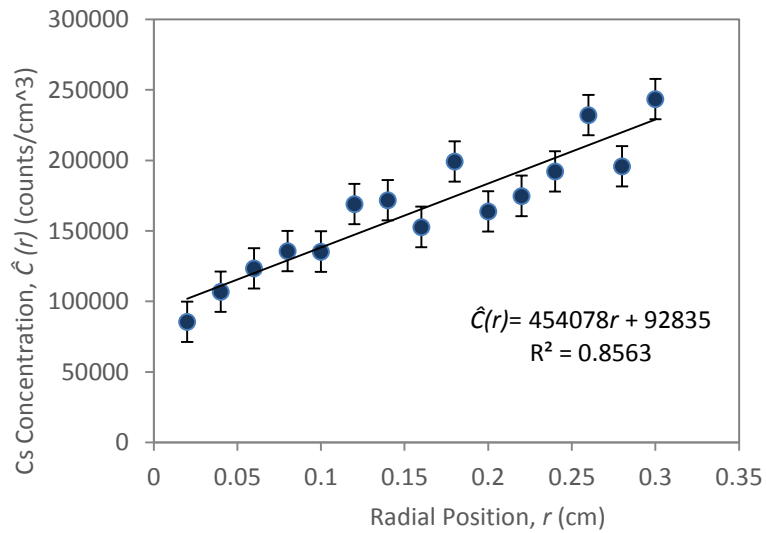


Figure 8.2: Initial Cs concentration profile measured by LA-ICP-MS

This profiles appears to be approximately linear, and therefore we have fit it with $\alpha + \beta(r/R)$, where α and β are constants (theoretically the profile should be flat at the center. We have discussed the infusion problem in appendix A, and estimated that this approximation is reasonable). We have found

$$\alpha = 4.21 m_0 \quad (g \text{ cm}^{-3}) \quad (8.14)$$

$$\beta = 6.18 m_0 \quad (g \text{ cm}^{-3}) \quad (8.15)$$

We have obtained diffusion coefficients for Cs in NBG-18 by fitting both Eqn. (8.11) and Eqn. (8.12) to the fractional release data via least squares regression analysis, described previously in [2]. The infinite series given by (11) has been approximated using the first 100 terms. The results obtained via the use of either equation are indistinguishable. Our results are reported in Table 8.1.

Table 8.1: Cs diffusion coefficients in NBG-18 graphite in the temperature range of 1090K to 1395K.

Initial Cs Content (μg)	Total Cs Release (μg)	Analysis Time (hr)	Temperature (K)	D (m^2/s)
14.3	0.80	5	1090	1.5×10^{-13}
15.1	1.2	5	1140	2.4×10^{-13}
15.0	1.3	5	1185	3.3×10^{-13}
14.3	1.1	5	1238	3.2×10^{-13}
15.7	2.8	5	1290	1.5×10^{-12}
14.6	3.0	5	1395	2.7×10^{-12}

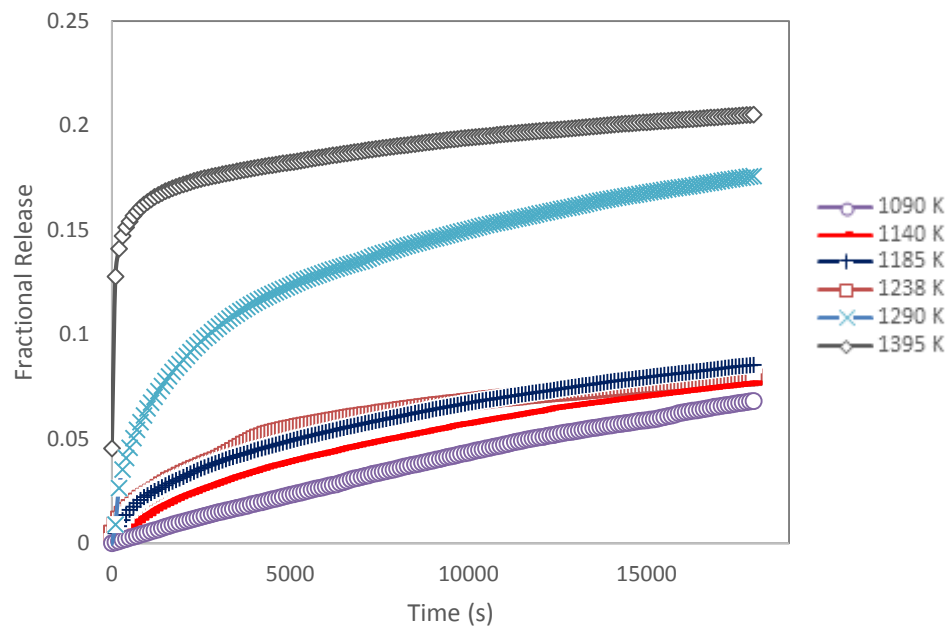


Figure 8.3: Fractional release curves for six $R=0.3$ cm NBG-18 graphite spheres as measured by ICP-MS.

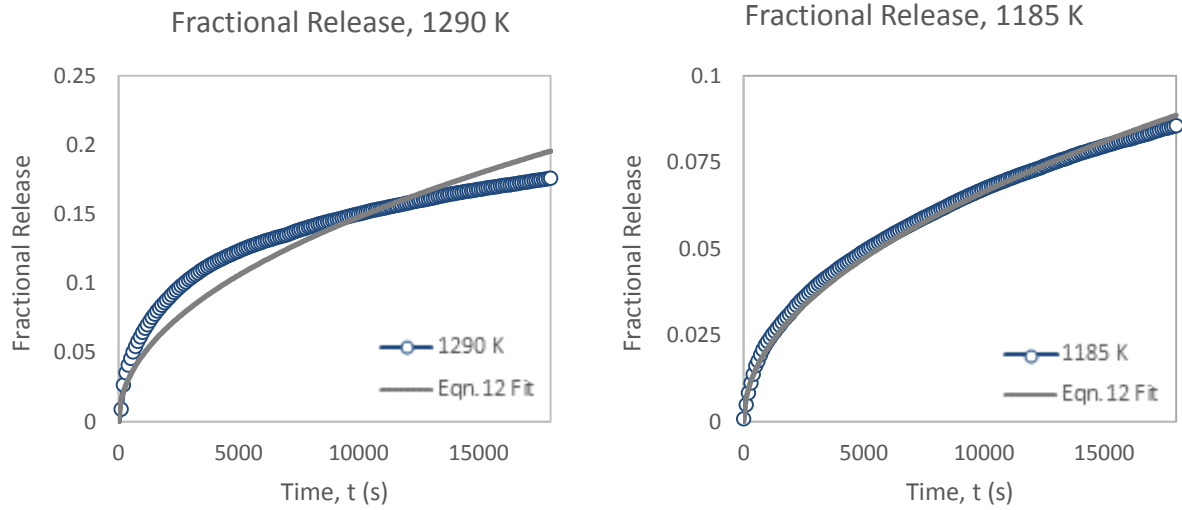


Figure 8.4: Fractional release curves and respective fit of Eqn. 11 for $R=0.30$ cm NBG-18 graphite spheres at 1290 and 1185 K.

The temperature dependence of the diffusion coefficient is reported in the Arrhenius form (Eqn. 8.1). The values of the pre-exponential factor D_0 and activation energy E_a over the temperature range of 1090-1395 K are reported in Table 8.2.

Table 8.2: Pre-exponential and activation parameters for diffusion of Cs in NBG-18 graphite between 1090K and 1395K.

Material	Diffusant	D_0 (m^2/s)	$\pm\Delta\ln D_0$	E_a (J/mol)	$\pm\Delta E_a$ (J/mol)
NBG-18	Cs	1.0×10^{-7}	2.10	1.23×10^5	2.1×10^4

8.7. Discussion

We have used classical diffusion theory for describing Cs transport in NBG-18 graphite using an effective diffusion coefficient and corresponding transport equation, (8.2). In doing so, we assume the transport of Cs obeys classical Fickian diffusion kinetics and diffusing material is continuously removed from the sphere surface. Our results suggest these assumptions are valid for the temperature range and experimental conditions tested here. Cs release during some trials showed an initially larger diffusant release rate which results in slight deviations from ideal transport behavior as evidenced by the 1290 K plot in Fig. 8.4. Initial rapid release of volatile diffusants is common in release experiments [12] but may indicate time dependence of the diffusion coefficient or multichannel transport processes. Additionally, initial rapid release may be a consequence of the pore structure of the particular graphite analyzed, where for some samples a larger “exposed” surface area may be present due to very large pores on the sample surface. Some variance is evident in the measured initial concentration profile in Fig. 8.2, which reflects the well-documented tendency of Cs to concentrate in the binder components of certain graphites [7-8,10].

It is common to perform the initial FP loading procedure for sufficient time for a macroscopically uniform distribution of FP to be achieved, as a uniform initial distribution simplifies extraction of diffusion coefficients [2,9,12-13]. It is sometimes possible to assume an initially uniform distribution *a priori* and extract diffusion coefficients from release data. The validity of this assumption may be checked by using the diffusion coefficients obtained to calculate the theoretical concentration profile that

should result based on the temperature, initial, and boundary conditions present during the loading procedure. In some experiments, it may be necessary to assume a uniform initial distribution or approximate the actual distribution by a uniform one; in the present case, such an assumption would result in an overestimate of the reported diffusion coefficient by approximately 10%.

Selected data for Cs diffusion in various graphites are presented in Fig. 8.5 for comparison with the NBG-18 data from this work.

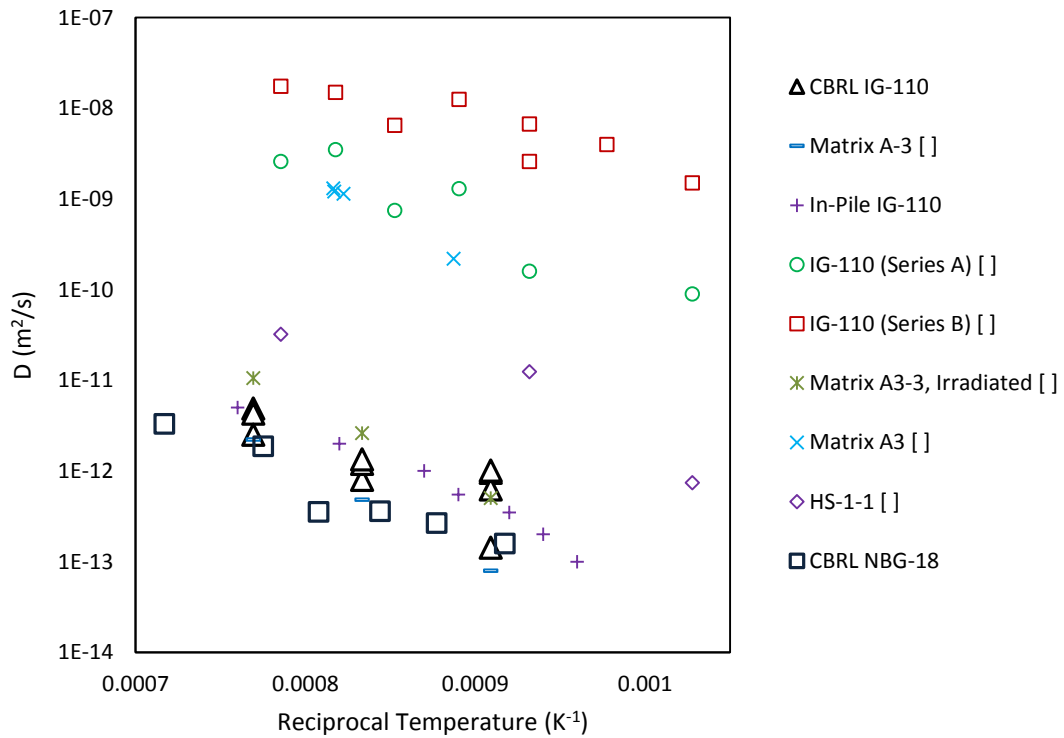


Figure 8.5: The measured diffusion coefficients from this experiment plotted versus reciprocal temperature with other values for various graphites reported in the literature.

Measured diffusion coefficients for Cs in NBG-18 appear lower than those for Cs in IG-110 graphite. This difference may be attributable to differences in pore structure or differences in the identity and concentration of impurities present in the graphites.

Diffusion of Cs in certain graphites has been shown to be dominated by surface diffusion mechanism wherein Cs migrates via transport along interior pore surfaces [6-10], as opposed to gas-phase diffusion through the bulk pore volume. This is consistent with the diffusion activation energies we have determined for IG-110 and NBG-18 graphites of 110 kJ/mol and 123 kJ/mol respectively, both of which are larger than the enthalpy of vaporization of cesium of 65 kJ/mol. Thus, transport of Cs in IG-110 and NBG-18 should occur primarily via a similar pore surface diffusion mechanism. IG-110 is a very fine-grained graphite and has a correspondingly large Brunauer-Emmett-Teller (BET) surface area in comparison to NBG-18. The larger surface area available for Cs transport in IG-110 may partially explain the larger observed diffusion coefficients in the material.

The presence of impurities in graphite has also been shown to affect diffusion coefficients of fission products in graphite. Impurities may sorb or dissolve diffusant atoms, lowering the diffusant vapor pressure and therefore lower the rate of transport [11]. Solid impurities may immobilize diffusant atoms if the activation energy for desorption from the impurity site is large. These effects have been shown to have a negligible effect on Cs diffusion in certain graphites [11]. While NBG-18 has a much

higher concentration of impurities than IG-110, it is unknown what effect this difference has on the differences observed in the current work. As the concentration of certain impurities may vary (whether the impurities are present in the graphite naturally, through production or machining processes, or those produced by fission) the present system was designed to be capable of studying multicomponent transport in graphite. Further investigation of the effects multiple components may have on the diffusion of one another will be undertaken in the future.

8.8. Conclusion

We have measured diffusion coefficients of Cs in NBG-18 graphite using the release method and ICP-MS coupled with a carbon aerosol helium gas-jet system. We have obtained:

$$D_{Cs/NBG-18} = (1.0 \times 10^{-7} \text{ m}^2/\text{s}) \exp\left(\frac{-123 \text{ kJ/mol}}{RT}\right) \quad (8.16)$$

This appears to be the first measurement of Cs diffusion coefficients in NBG-18 graphite, and therefore there are no data for direct comparison at this point. However, the results are in agreement with measurements Cs diffusion coefficients in similar graphites reported in the literature. The diffusion coefficients for Cs in NBG-18 are lower than those we have measured in IG-110, and by extrapolation may remain so up

to temperatures exceeding the loss of coolant scenario maximum attainable core temperature of the VHTR.

8.9. Acknowledgements

This research has been supported by the U.S. Department of Energy Nuclear Energy University Program (NEUP-2982). The authors express gratitude to Drs. Tushar Ghosh, Matthew Simones, and Rajesh Gutti for helpful discussion and assistance with instrumentation, and to Saint Gobain-Hexaloy and the MURR Science Instrument Shop for mechanical support.

8.10. References

- [1] C.I. Contescu, T. Guldan, P. Wang, T.D. Burchell. Effect of microstructure on air oxidation resistance of nuclear graphite. *Carbon* 50 (9) 3354-3366.
- [2] L.M. Carter, J.D. Brockman, S.K. Loyalka, J.D. Robertson. Measurement of Cs diffusion coefficients in IG-110 graphite. *J. Nuc. Materials* 460 (2015) 30-36.
- [3] L.M. Carter, J.D. Brockman, S.K. Loyalka, J.D. Robertson. Calibration of system for measurements of Cs diffusion coefficients in graphite. *JRNC* (submitted)
- [4] G. Zheng, P. Xu, K. Sridarhan, T. Allen. Characterization of structural defects in nuclear graphite IG-110 and NBG-18. *Journal of Nuclear Materials* 446 (2014) 193–199
- [5] J. Lee, T.K. Ghosh, S.K. Loyalka. Oxidation rate of nuclear-grade graphite IG-110 in the kinetic regime for VHTR air ingress accident scenarios. *J. Nuc. Materials* 446 (2014) 38-48.
- [6] E. Hoinkis, Editor. Transport of fission products in matrix and graphite. HMI-B372. Proceedings of a colloquium held at Hahn-Meitner-Institut, Berlin, 1981 (published, June

1983). These proceedings contain many papers of interest, we cite relating to the release method below.

[7] B. F. Meyers. A Review of the diffusion of selected fission product metals in polycrystalline graphite. *ibid*, p. 56.

[8] B. F. Meyers and D. W. Hill. Cesium diffusion in H-451 graphite. *ibid* p. 68.

[9] H. J. Leyers. Cesium release out of graphite matrix A3 in flowing helium. *ibid* p. 103.

[10] E. Hoinkis. The determination of diffusion coefficients of cesium and silver by the release method in as received, oxidized and neutron irradiated graphite-matrix. *ibid* p. 77.

[11] R. Forthmann. Influence of metallic traps on the diffusion of silver and caesium in graphitic matrix. *Ibid* p. 108

[12] D. R. Olander, Fundamental Aspects of Nuclear fuel Elements. Energy Research and Development Administration. 1976.

[13] A.H. Booth, A Method of Calculating Fission Gas Diffusion from UO₂ Fuel and its Application to the X-2-f Loop Test, Atomic Energy of Canada Ltd., Technical, Report AECL-496, 1957.

[14] M., Eibach , T. Beyer, K. Blaum, M. Block, K. Eberhardt, F. Herfurth, C. Geppar, J. Ketalaeer, J. Ketter, J. Kramer, A. Krieger, K. Knuth, S. Nagy, W. Narthershauser, and C. Smorra “Transport of fission products with a helium gas-jet at TRIGA-SPEC”. *Nucl. Instrum. Methods Phys. Res., Sect. A*, 613:226-231 (2010).

[15] R. B. Evans, W. Davis, A.L. Sutton. “Cesium diffusion in graphite”. ORNL-5648, Oak Ridge National Laboratory, Tennessee, US. (1980)

[16] M. P. Simones, M. L. Reinig, S.K. Loyalka, “A Mathematical Model for the Release of Noble Gas and Cs from Porous Nuclear Fuel Based on VEGA 1&2 Experiments.” *J. Nuc. Materials* 448 (2014) 217-229.

8.11. Appendix A: The infusion Profile of Cs in NBG-18

Our measurements indicated that the final infusion profile of Cs in the graphite sphere was approximately linear, and we used this linear profile to obtain the diffusion

coefficients from the release data. Theoretical considerations would indicate that the profile should have some flatness (zero gradient) at the center of the sphere. To clarify it further, we note that the solution of the infusion problem is closely related to the solution of the release problem (particularly when the initial concentration profile $C(r,0)$ is a constant). Thus for infusion, one considers the problem (we have put a tilde to distinguish it from the release problem, note that $\tilde{C}(r,t)$ is finite everywhere),

$$\frac{\partial \tilde{C}(r,t)}{\partial t} = \frac{1}{r^2} \frac{\partial}{\partial r} \left(D r^2 \frac{\partial \tilde{C}(r,t)}{\partial r} \right) \quad (8.17)$$

with boundary condition: (8.18)

$$\tilde{C}(R,t) = \tilde{C}_\infty \quad (8.19)$$

And the initial condition:

$$\tilde{C}(r,0) = 0 \quad (8.20)$$

Then we can show that,

$$\tilde{C}(r,t) = C(r,t) |_{C(r,0)=\tilde{C}_\infty} + \tilde{C}_\infty \quad (8.21)$$

And, assuming \tilde{C}_∞ is known (vapor pressure of FP at the infusion temperature), it is possible to extract the diffusion coefficient from the measurements of concentration profile (or the total mass infusion) in the infusion part of the experiments also.

We note that the infusion problem has the solution:

$$\tilde{C}(r,t) = \sum_{n=1}^{\infty} A_n \psi_n(r) \text{Exp}(-\lambda_n^2 Dt) \Big|_{C(r,0)=-\tilde{C}_{\infty}} + \tilde{C}_{\infty} \quad (8.22)$$

Where,

$$A_n = \frac{2}{R} \int_0^R r^2 C(r,0) \psi_n(r) dr = - \left(\frac{2}{R} \int_0^R r^2 \psi_n(r) dr \right) \tilde{C}_{\infty} = - \frac{2}{\lambda_n} (-1)^{n-1} \tilde{C}_{\infty} \quad (8.23)$$

Which gives

$$\tilde{C}(r,t) = \left(1 - \sum_{n=1}^{\infty} \frac{2}{\lambda_n} (-1)^{n-1} \psi_n(r) \text{Exp}(-\lambda_n^2 Dt) \right) \tilde{C}_{\infty} \quad (8.24)$$

Indicating that for a large time t , the infusion profile should be:

$$\tilde{C}(r,t) = \left(1 - \frac{2}{\lambda_1} \psi_1(r) \text{Exp}(-\lambda_1^2 Dt) \right) \tilde{C}_{\infty} = \left(1 - 2 \frac{\sin(\pi r / R)}{(\pi r / R)} \text{Exp}(-\pi^2 Dt / R^2) \right) \tilde{C}_{\infty} \quad (8.25)$$

Our computations confirm that for the case at hand the above expression is both useful and adequate (it gives results that agree with those obtained by using more terms in the series).

We have therefore fit the normalized infusion profile (temperature of 1373 K, for $t=8$ days) with the above (A.9), and we obtain approximately:

$$D = 1.90 \times 10^{-12} \text{ m}^2 / \text{s} \quad (8.26)$$

Which agrees well with the value ($D = 2.7 \times 10^{-12} \text{ m}^2 / \text{s}$) obtained from the release measurements (at 1395 K).

One can estimate \tilde{C}_∞ in several ways (using the infusion profile, the vapor pressure for Cs, or by the INAA mass measurements). Considering the INAA data, one would have:

$$\tilde{C}_\infty = \frac{m_0}{4\pi \int_0^R r^2 \left(1 - 2 \frac{\sin(\pi r / R)}{(\pi r / R)} \text{Exp}(-\pi^2 Dt / R^2) \right) dr} = \frac{m_0}{\frac{4\pi R^3}{3} \left(1 - \frac{6}{\pi^2} \text{Exp}(-\pi^2 Dt / R^2) \right)} \quad (8.27)$$

Thus, the initial profile for each sphere can be approximated by (the subscript *inf* indicates values corresponding to infusion conditions):

$$C(r, 0) = \frac{m_{0, \text{INAA}, j}}{\frac{4\pi R^3}{3} \left(1 - \frac{6}{\pi^2} \text{Exp}(-\pi^2 D_{\text{inf}} t_{\text{inf}} / R^2) \right)} \left(1 - 2 \frac{\sin(\pi r / R)}{(\pi r / R)} \text{Exp}(-\pi^2 D_{\text{inf}} t_{\text{inf}} / R^2) \right) \quad (8.28)$$

We can write this for convenience as:

$$C(r,0) = \tilde{m}_0 \left(1 - b \frac{\sin(\pi r / R)}{(\pi r / R)} \right) \quad (8.29)$$

And, calculate release rates based on this expression rather than a linear profile. In our infusion part of the experiments, however, \tilde{C}_∞ was not kept constant. It decreased with time as Cs was infused in the sphere(s), and hence we concluded that it was better to use the experimentally measured infusion profile rather than the above (the linear profile matches well with the above up to more than half way in the sphere as seen below). We have shown fits to the infusion data with Eqn. (8.25) in the Fig. 8.6 below. Future numerical analysis on the lines of Ref. [16], and comparisons with experiments, however would be of interest.

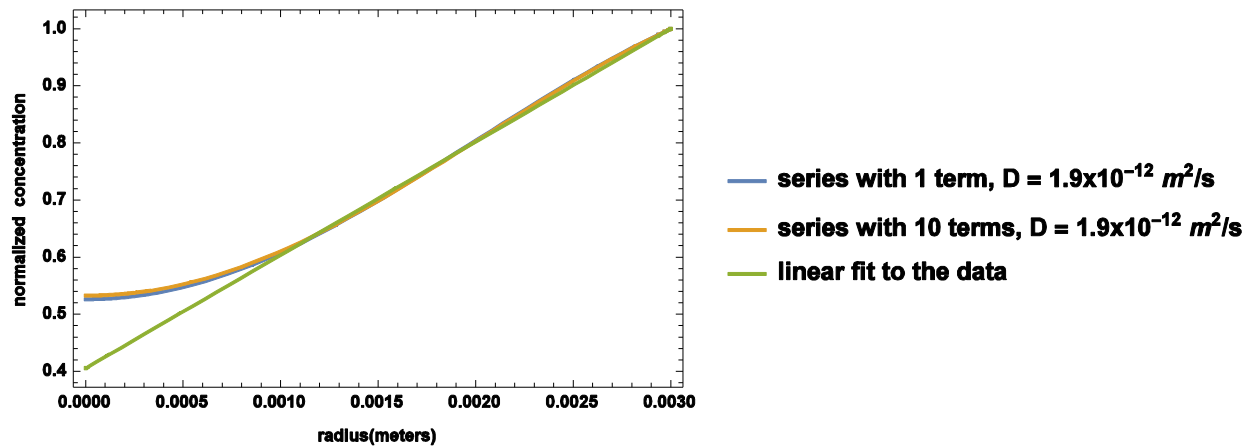


Figure 8.6: The normalized infusion profile (mass concentration vs radius), measurements and theory.

CHAPTER 9:

SILVER AND STRONTIUM INFUSION EXPERIMENTS

9.1. Overview

Multiple approaches were attempted in an effort to infuse IG-110 graphite spheres with strontium and silver for subsequent diffusion measurements.

9.2. Gas phase infusion

Following the success of loading IG-110 spheres with Cs by heating CsNO₃ salt to decomposition within sealed quartz tubes via the procedure described previously, the procedure was modified to attempt silver or strontium infusion by placing AgNO₃ or Sr(NO₃)₂ salts into quartz vials with $R=1/16''$ IG-110 spheres. The sealed vials were heated to 1100°C for four days.

The the Ag/IG-110 samples were irradiated along with 10 µg Ag standards for 30 seconds at $6.5 \times 10^{13} \text{ n}_{\text{th}}/\text{cm}^2/\text{s}$ to determine the mass of Ag present in the spheres via INAA. No detectable photopeaks were observed in the 632.9 keV or 657.8 keV regions after a 1 min decay, indicating the infusion was unsuccessful. The minimum detectable amount of silver in these measurements is approximately 0.1 ng.

The Sr/IG-110 samples and 10 µg Sr standards were irradiated for two minutes at $6.5 \times 10^{13} \text{ n}_{\text{th}}/\text{cm}^2/\text{s}$ to determine Sr mass within the spheres. The expected 388.5 keV photopeak from the decay of Sr-87m was absent, indicating no appreciable Sr loading.

The failure of Sr or Ag to infuse into the IG-110 spheres may be due to one or a combination of factors. It is likely the vapor pressure of silver metal at 1100°C is sufficient to induce appreciable gas phase diffusion into the graphite. The decomposition of strontium nitrate under the conditions of the procedure here likely produces strontium oxide, which also has a very low vapor pressure under the present temperature condition. In this particular graphite, the diffusion coefficients for Sr and Ag may be much smaller than expected based on results from other graphites reported in the literature. Additionally, one has to consider the equilibrium that exists between the Ag or Sr metals in the gas phase and adsorbed states. At low concentration, adsorption of many species to graphite is well-described by Henry's law:

$$C = k_H P_{\text{vap}} \tag{9.1}$$

Where:

C = Concentration of adsorbed species $\left(\frac{\text{mol}}{\text{L}}\right)$

k_H = Henry's law constant $\left(\frac{\text{mol}}{\text{L} \cdot \text{atm}}\right)$

P_{vap} = Vapor pressure (atm)

Henry's law constants have yet to be determined for Ag and Sr in IG-110 graphite, and therefore it is possible that equilibrium does not favor the adsorbed phase under the conditions used here.

9.3. Powdered graphite infusion

The problem of low vapor pressure of silver and strontium species was addressed by attempting diffusion from a Ag or Sr laden graphite powder source, which avoids the requirement of the graphite to sorb material from the gas phase. In this case, Ag and Sr were expected to be transported into the IG-110 spheres via a bulk diffusion process.

9.3.1. Quartz container

The first attempts used quartz tubing used previously for gas-phase infusion experiments.

5 mL of 1.00 mg/mL silver nitrate in 2% HNO₃ purchased from High Purity Standards was pipetted onto 5 g of powdered graphite purchased from Fisher Scientific. The resulting slurry was well stirred, and excess liquid was allowed to evaporate in air. The dried powder was placed in a vacuum oven at approximately 100°C for five days to drive off much of the remaining moisture. 1 g of the powder and five 0.125" diameter IG-110 spheres were added to a quartz vial and 100 mtorr vacuum was applied. The closed end of the tube containing the sample was heated to 550°C for 5 min to allow the nitrate to decompose and to off-gas as much adsorbed water as possible. The closed end of the tube was then removed from the furnace and sealed off with a methane/oxygen torch. Finally, the sealed sample was heated to 1100°C for 6 days. The tube had noticeably expanded during the annealing procedure.



Figure 9.1: Metal nitrate decomposition under vacuum in quartz tubing



Figure 9.2: Sealed quartz tube containing 1 g graphite powder and five R=1/16" IG-110 spheres before annealing procedure



Figure 9.3: Sealed quartz tube after annealing procedure

Each of the spheres was irradiated for 30 s at $6.5 \times 10^{13} \text{ n}_{\text{th}}/\text{cm}^2/\text{s}$ along with a 10 μg Ag standard. No detectable photopeaks were observed in the 632.9 keV or 657.8 keV regions after a 1 min decay, indicating the infusion was unsuccessful.

It was desirable to know whether silver had escaped the quartz container, or simply had not diffused into the spheres. Therefore 25 mg of the silver laden graphite powder used in the Ag infusion (equilibrated with the IG-110 spheres at 1100°C) was analyzed for remaining Ag content by INAA, and compared with the silver content of 25 mg of the silver laden powder not used in the Ag infusion. It was found that approximately 40% of the initial Ag mass remained in the powder, suggesting that some Ag had escaped through a leak in the tube, or had sorbed onto or diffused through the quartz tubing.

9.3.2. Molybdenum container

Higher temperatures were desirable for Sr and Ag loading due to the failure of these metals to appreciably diffuse into IG-110 at 1100°C. It was found that quartz tubing becomes plastic at the 1400°C temperature condition we desired, and therefore molybdenum was considered as a material for containment of the Sr/Ag/powdered graphite/IG-110 sphere mixture due to its high melting point and previous use in the literature. An inert atmosphere furnace was required for this experiment because Mo oxidizes in air at high temperatures to form volatile MoO_2 .

A screw-top molybdenum container with $\frac{3}{4}$ " diameter x $\frac{3}{4}$ " height cylindrical interior dimensions was machined from stock by the MURR Science Instrument shop.

Strontium laden graphite powder was prepared using the same procedure outlined in 9.3.1, and placed into the bore of the container and well-packed along with five R=1/16" IG-110 spheres.



Figure 9.4: Unused molybdenum container



Figure 9.5: Molybdenum container filled with Sr laden graphite powder and IG-110 spheres



Figure 9.6: Molybdenum container after annealing attempt, with dark purple MoO₂ oxidation layer visible

The container was placed into a 1400°C inert atmosphere furnace operating with argon flow of 10 mL/min. The molybdenum container began to oxidize within minutes, and the experiment had to be stopped to avoid damage and MoO₂ contamination of the laboratory.

9.3.3. Graphite container

A final attempt to load IG-110 spheres with Ag, Sr, and a mixture of Ag, Sr, and Cs was attempted by using metal laden graphite powder in contact with IG-110 spheres in cement-sealed graphite containers, which would avoid the problem of molybdenum oxidation experienced previously. Three graphite canisters were packed with five IG-110 spheres and metal laden graphite powder, and sealed using Aremco 890 cement. The canisters were annealed at 1400°C in an evacuated graphite element furnace for five days at the University of Missouri-Rolla high temperature materials facility.



Figure 9.7: Annealed graphite canisters

The cement seals were found to have failed during the annealing procedure, allowing the volatile metals to escape the containers. No appreciable amounts of Ag or Cs were observed in any of the spheres via INAA. The spheres contained approximately 340 ng/sphere of Sr following the procedure despite the seal failure. Additionally, the furnace introduced small amounts of contamination of several materials into the spheres, including iodine, manganese, bromine, zinc, and europium. A diffusion experiment at 1000°C was conducted with one of the spheres in an effort to determine diffusion coefficients for Sr and contaminant materials present. No diffusion was seen, which for the metals is likely attributable to a combination of small diffusion coefficients at this temperature and small masses present; for iodine and bromine, although diffusion coefficients are expected to be high, the small masses present likely generate release rates below the limit of detection of the setup given the instrumentation parameters used. Here, the failure of Ag and Cs to load into the spheres is expected to be due to seal failure.

Table 9.1: Graphite canister annealed IG-110 sphere elemental component analysis (2 min irradiation at 5×10^{13} n_{th}/cm²/s, 5 hr count).

Nuclide	γ-line (keV)	Counts	Total element mass (ng)
Sr-87m	388	6748	340
I-128	442.9	12832	22
Br-80	617	1487	Not obtained
Mn-56	846	11128	Not obtained

Zn-65	1115	946	Not obtained
Eu-152m	121	13669	Not obtained

CHAPTER 10:

MEASUREMENT OF IODINE TRANSPORT IN IG-110 GRAPHITE FOR HTGR/VHTR

10.1. Highlights

- A method for real time analysis of fission product transport of iodine by ICP-MS was applied to nuclear-grade graphite IG-110
- The design simulates HTGR conditions
- Diffusion coefficients for iodine in IG-110 were obtained

10.2. Abstract

Graphite functions as a structural material and as a barrier to fission product release in the pebble bed and prismatic HTGR/VHTR designs, and elucidation of transport parameters for fission products in reactor-grade graphite is thus required for reactor source terms calculations. We have conducted transport rate measurements of iodine in IG-110 graphite, wherein we impregnated spheres of IG-110 with iodine and measured the release rates in the temperature range of 873-1293 K. We have characterized iodine transport using an effective diffusion coefficient and, compared our results with those available in the literature.

10.3. Introduction

Release of iodine radioisotopes, particularly I-131, is of concern during both normal operation and accident scenarios involving HTGRs. In predicting iodine release from such reactors, one must consider complex mechanisms of interaction (e.g. diffusion, sorption, chemistry) of iodine with the fuel, core materials, and materials comprising the reactor cooling circuit. Nuclear graphite grade IG-110 comprises multiple permanent and replaceable core structures in the High-Temperature Test Reactor (HTTR) in Japan, and is currently a candidate graphite for use in other contemporary HTGR designs. The present work focuses on analysis of iodine transport in IG-110 by diffusion. Historically, computer codes (e.g. FRESCO) have been designed to estimate fission product release rates from HTGRs based on an effective diffusion coefficient [1], and therefore we apply the classical Fickian diffusion model to iodine transport in IG-110.

10.4. Theory

The diffusion coefficient characterizes classical diffusive transport of a particular substance (fission product, or fission product surrogate) in a particular medium (graphite). The concentration of FP in the sample is given by Fick's law:

$$\frac{\partial C}{\partial t} = D\nabla^2 C \tag{10.1}$$

where t is the time, C is the concentration (kg/m^3) of FP as function of position and time, D is the diffusion coefficient, and ∇ is the spatial gradient operator.

Diffusion coefficients for FP's in graphite are commonly determined experimentally using the release method [2-7], wherein spheres of graphite material are uniformly infused with a fission product surrogate(s), and release of the FP in time is monitored isothermally in a separate experiment. In practice, it typical to measure the release rate or fractional release; the latter defined as the total cumulative mass release of FP divided by the total initial mass of FP present within the sample. For a spherically symmetric geometry, we have:

$$\dot{m}(t) = 8\pi RDC_0 \sum_{n=1}^{\infty} e^{-\left(\frac{n\pi}{\ell}\right)^2 Dt} \quad (10.2)$$

And,

$$F(t) = 1 - \frac{6}{\pi^2} \sum_{n=1}^{\infty} \frac{1}{n^2} e^{-\left(\frac{n\pi}{R}\right)^2 Dt} \quad (10.3)$$

The diffusion coefficient may be obtained by fitting solutions of eqn's (10.2) or (10.3) to the experimental data.

10.5. Experimental

10.5.1. Instrumentation

A specialized SiC diffusion cell coupled to a Nexion 300X QD-ICP-MS calibrated via INAA was used for quantification of the fractional release. Transport of FP from the

sample to the ICP-MS was facilitated using an aerosol laden He jet system. A complete description of the instrumentation and INAA calibration procedures is given in Ref. [1-3].

10.5.2. Materials and Methods

10.5.2.1. Sample preparation

Spheres with radius $R=0.16$ cm were milled from as-received IG-110 stock material by the MURR Science Instrument shop. The spheres were added to a cylindrical quartz vial along with approximately 200 μg each of solid CsI and RbNO_3 (as-received from Fisher Scientific). The vial was sealed under 100 mtorr vacuum with a flame sealing torch. The sample was annealed at 1100°C and maintained for 4 days in an effort to infuse iodine, cesium, and rubidium within the spheres. The spheres were further machined diameter 0.3 cm using SiC sandpaper. Machining dust was removed with compressed air.

10.5.2.2. Initial iodine content analysis

Instrumental neutron activation analysis was conducted to determine the masses of Cs, I, and Rb present within the spheres following the annealing procedure. Each sphere was irradiated in the row 2 pneumatic tube irradiation position of the MURR facility for 10 seconds at a thermal neutron flux of 5.0×10^{13} n/cm²/s to produce trace Cs-134m, I-128, and Rb-88 via n, γ reactions, respectively.

Cs and Rb standards were prepared by drying aliquots of CsNO_3 and RbNO_3 (2% HNO_3 ICP-MS standards as received from High Purity Standards) onto stacked filter

paper in polyethylene vials. Iodine standards were prepared by drying aliquots of iodide present in 0.01% KOH (as received from High Purity Standards) onto stacked filter paper in polyethylene vials. The samples and standards were irradiated simultaneously. The samples were counted 5 cm from the face of a 20% relative efficiency HPGe detector. Detector dead time was managed using the loss free counting technique.

Only iodine was found to have diffused into the spheres in appreciable amounts ($\approx 1 \mu\text{g/sphere}$). The minimal detectable amount of Cs and Rb in the measurements was 0.1 ng and 1 ng, respectively.

10.5.2.3. Diffusion measurements

The ICP-MS was set up to measure release of I, Cs, and Rb in time under isothermal temperature conditions in the range of 873K to 1293K. Release was measured for a period of approximately five hours at all temperatures. The I, Cs, and Rb signals were monitored for approximately one hour before a sphere is introduced into the cell to allow for correction due to detector background. Cs and Rb release was not observed, which was expected considering the results of the INAA measurement in 10.2.2.

10.5.2.4. Final iodine content analysis

Following ICP-MS release measurements, the iodine content of each sphere was determined again using standard comparator INAA as described in Section 10.2.2. The iodine mass difference before and after release measurements was used to determine

the ICP-MS calibration factor, which scales the ICP-MS count rate to units of grams I/s, or cumulative release rate to grams Cs, respectively. The calibration method and related calculations are described in detail in Ref's [2-4].

10.6. Results

The masses of iodine present in each sphere before and after release measurements are given in Table 10.1.

Table 10.1: IG-110 sphere iodine content and effective diffusion coefficients calculated from Eqn. 10.3.

Temperature (K)	$m_{i,initial}$ (μg)	$m_{i,final}$ (μg)	D_{eff} (m^2/s)
873	1.71	0.104	5.7×10^{-10}
983	0.790	0.0265	5.6×10^{-10}
1108	1.17	0.0730	3.6×10^{-10}
1193	1.41	0.0644	1.6×10^{-10}
1293	0.819	0.0837	8.3×10^{-11}

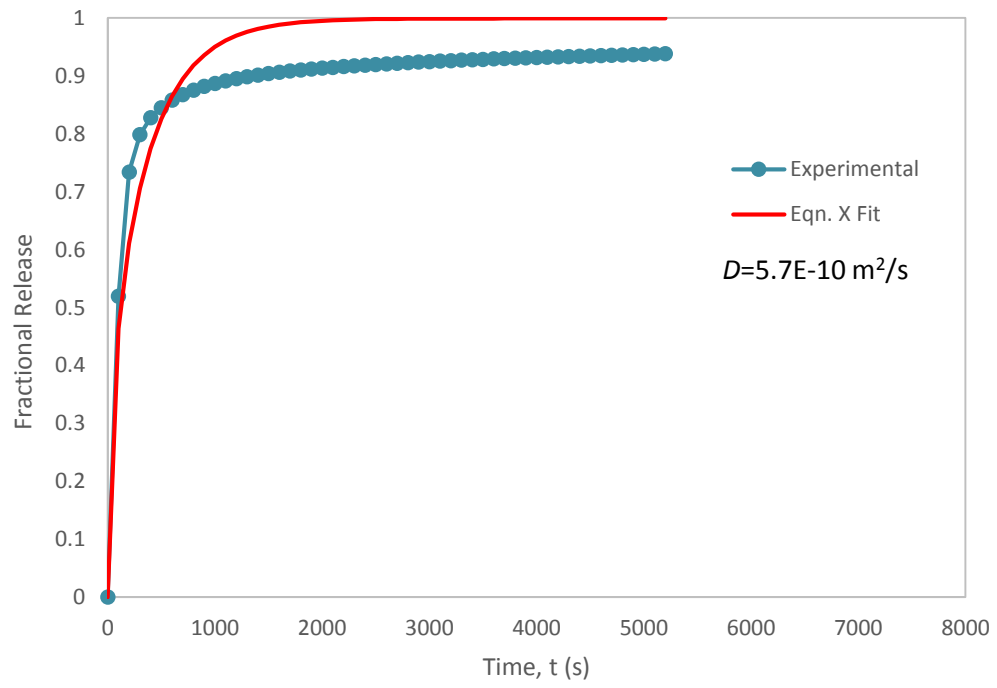


Figure 10.1: I/IG-110, R=0.15 cm, T=873 K

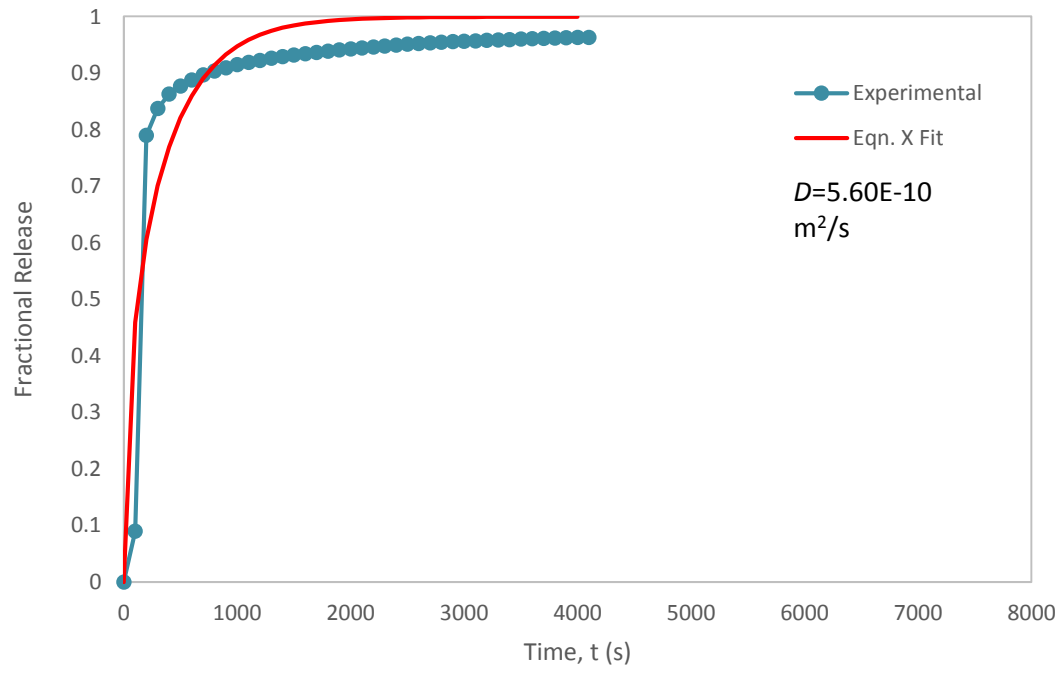


Figure 10.2: I/IG-110, R=0.15 cm, T=983 K

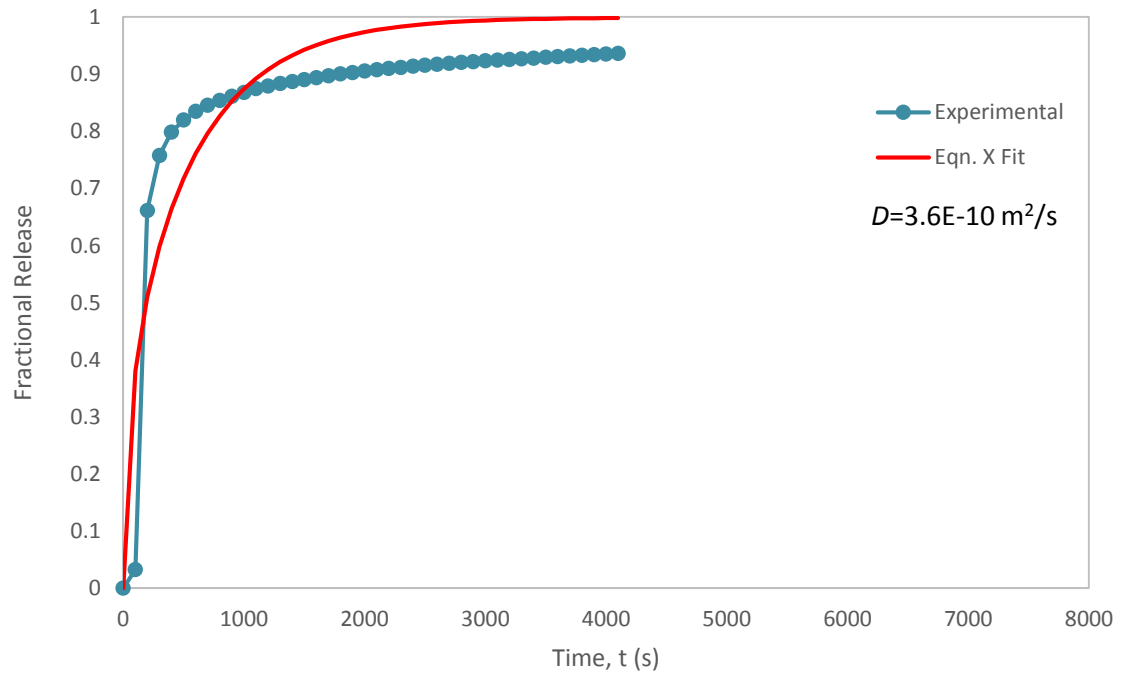


Figure 10.3: I/IG-110, R=0.15 cm, T=1108 K

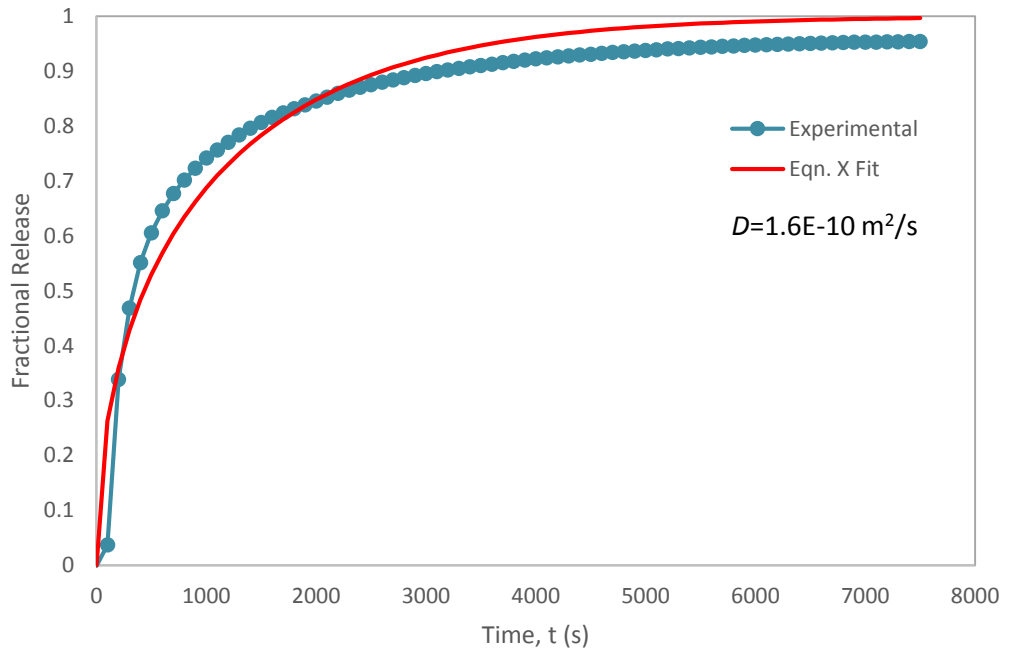


Figure 10.4: I/IG-110, $R=0.15 \text{ cm}$, $T=1193 \text{ K}$

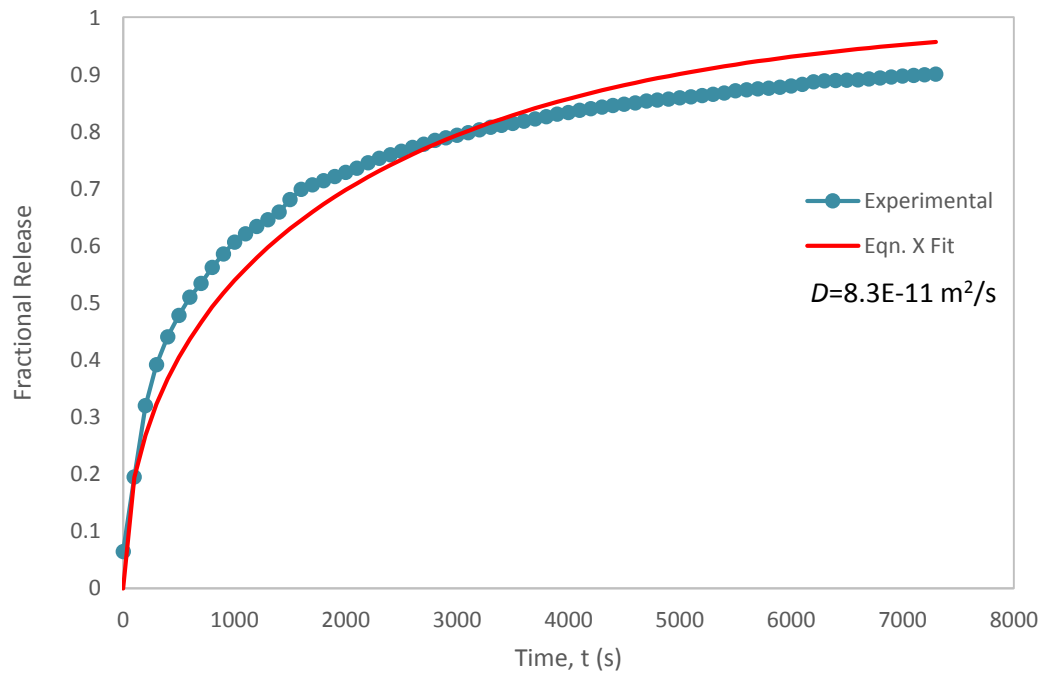


Figure 10.5: I/IG-110, R=0.15 cm, T=1293 K

As a function of temperature, the effective diffusion coefficient is reasonably well described by a linear function, and thus we may report:

$$D_{I,IG-110} = (-1 \times 10^{-12})T + (2 \times 10^{-9}) \quad (3)$$

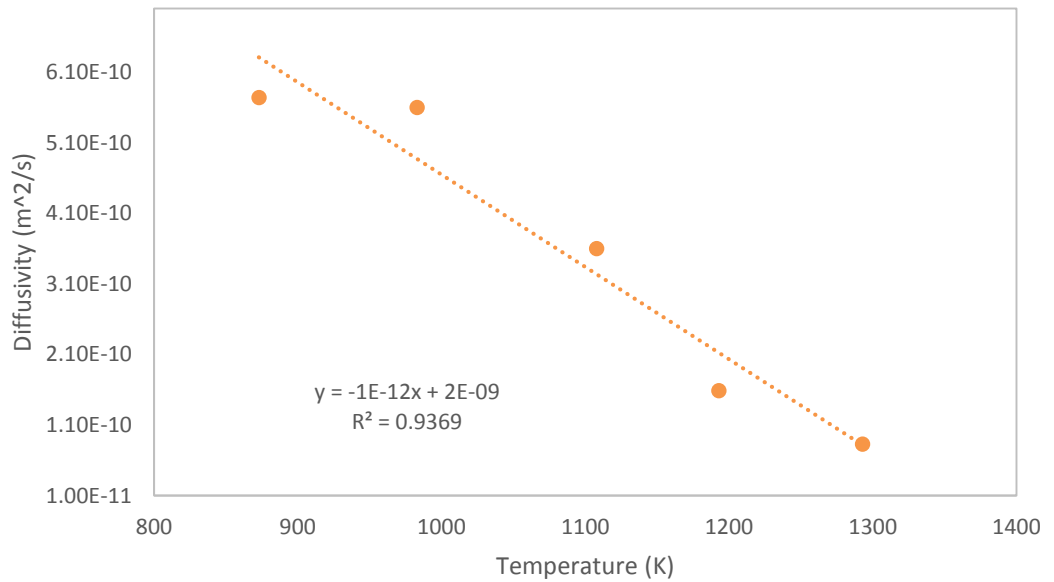


Figure 10.6: Variation of D as function of T

10.7. Discussion

It is clear that at temperatures appreciably below 1200 K, transport of iodine in IG-110 is not well-described by classical transport theory. Further, the initial release

rate as well as the calculated effective diffusion coefficient, was observed to decrease with increasing temperature; the opposite of what would be expected based purely on classical diffusion theory. These results suggest that at higher temperatures, iodine is chemically converted to a more strongly bound form. It is well known that the degree of dissociation of molecular iodine increases as a function of temperature, according to the reaction:



where k_f and k_r denote rate constants for the forward (1st order) and reverse (2nd order) reactions, respectively. We expect that I_2 would be weakly bound (physisorbed) to the graphite, and because I is a reactive radical species, would be in a strongly bound state when sorbed to the graphite.

We consider simultaneous diffusion of both iodine species, with reaction (10.4).

The rate of change of concentration of molecular iodine may be given (in the one-dimensional case) as:

$$\frac{d[I_2]}{dt} = D_{I_2} \frac{d^2[I_2]}{dx^2} - k_f[I_2] + \frac{1}{2}k_r[I']^2 \quad (10.5)$$

The first term in (10.4) is the usual diffusive accumulation term, the second term represents the first-order sink for the dissociation of molecular iodine in (10.4), and the last term is the source term for generation of molecular iodine given by the reverse

reaction in (10.4), which is assumed to be second order. Likewise, transport of the radical iodine species may be given by:

$$\frac{d[I\cdot]}{dt} = D_I \frac{d^2[I\cdot]}{dx^2} - k_r [I\cdot]^2 + 2k_f [I_2] \quad (10.6)$$

If the total iodine concentration is defined as:

$$[I_{tot}] = [I\cdot] + 2[I_2] \quad (10.7)$$

And,

$$\frac{d[I_{tot}]}{dt} = \frac{d[I\cdot]}{dt} + 2 \frac{d[I_2]}{dt} \quad (10.8)$$

Then by substitution of (10.5) and (10.6) into (10.8) we may write:

$$\frac{d[I_{tot}]}{dt} = D_{I_2} \frac{d^2[I_2]}{dx^2} + D_I \frac{d^2[I\cdot]}{dx^2} \quad (10.9)$$

If one defines iodine transport in terms of an overall effective diffusion coefficient,

$$\frac{d[I_{tot}]}{dt} = D_{I_2} \frac{d^2[I_2]}{dx^2} + D_I \frac{d^2[I\cdot]}{dx^2} \approx D_{eff} \frac{d^2[I_{tot}]}{dx^2} \quad (10.10)$$

In the case that iodine is present largely as the radical species, then

$$[I\cdot] \gg [I_2] \quad (10.11)$$

And thus:

$$D_{eff} \rightarrow D_I \quad (10.12)$$

Because $D_{I_2} \gg D_I$ due to the radical species being strongly bound and the molecular species being weakly bound, (10.12) is consistent with the observed decrease

of the effective diffusion coefficient with increasing temperature, in a certain temperature region.

At very high temperature, when only the radical species is present, the diffusion coefficient should increase. At very low temperature, when only the molecular species is present, the diffusion coefficient should decrease. The particular temperature range tested, is believed to be a region of temperature in which the rate of change of the equilibrium constant (i.e. $K_{eq}=k_f/k_r$) is comparable to the rate of change of the diffusion coefficient of the radical species. The following behavior of D as a function of T would perhaps be expected over a broader range of temperature, which is implied by the curvature of the data in Figure 10.6.

At all temperatures, small residual amounts (~5%) of I remained in the graphite even at long times. We expect this represents iodine that is very strongly bound to impurity sites in the graphite.

10.8. Conclusion

We have measured diffusion coefficients of iodine in IG-110 graphite using ICP-MS coupled to a carbon aerosol helium gas-jet system.

Other data for diffusion of iodine in IG-110 are non-existent as of yet. However, the results are in agreement with adsorption characteristics of iodine on graphites reported in the literature.

10.9. References

- [1] A Review of Radionuclide Release from HTGR Cores During Normal Operation. www.ngnpalliance.org/index.php/resources/download/czo0NDoiL2ItYWdlcy9nZW5lcmFsX2ZpbGVzLzAwMDAwMDAwMDAwMTAwOTM4Mi5QREYiOw__ A Review of Radionuclide Release From HTGR Cores During Normal Operation
- [2] L.M. Carter, J.D. Brockman, S.K. Loyalka, J.D. Robertson. Measurement of Cs diffusion coefficients in IG-110 graphite. *J. Nuc. Materials* 460 (2015) 30-36.
- [3] L.M. Carter, J.D. Brockman, S.K. Loyalka, J.D. Robertson. Calibration of system for measurements of Cs diffusion coefficients in graphite. *JRNC* (submitted)
- [4] L.M. Carter, J.D. Brockman, S.K. Loyalka, J.D. Robertson. Measurement of Cs diffusion coefficients in NBG-18 graphite for VHTRs. *J. Nuc. Materials* (in press).
- [5] Leyers, H. J. "Cesium Release out of Matrix A3 in Flowing Helium". E. Hoinkis. *Transport of Fission Products in Matrix and Graphite: Proceedings of a Colloquium Held at the Hahn-Meitner Institut Berlin from 9-11 November 1981*.
- [6] D. R. Olander, *Fundamental Aspects of Nuclear fuel Elements*. Energy Research and Development Administration. 1976.
- [7] Booth, A. H. *A Method of Calculating Fission Gas Diffusion from UO₂ Fuel and its Application to the X-2-F Loop Test*. 1957.

CHAPTER 11:

CONCLUSIONS AND FUTURE WORK

Based on the success of the diffusion analyses of Cs in IG-110 and NBG-18 graphites, and I in IG-110 graphite, it can be concluded that the present setup is an effective method for determination of diffusion coefficients of multiple fission products in graphite. Many other candidate graphites for the HTGR/VHTR exist in addition to IG-110 and NBG-18, and similar fission product diffusion measurements should be conducted with these graphites in the future. Experiments to infuse Sr, Ag, Te, and other surrogate fission products into graphite samples should be conducted in order to further investigate the effects of multiple diffusing substances on one another.

Of additional interest is the capability of the present system to measure release rates of fission products from a designed-to-fail TRISO fuel. Under normal reactor conditions, the intact SiC shell of the TRISO particle retains almost all fission products, and therefore a primary practical FP release mechanism is failed, broken, or defective SiC barrier layers in the TRISO fuel. The designed-to-fail fuel is essentially TRISO fuel manufactured without the SiC barrier layer for laboratory simulations and analyses of SiC failure. In particular, we have considered whether a sufficient quantity of certain fission products can be generated by irradiation of a single designed-to-fail TRISO fuel pellet, from which diffusion rates could be measured using the current system. The

possibility for this type of measurement would be primarily determined by the instrument detection limit, neutron fluence during irradiation, and diffusion coefficients for FPs in the TRISO buffer and PyC layers. We have estimated the detection limit for Cs at 10 pg/s by determining what release rate of Cs would generate a signal 5x the Cs background.

As an example if one assumes the diffusion coefficient for Cs-137 in the buffer and PyC layers is similar to that of Cs in IG-110 (we shall take $T=900^{\circ}\text{C}$, $D=1.3\times 10^{-8}$ cm^2/s), that the dominant resistance to diffusion is in the barrier layers (as opposed to the fuel kernel), that the concentration of Cs at the kernel/buffer interface is approximately equal to the average Cs mass in the kernel divided by the kernel volume, and using a 10% enriched UO_2 kernel diameter of 0.05 cm with barrier thickness of 0.013 cm, one can calculate the expected release rate given initial irradiation parameters. Assuming a 240 hr irradiation at a thermal flux of 1×10^{14} $n_{\text{th}}/\text{cm}^2\cdot\text{s}$ and resonance flux of 3×10^{12} $n_r/\text{cm}^2\cdot\text{s}$, $\sigma_{\text{th}}=584$ b and $\sigma_r=280$ b, and 6% cumulative fission yield, the resulting Cs-137 activity can be calculated as 8 uCi. This corresponds to a mass of approximately 7×10^{-10} g, and given the kernel dimensions, $[\text{Cs-137}]=1\times 10^{-5}$ g/cm^3 . Assuming pseudo steady state conditions and Fick's first law, the concentration gradient would be approximately $[\text{Cs-137}]$ divided by barrier thickness. The gradient is therefore equal to 8×10^{-4} g/cm^4 , and the pseudo steady state release rate can be calculated by multiplication of the gradient by the diffusion coefficient and surface area, which is approximately 1 ng/s.

By comparison with the estimated detection limit, one can conclude the current setup is capable of this measurement, at least for Cs-137. Detection limits for other elements may be different and largely depend on transport efficiency with the aerosol, ionization efficiency in the plasma, instrument background and interfering species. Several steps may be readily taken to improve the measurement sensitivity. These steps could include replacement of the standard spray chamber/nebulizer with a desolvating nebulizer, and increasing the aerosol mass flow rate by increasing the spark generation frequency or by concentrating it using a virtual impactor. As an alternative to an ICP-MS measurement, one could also consider a collimated γ -spectrometric measurement of the present activity as a function of time, similar to Leyers' technique described previously. Coupling the two methods is certainly possible as well.

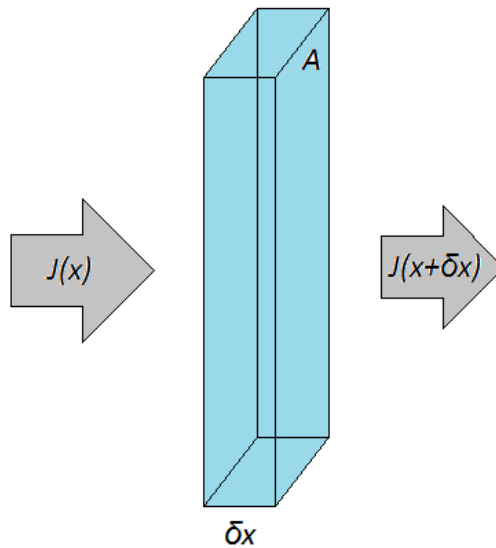
CHAPTER 12:

APPENDICES

12.1. Derivation of Commonly Used Equations

12.1.1. Diffusion Equation (Fick's second law)

We wish to determine the rate of accumulation (change in concentration) in a slab of width δx . We consider the following:



The rate of change of concentration C in the slab is:

$$\frac{\partial C}{\partial t} = \frac{\text{rate in} - \text{rate out}}{V} = \frac{A \cdot J(x) - A \cdot J(x + \delta x)}{A \cdot \delta x} \quad (12.1)$$

If $J(x+\delta x)$ is expanded about x using a Taylor series, where the Taylor series of $f(y)$ about $y=a$ is defined in compact sigma notation as:

$$\sum_{n=0}^{\infty} \frac{f^n(a)}{n!} (y - a)^n \quad (12.2)$$

One obtains for $J(x+\delta x)$:

$$J(x + \delta x) = \frac{J(x)}{0!} (\delta x)^0 + \frac{\partial J(x)}{1!} (\delta x)^1 + \dots \quad (12.3)$$

And the additional terms ... may be neglected. Substituting 12.3 into 12.1 yields:

$$\frac{\partial C}{\partial t} = - \frac{\partial J(x)}{\partial x} \quad (12.4)$$

And because $J(x)$ is given by Fick's first law as:

$$J(x) = -D \frac{\partial C}{\partial x} \quad (12.5)$$

One immediately obtains Fick's second law:

$$\frac{\partial C}{\partial t} = D \frac{\partial^2 C}{\partial x^2} \quad (12.6)$$

In three dimensions, this becomes:

$$\frac{\partial C}{\partial t} = D \nabla^2 C \quad (12.7)$$

12.1.2. Spherical Release Series Solutions

Due to the usefulness of the spherical release configuration for determination of diffusion coefficients in the present work, a derivation of equations presented in Section 2.4.2. Transforming (12.7) into spherical coordinates, and assuming spherical symmetry, yields:

$$\frac{\partial C(r,t)}{\partial t} = \frac{1}{r^2} \frac{\partial}{\partial r} \left(D r^2 \frac{\partial C(r,t)}{\partial r} \right) \quad (12.8)$$

And we consider boundary and initial conditions (as in 2.4.2):

$$C(r, 0) = C_0$$

$$C(0, t) = \text{finite}$$

$$C(R, t) = 0$$

It is generally only possible to obtain non-trivial solutions of PDE's of this form using standard methods (non-numerical) if the boundary conditions are homogeneous, i.e. zero. Therefore we begin by implementing a change of variables, which reduces the problem to a 1D slab geometry and homogenizes the boundary conditions. Noting that the offending BC is at the sphere center $r=0$, if one makes the clever substitution:

$$\gamma(r, t) = r \cdot C(r, t) \tag{12.9}$$

The BC at the center will become zero because $r=0$, and the BC at the surface will become zero because $C(R,t)=0$.

From 12.9 one can write:

$$C(r, t) = \frac{\gamma(r, t)}{r} \tag{12.10}$$

And substitution of 12.10 into 12.8 yields:

$$\frac{\partial \left(\frac{\gamma(r, t)}{r} \right)}{\partial t} = \frac{1}{r^2} \frac{\partial}{\partial r} \left(D r^2 \frac{\partial \left(\frac{\gamma(r, t)}{r} \right)}{\partial r} \right) \tag{12.11}$$

Using the product rule:

$$\frac{1}{r} \frac{\partial \gamma(r, t)}{\partial t} = \frac{1}{r^2} \left[\left(D \frac{\partial \gamma(r, t)}{\partial r} + D r \frac{\partial^2 \gamma(r, t)}{\partial r^2} \right) - D \frac{\partial \gamma(r, t)}{\partial r} \right] \tag{12.12}$$

And therefore:

$$\frac{\partial \gamma(r, t)}{\partial t} = D \frac{\partial^2 \gamma(r, t)}{\partial r^2} \tag{12.13}$$

With IC and BC's:

$$\gamma(r, 0) = r \cdot C(r, 0) = rC_0$$

$$\gamma(0, t) = 0 \cdot \text{finite} = 0$$

$$\gamma(R, t) = R \cdot 0 = 0$$

12.13 may now be solved using separation of variables (which we see later yields series solutions very useful for long times) or by Laplace's method (which yields simple analytical solutions very useful for short times) which is treated in the proceeding section.

To use the technique of separation of variables, we assume the original function $\gamma(r, t)$ is a product of two independent functions; a spatially dependent function $f(r)$, and a time dependent function $g(t)$. If this assumption is false, we will find out very quickly.

If true, we may proceed with the solution. We assume specifically:

$$\gamma(r, t) = f(r) \cdot g(t) \tag{12.14}$$

And, substituting 12.14 into 12.13:

$$\frac{\partial[f(r) \cdot g(t)]}{\partial t} = D \frac{\partial^2[f(r) \cdot g(t)]}{\partial r^2} \tag{12.15}$$

Then, because $f(r)$ is independent of t and $g(t)$ is independent of r :

$$f(r) \frac{\partial g(t)}{\partial t} = D \cdot g(t) \frac{\partial^2 f(r)}{\partial r^2} \tag{12.16}$$

Rearranging, we obtain:

$$\frac{1}{D \cdot g(t)} \frac{\partial g(t)}{\partial t} = \frac{1}{f(r)} \frac{\partial^2 f(r)}{\partial r^2} \tag{12.17}$$

And thus we find that 12.13 separates into two functions, with the left depending only on time, and the right depending only on spatial coordinate. We may replace the partial differential notation with the total differential.

Now we note that two equivalent functions of different variables must be equal to the same constant. Here, for convenience, we choose the constant to be $-\lambda^2$.

Therefore we have:

$$\frac{1}{D \cdot g(t)} \frac{dg(t)}{dt} = -\lambda^2 \quad (12.18)$$

And,

$$\frac{1}{f(r)} \frac{d^2 f(r)}{dr^2} = -\lambda^2 \quad (12.19)$$

We solve the spatially dependent eqn. 12.19 first, as it fixes the values for λ .

Rearranging, we have:

$$\frac{d^2 f(r)}{dr^2} + \lambda^2 f(r) = 0 \quad (12.20)$$

And we may form the characteristic equation of 12.20, viz.:

$$a^2 + \lambda^2 = 0 \quad (12.21)$$

The solution of the characteristic equation is:

$$a = \pm \lambda i \quad (12.22)$$

And thus, the solution of 12.19 may be written as:

$$f(r) = c_1 e^{i\lambda r} + c_2 e^{-i\lambda r} \quad (12.23)$$

12.23 may be written as a sum of sines and cosines using Euler's famous formula, and taking a linear combination to eliminate the imaginary component, we may write the general solution as:

$$f(r) = c_3 \sin(\lambda r) + c_4 \cos(\lambda r) \quad (12.24)$$

The coefficients c_3 and c_4 are determined from the boundary conditions of 12.13.

Because $\gamma(0,t)=0$, it must be the case that $f(0)=0$, and therefore:

$$f(0) = 0 = c_3 \sin(\lambda \cdot 0) + c_4 \cos(\lambda \cdot 0) \quad (12.25)$$

So,

$$c_4 = 0 \quad (12.26)$$

Because $\gamma(R,t)=0$, it must be the case that $f(R)=0$, and therefore:

$$f(R) = 0 = c_3 \sin(\lambda R) \quad (12.27)$$

Here, there are two possibilities: $c_3=0$ gives a trivial solution, so it must be that $\sin(\lambda R)=0$, and therefore λR must be a multiple of π . Thus,

$$\lambda = \frac{n\pi}{R} \quad (12.28)$$

And the solution of 12.13 is:

$$f(r) = c_3 \sin\left(\frac{n\pi r}{R}\right), n = 1, 2, 3, \dots \quad (12.29)$$

We now return to 12.18 and solve. Rearranging 12.18, we have:

$$\frac{1}{g(t)} dg(t) = -\lambda^2 D dt \quad (12.30)$$

Integrating both sides, we have:

$$\ln[g(t)] = -\lambda^2 D t + c_5 \quad (12.31)$$

And thus:

$$g(t) = c_6 e^{-\lambda^2 D t} \quad (12.32)$$

And because $\lambda = n\pi/R$, we have:

$$g(t) = c_6 e^{-\left(\frac{n\pi}{R}\right)^2 D t}, n = 1, 2, 3, \dots \quad (12.33)$$

We now have the component functions $f(r)$ and $g(t)$ that comprise $\gamma(r,t)$ and can combine them, which yields:

$$\gamma(r, t) = c_n \sin\left(\frac{n\pi r}{R}\right) e^{-\left(\frac{n\pi}{R}\right)^2 D t}, n = 1, 2, 3, \dots \quad (12.34)$$

Where the subscript n has been added to the coefficient c to indicate that it will likely be different for different values of n . Because different values of n correspond to different solutions, and the principle of superposition states that any sum of solutions is also a solution, we may write:

$$\gamma(r, t) = \sum_{n=1}^{\infty} c_n \sin\left(\frac{n\pi r}{R}\right) e^{-\left(\frac{n\pi}{R}\right)^2 D t} \quad (12.35)$$

The constants c_n are determined by the initial condition, viz.:

$$\gamma(r, 0) = \sum_{n=1}^{\infty} c_n \sin\left(\frac{n\pi r}{R}\right) e^{-\left(\frac{n\pi}{R}\right)^2 D \cdot 0} \quad (12.36)$$

And thus:

$$\gamma(r, 0) = rC_0 = \sum_{n=1}^{\infty} c_n \sin\left(\frac{n\pi r}{R}\right) \quad (12.37)$$

12.37 is in the form of a Fourier sine series, and thus c_n are the coefficients of the Fourier sine series representation of the initial condition. Fourier showed from the orthogonality of the sines that the coefficients are given by:

$$c_n = \frac{2}{R} \int_0^R \gamma(r, 0) \sin\left(\frac{n\pi r}{R}\right) dr = \frac{2}{R} \int_0^R rC_0 \sin\left(\frac{n\pi r}{R}\right) dr \quad (12.38)$$

And integrating by parts yields:

$$c_n = \frac{2C_0R}{n\pi} (-1)^{n+1} \quad (12.39)$$

Substituting 12.39 into 12.35 and rearranging, we have:

$$\gamma(r, t) = \frac{2C_0R}{\pi} \sum_{n=1}^{\infty} \frac{(-1)^{n+1}}{n} \sin\left(\frac{n\pi r}{R}\right) e^{-\left(\frac{n\pi}{R}\right)^2 Dt} \quad (12.40)$$

And finally, substitution of 12.35 into 12.10 yields the series solution of Fick's second

law, viz.:

$$C(r, t) = \frac{2C_0R}{\pi r} \sum_{n=1}^{\infty} \frac{(-1)^{n+1}}{n} \sin\left(\frac{n\pi r}{R}\right) e^{-\left(\frac{n\pi}{R}\right)^2 Dt} \quad (12.41)$$

Which is the concentration profile in the sphere as a function of time and position.

Fick's first law may be applied to 12.41 to give the flux $J(r, t)$ as a function of time and position in the sphere:

$$J(r, t) = -D \frac{\partial C(r, t)}{\partial r} = -D \frac{\partial}{\partial r} \left[\frac{2C_0R}{\pi r} \sum_{n=1}^{\infty} \frac{(-1)^{n+1}}{n} \sin\left(\frac{n\pi r}{R}\right) e^{-\left(\frac{n\pi}{R}\right)^2 Dt} \right] \quad (12.42)$$

Which, using the product rule, gives:

$$J(r, t) = \frac{2DC_0R}{\pi} \sum_{n=1}^{\infty} \left[\frac{(-1)^n}{nr^2} \sin\left(\frac{n\pi r}{R}\right) e^{-\left(\frac{n\pi}{R}\right)^2 Dt} + \frac{\pi(-1)^{n+1}}{rR} \cos\left(\frac{n\pi r}{R}\right) e^{-\left(\frac{n\pi}{R}\right)^2 Dt} \right] \quad (12.43)$$

Of particular interest is the flux through the sphere surface, i.e. at $r=R$, which by substitution is:

$$J(r, t)|_{r=R} = J_R(t) = \frac{2DC_0}{R} \sum_{n=1}^{\infty} e^{-\left(\frac{n\pi}{R}\right)^2 Dt} \quad (12.44)$$

The mass flow rate through the surface is thus:

$$\dot{m}(t) = 4\pi R^2 \cdot J_R(t) = 8\pi RDC_0 \sum_{n=1}^{\infty} e^{-\left(\frac{n\pi}{R}\right)^2 Dt} \quad (12.45)$$

And because $C_0=m_0/V$, and for a sphere $V=4/3\pi R^3$, we can write:

$$\dot{m}(t) = \frac{6Dm_0}{R^2} \sum_{n=1}^{\infty} e^{-\left(\frac{n\pi}{R}\right)^2 Dt} \quad (12.46)$$

The time integral of the mass flow rate gives the cumulative mass diffused

$m_{diffused}(t)$ through the surface, viz.:

$$m_{diffused}(t) = \int_0^t \dot{m}(t) dt = m_0 - \frac{6m_0}{\pi^2} \sum_{n=1}^{\infty} \frac{1}{n^2} e^{-\left(\frac{n\pi}{R}\right)^2 Dt} \quad (12.47)$$

And the fractional release $F(t)$, defined as the cumulative mass diffused divided by the initial mass, is therefore:

$$F(t) = \frac{m_{diffused}(t)}{m_0} = 1 - \frac{6}{\pi^2} \sum_{n=1}^{\infty} \frac{1}{n^2} e^{-\left(\frac{n\pi}{R}\right)^2 Dt} \quad (12.48)$$

12.1.3. Spherical Release Short Time Solution

Use of the Laplace transform (LT) technique to solve A-8 is presented here. The Laplace transform is a mathematical tool used to solve certain differential equations by mapping them into a frequency domain where they can be solved algebraically. We begin by transforming the problem into one with homogeneous BC's as described in the previous section. Applying the Laplace transform to 12.13, we have:

$$\mathcal{L}\left\{\frac{\partial \gamma(r,t)}{\partial t}\right\} = \mathcal{L}\left\{D \frac{\partial^2 \gamma(r,t)}{\partial r^2}\right\} \quad (12.49)$$

And using the definition of the LT, viz:

$$\mathcal{L}\{f(t)\} = f^*(s) = \int_0^{\infty} e^{-st} f(t) dt \quad (12.50)$$

We have:

$$\int_0^{\infty} e^{-st} \frac{\partial \gamma(r,t)}{\partial t} dt = \int_0^{\infty} e^{-st} D \frac{\partial^2 \gamma(r,t)}{\partial r^2} dt \quad (12.51)$$

Integration of 12.51 by parts yields:

$$e^{-st} \gamma(r,t) \Big|_0^{\infty} + s \int_0^{\infty} e^{-st} \gamma(r,t) dt = D \frac{\partial^2}{\partial r^2} \int_0^{\infty} e^{-st} \gamma(r,t) dt \quad (12.52)$$

And, because $\gamma(r,0)=rC_0$ (the initial condition) we can simplify 12.52 to:

$$-rC_0 + s\gamma^*(r,s) = D \frac{\partial^2 \gamma^*(r,s)}{\partial r^2} \quad (12.53)$$

And rearranging 12.53 to standard form, we have:

$$\frac{\partial^2 \gamma^*(r,s)}{\partial r^2} - \frac{s}{D} \gamma^*(r,s) = -\frac{rC_0}{D} \quad (12.54)$$

Where 12.13 is a partial differential equation, 12.54 is an 2nd order non-homogeneous ordinary differential equation that may be solved by standard methods.

We start with the solution of the complimentary problem (where the problem is homogeneous, i.e. $-rC_0/D=0$). We form the characteristic equation:

$$a^2 - \frac{s}{D} = 0 \quad (12.55)$$

And thus:

$$a = \pm \sqrt{\frac{s}{D}} \quad (12.56)$$

And the complimentary solution of 12.54 is therefore:

$$\gamma^*(r,s) = c_1 e^{r\sqrt{\frac{s}{D}}} + c_2 e^{-r\sqrt{\frac{s}{D}}} \quad (12.57)$$

We now use the method of undetermined coefficients to obtain the general solution of 12.54. Because the right side of 12.54 is a 1st order polynomial in r , we look for a particular solution of the form $\gamma^*(r,s)=Ar+B$. Substitution yields:

$$\frac{\partial^2(Ar+B)}{\partial r^2} - \frac{s}{D}(Ar + B) = -\frac{rC_0}{D} \quad (12.58)$$

And thus:

$$0 - \frac{sA}{D}r - \frac{sB}{D} = -\frac{rC_0}{D} \quad (12.59)$$

Solving for A and B:

$$-\frac{sA}{D}r = -\frac{rC_0}{D} \therefore A = \frac{C_0}{s} \quad (12.60)$$

$$-\frac{sB}{D} = 0 \therefore B = 0 \quad (12.61)$$

We find a particular solution is thus:

$$\gamma^*(r, s) = \frac{rC_0}{s} \quad (12.62)$$

And the general solution is thus:

$$\gamma^*(r, s) = c_1 e^{r\sqrt{\frac{s}{D}}} + c_2 e^{-r\sqrt{\frac{s}{D}}} + \frac{rC_0}{s} \quad (12.63)$$

We may now solve for the coefficients c_1 and c_2 using the Laplace transform of the original boundary conditions of 12.13. Using the BC at the sphere center:

$$\gamma^*(0, s) = \int_0^\infty e^{-st} \gamma(0, t) dt = \int_0^\infty e^{-st} \cdot 0 dt = 0 = c_1 e^{0\sqrt{\frac{s}{D}}} + c_2 e^{-0\sqrt{\frac{s}{D}}} + \frac{0 \cdot C_0}{s} \quad (12.64)$$

And thus:

$$c_1 = -c_2 \quad (12.65)$$

Using the BC at the surface:

$$\gamma^*(R, s) = \int_0^\infty e^{-st} \gamma(R, t) dt = \int_0^\infty e^{-st} \cdot 0 dt = 0 = c_1 e^{R\sqrt{\frac{s}{D}}} + c_2 e^{-R\sqrt{\frac{s}{D}}} + \frac{R \cdot C_0}{s} =$$

$$c_1 e^{R\sqrt{\frac{s}{D}}} - c_1 e^{-R\sqrt{\frac{s}{D}}} + \frac{RC_0}{s} \quad (12.66)$$

And thus:

$$c_1 = -\frac{RC_0}{s \left(e^{R\sqrt{\frac{s}{D}}} - e^{-R\sqrt{\frac{s}{D}}} \right)} \quad (12.67)$$

$$c_2 = \frac{RC_0}{s \left(e^{R\sqrt{\frac{s}{D}}} - e^{-R\sqrt{\frac{s}{D}}} \right)} \quad (12.68)$$

And the solution of the the transformed boundary value problem is therefore:

$$\gamma^*(r, s) = -\frac{RC_0}{s} \left(\frac{e^{r\sqrt{\frac{s}{D}}} - e^{-r\sqrt{\frac{s}{D}}}}{e^{R\sqrt{\frac{s}{D}}} - e^{-R\sqrt{\frac{s}{D}}}} \right) + \frac{rC_0}{s} \quad (12.69)$$

We may apply the Laplace transform to our original substitution 12.9, to obtain the relationship between $\gamma^*(r, s)$ and $C^*(r, s)$. Taking the Laplace transform of 12.9:

$$\mathcal{L}\{\gamma(r, t)\} = \mathcal{L}\{r \cdot C(r, t)\} \quad (12.70)$$

We have:

$$\int_0^\infty e^{-st} \gamma(r, t) dt = \int_0^\infty e^{-st} r \cdot C(r, t) dt \quad (12.71)$$

And simplifying:

$$\gamma^*(r, s) = r \cdot C^*(r, s) \quad (12.72)$$

Rearranging 12.66:

$$C^*(r, s) = \frac{\gamma^*(r, s)}{r} \quad (12.73)$$

And the transformed concentration profile is therefore:

$$C^*(r, s) = -\frac{RC_0}{sr} \left(\frac{e^{r\sqrt{\frac{s}{D}}} - e^{-r\sqrt{\frac{s}{D}}}}{e^{R\sqrt{\frac{s}{D}}} - e^{-R\sqrt{\frac{s}{D}}}} \right) + \frac{C_0}{s} \quad (12.74)$$

We may now invert the transform to give the concentration profile as a function of time and position. When modeling release of diffusant from a spherical particle, however, it is often more useful to know the theoretical rate of loss of diffusant from the surface, or the fractional release, as these are more conveniently measured than the concentration profile within the sphere and therefore more useful in extracting the diffusion coefficient from a spherical release experiment. In particular, the flux at $r=R$ is desired, we may put Fick's first law in terms of $C^*(r, s)$ and $J^*(r, s)$ by applying the Laplace transform.

Applying the Laplace transform to Fick's 1st law, we have:

$$\mathcal{L}\{J(r, t)\} = \mathcal{L}\left\{-D \frac{\partial C(r, t)}{\partial r}\right\} \quad (12.75)$$

Which gives:

$$\int_0^\infty e^{-st} J(r, t) dt = -\int_0^\infty e^{-st} D \frac{\partial C(r, t)}{\partial r} dt \quad (12.76)$$

Which can be written as:

$$J^*(r, s) = -D \frac{\partial C^*(r, s)}{\partial r} \quad (12.77)$$

Substituting 12.68 into 12.71 and using the product rule, we have:

$$J^*(r, s) = -\frac{DRC_0}{sr^2} \left(\frac{e^{r\sqrt{\frac{s}{D}}} - e^{-r\sqrt{\frac{s}{D}}}}{e^{R\sqrt{\frac{s}{D}}} - e^{-R\sqrt{\frac{s}{D}}}} \right) + \frac{DRC_0}{sr} \sqrt{\frac{s}{D}} \left(\frac{e^{r\sqrt{\frac{s}{D}}} + e^{-r\sqrt{\frac{s}{D}}}}{e^{R\sqrt{\frac{s}{D}}} - e^{-R\sqrt{\frac{s}{D}}}} \right) \quad (12.78)$$

At $r=R$ this simplifies to:

$$J^*(R, s) = -\frac{DC_0}{sR} + \frac{DC_0}{s} \sqrt{\frac{s}{D}} \left(\frac{e^{R\sqrt{\frac{s}{D}}} + e^{-R\sqrt{\frac{s}{D}}}}{e^{R\sqrt{\frac{s}{D}}} - e^{-R\sqrt{\frac{s}{D}}}} \right) \quad (12.79)$$

THE SHORT TIME APPROXIMATION: when the time t is small, the Laplace variable s is large. Therefore at short times, the term in parentheses in 12.73 may be set to unity. We now have:

$$J^*_{short}(R, s) = -\frac{DC_0}{sR} + \frac{DC_0}{s} \sqrt{\frac{s}{D}} \quad (12.80)$$

Which may readily be inverted using a table of Laplace transforms or mathematical software. Rearranging 12.73 for convenience, we have:

$$J^*_{short}(R, s) = -\frac{DC_0}{R} \left(\frac{1}{s} \right) + \frac{C_0\sqrt{D}}{\sqrt{\pi}} \sqrt{\frac{\pi}{s}} \quad (12.81)$$

Taking the inverse of 12.74:

$$\mathcal{L}\{J^*_{short}(R, s)\} = \mathcal{L}\left\{-\frac{DC_0}{R} \left(\frac{1}{s} \right) + \frac{C_0\sqrt{D}}{\sqrt{\pi}} \sqrt{\frac{\pi}{s}}\right\} = -\frac{DC_0}{R} + \frac{C_0\sqrt{D}}{\sqrt{\pi t}} = J(R, t) \quad (12.82)$$

The flux may be used to calculate the fractional release as described in the previous section. Multiplication by the surface area, integration with respect to time, and division by the initial mass gives $F_{short}(t)$, which is:

$$F_{short}(t) = 6\sqrt{\frac{Dt}{\pi R^2}} - 3\frac{Dt}{R^2} \quad (12.83)$$

12.2. Development of a MS Excel Program for Calculation of Diffusion Coefficients

12.2.1. Introduction

An Excel program set was desirable for extraction of diffusion coefficients in the current work, particularly for compatibility with current instrument software and existing Excel spreadsheets developed at MURR for ICP-MS data analysis. Requirements for the spreadsheets included:

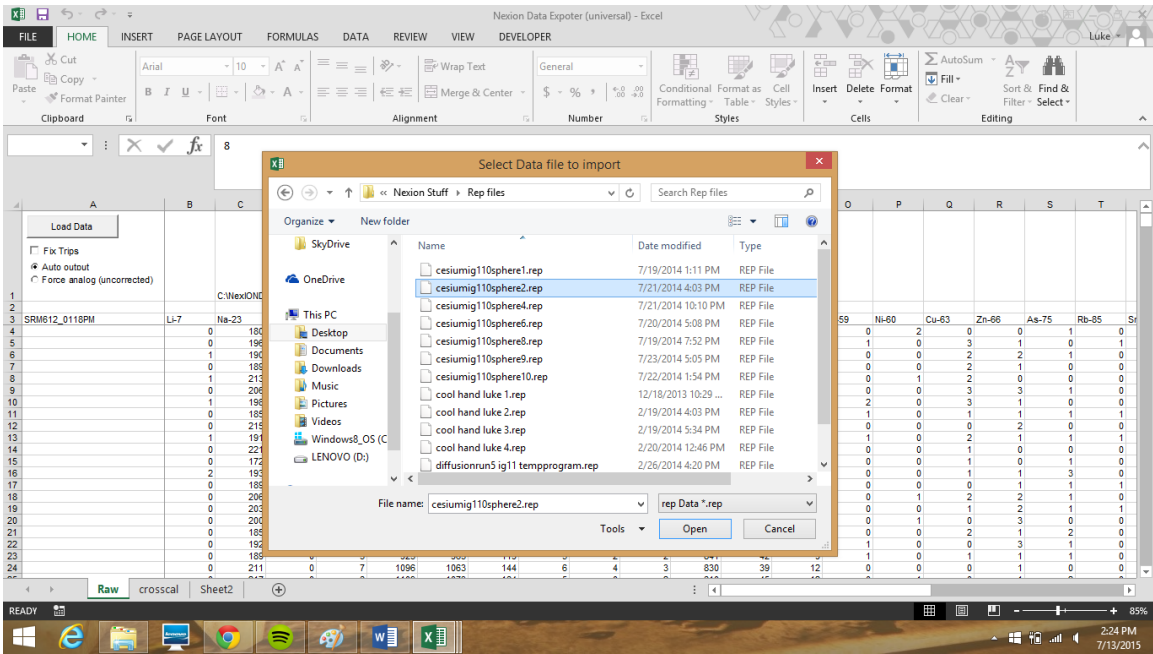
- ICP-MS data analysis spreadsheet for importation of ICP-MS data, signal normalization, instrument background subtraction, and calibration
- Spherical release diffusion simulator/calculator for visualization of expected phenomena and calculation of diffusion coefficients from experimental release data via least squares regression
- Spherical infusion simulator/calculator for selection of appropriate infusion times/temperatures and sample dimensions, and calculation of diffusion coefficients from experimental infusion data (measured concentration profile)

12.2.2. ICP-MS Data Analysis Spreadsheet

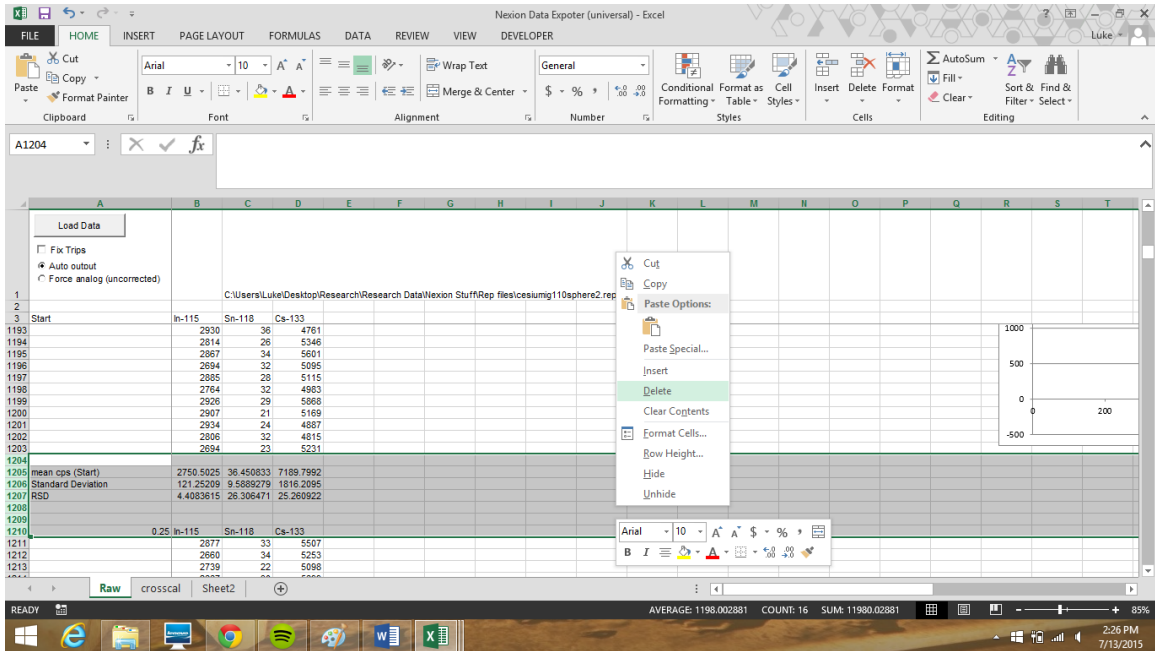
The ICP-MS diffusion data analysis spreadsheet is a modified form of the Nexion Data Expoter (Universal) developed by Barry Higgins at MURR (Note the “Expoter” and “Expoter” are different). The spreadsheet normalizes the internal standard response of the instrument to a constant value and scales the analyte signal relative to the normalization factor. The background may then be subtracted from the signal, and the

calibration factor determined. Finally, the spreadsheet calculates the actual mass transport rate or flux from the sample to the ICP-MS. The procedure for use is as follows:

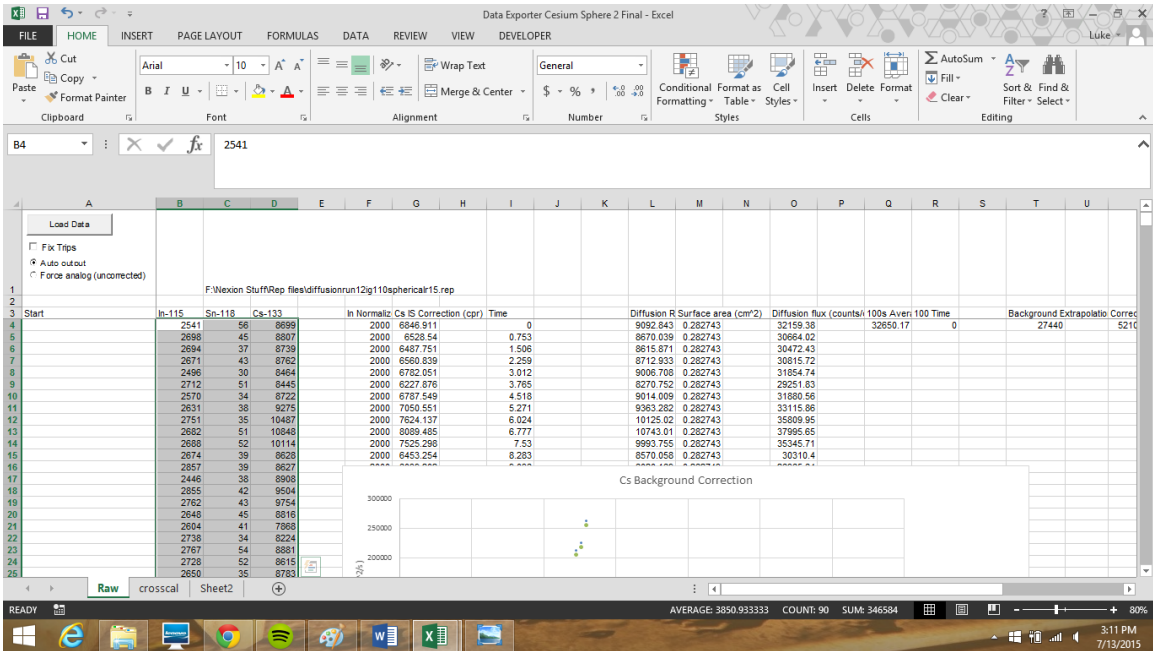
- Open the Nexion Data Expoter, and import the Report Output file to be analyzed using the “Load Data” button.



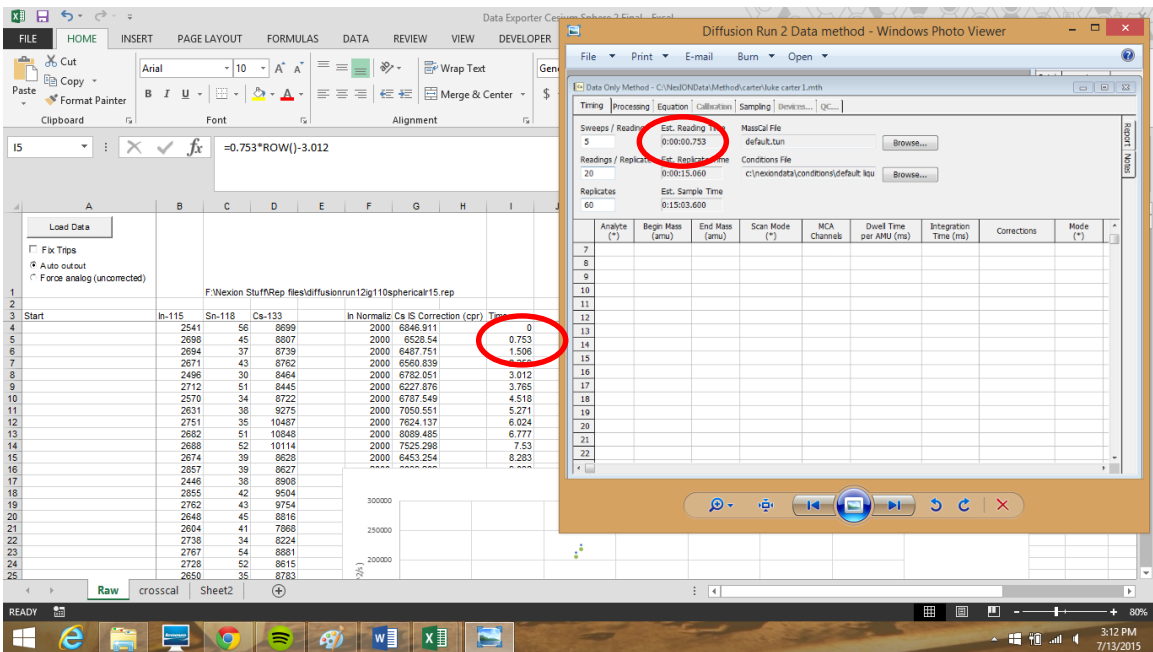
- Delete all discontinuities in the data series where average, RSD, and blank spaces are computed.



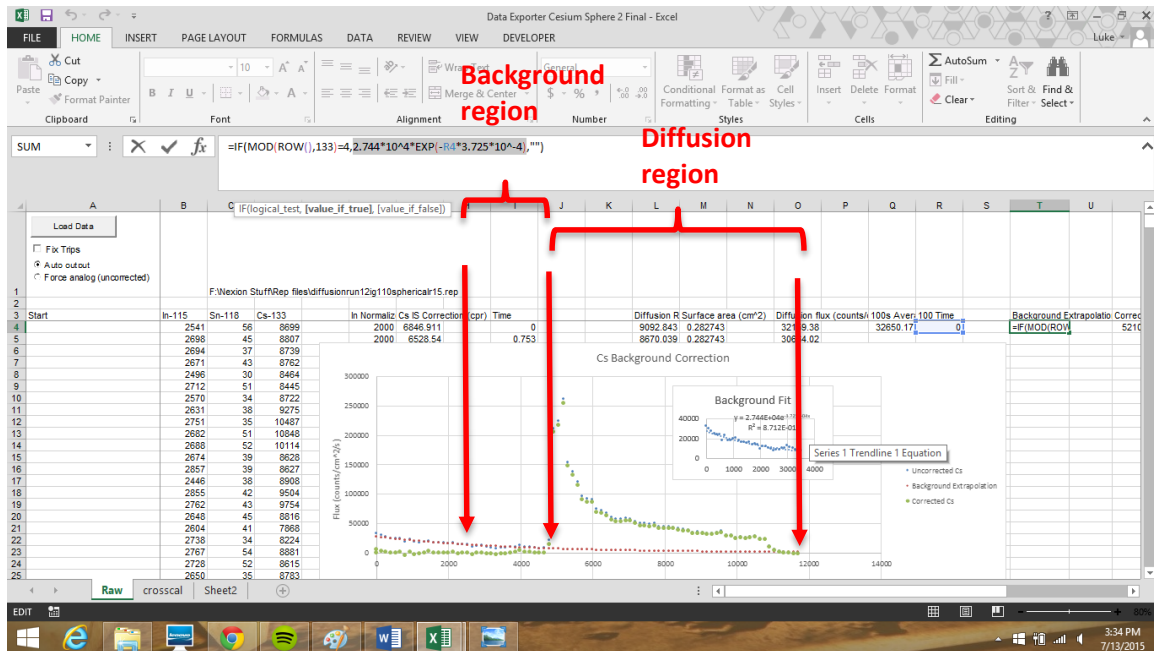
- Copy the data (columns B-D from row 4 to end of data) from the Nexion Data Expoter and paste into the ICP-MS diffusion data analysis spreadsheet. The spreadsheet will automatically normalize the In internal standard response to 2000 counts/reading and scale the Cs (or other analyte) response by the appropriate factor.



- If the data acquisition parameters are different than those used presently (see insert), adjust the time step in column I to the actual value used.



- Input sample radius (centimeters) into surface area formula in column M. The spreadsheet will calculate the material flux (counts/s·cm²).
- Determine the background region of the diffusion curve. To do this properly, one must set the furnace to target temperature and note the time at which the temperature in the diffusion cell comes to thermal equilibrium (the furnace tends to overheat the cell initially, and gradually descends to an equilibrium temperature approximately 20° higher than the furnace thermocouple reading). Modify as necessary for particular furnace used. The background may be taken as well-described by the part of the curve from when thermal equilibrium is reached to sample introduction. This part of the curve is generally well-fit with either a slowly-decaying exponential function, or a constant.
- Enter the coefficients from the background fit into the equation in column T, and fill down. The spreadsheet will subtract the background from the experimental data to give a corrected flux curve in column V. If the plot does not show discrete points, delete any formulas which may show as *empty cells* present in the data range plotted.



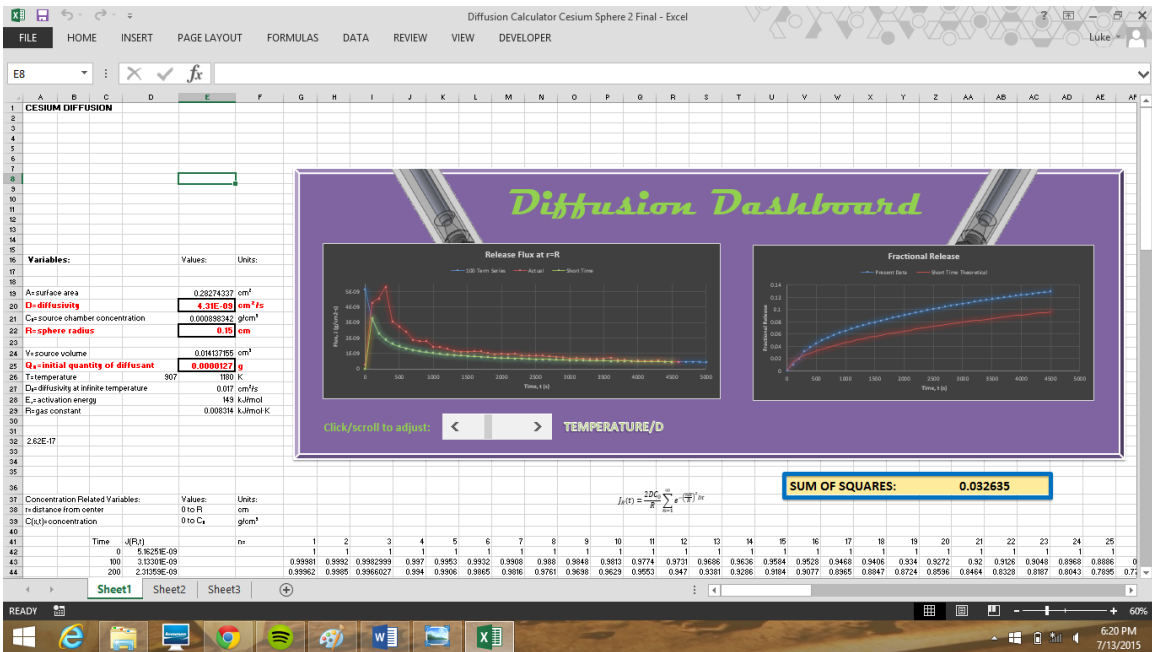
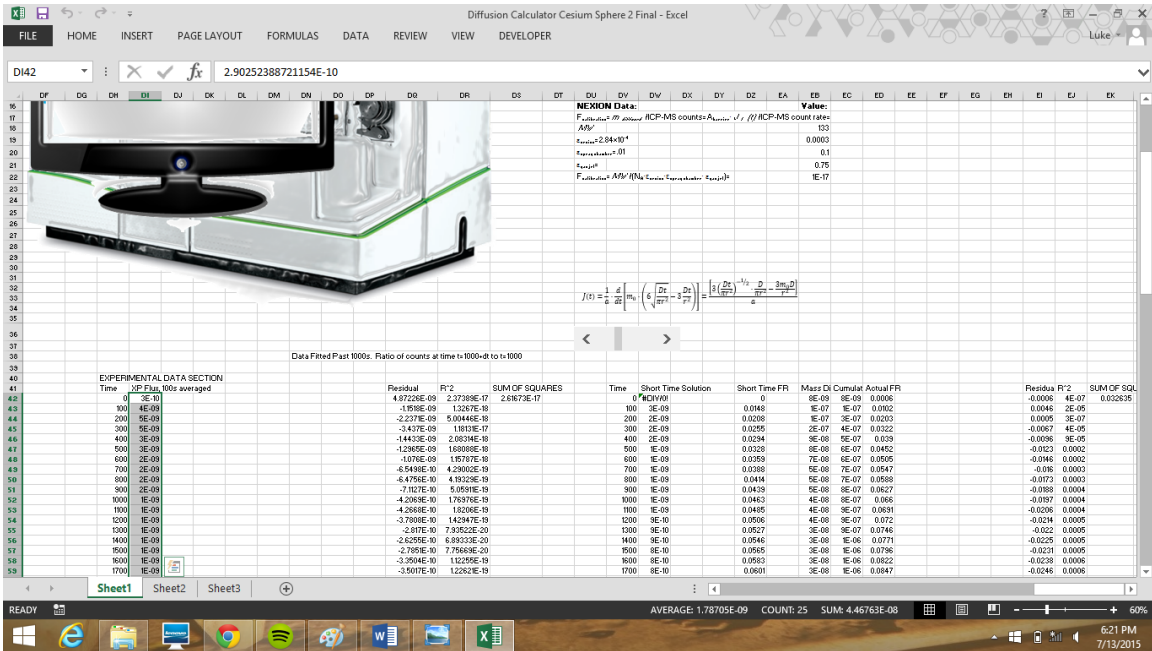
- Determine the total counts acquired in the diffusion region. This is taken as the cumulative counts acquired from sample introduction until after furnace shutdown. Enter the cell numbers for the range into the formula in column X.
- The total mass diffused divided by counts acquired is the calibration factor. Enter the total mass diffused (g) from INAA into the formula in column Z. The spreadsheet will calculate the actual mass flux from the sample, which may be used for extraction of the diffusion coefficient.

12.2.3. Spherical Release Diffusion Calculator/Simulator

The spherical release calculator allows one to extract diffusion coefficients from the data obtained with the ICP-MS if the initial distribution of diffusant in the sample is

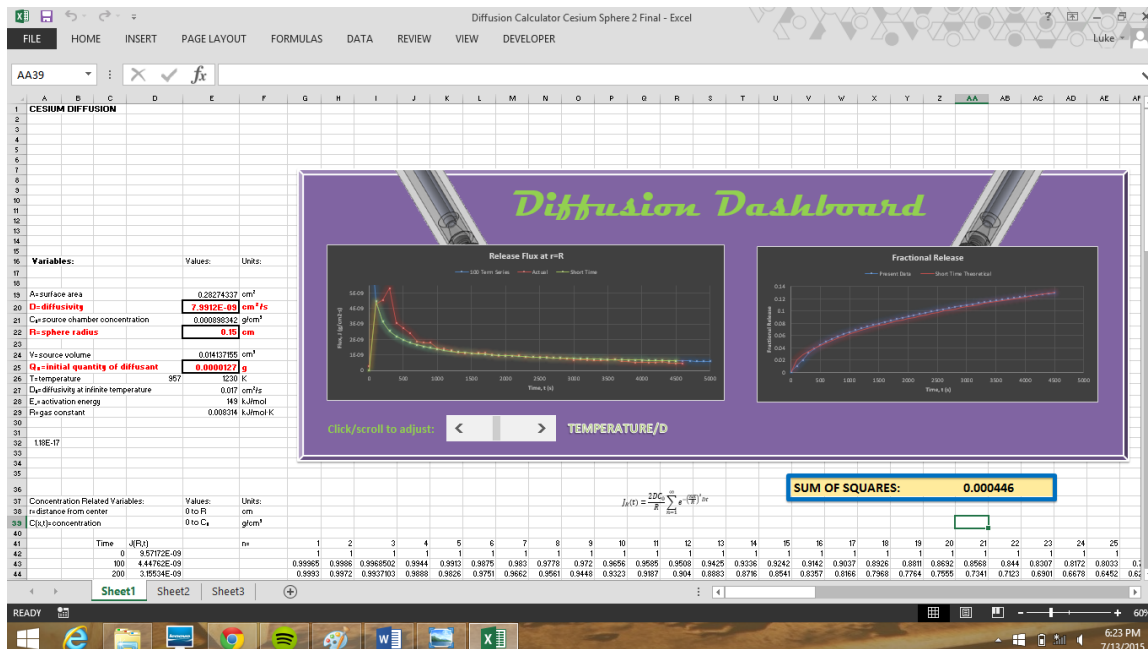
known. Use of the spreadsheet is illustrated for a sphere with a uniform initial distribution of diffusant.

- Open the Spherical Release Diffusion Calculator
- Copy the release flux data (corresponding the diffusion region only) from the ICP-MS Data Analysis Spreadsheet and paste into column *DI* of the Spherical Release Diffusion Calculator. Enter the sphere radius (cm) into cell *E22* and the initial diffusant mass as determined by INAA into cell *E25*. The spreadsheet will calculate the experimental fractional release and will plot both the flux and fractional release. The calculator will also plot the theoretical flux and fractional release. As discussed in Chapter 5, we believe the fractional release gives the most appropriate form of the data for extraction of the diffusion coefficient, and therefore the calculator's regression function uses only the fractional release data. Note in the release and flux plots below, the theoretical curves are below the experimental ones, indicating the diffusion coefficient should be increased to obtain a better fit.



- The scroll bar/spin button beneath the flux and fractional release curves allows one to plot the theoretical flux/FR for different values of the diffusion coefficient. Cell V36 gives the sum of squares of the differences between each
- 185

point on the experimental and theoretical data curves. Adjust the value of the diffusion coefficient using the scroll bar/spin button until the sum of squares reaches a minimum value. Note the better fit and smaller sum of squares in the figure below.



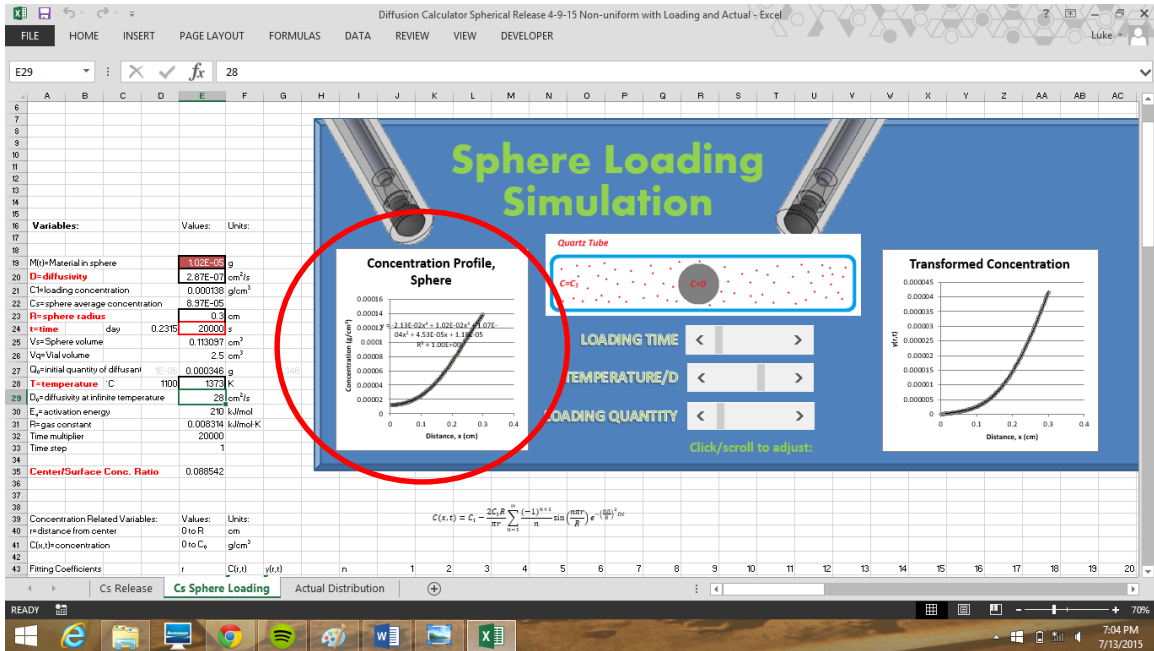
12.2.4. Spherical Infusion Calculator/Simulator

The spherical infusion calculator/simulator calculates the expected diffusant concentration profile given an assumed value of the diffusion coefficient (e.g. from the literature), loading time, and source concentration. The boundary conditions of the model specify a constant source concentration (i.e. $C(R,t)=C_0$) which experimentally can be challenging to realize. Therefore, generally, this calculator is best suited to

determining appropriate infusion time and temperature conditions, in preparation for a subsequent release experiment. The infusion calculator also simulates release experiments from spheres infused for an arbitrary amount of time given an assumed diffusion coefficient, i.e. for both uniform distributions as well as non-uniform initial distributions well-described by a 4th order polynomial. An example of its use is illustrated below.

Example problem: Fukuda [16] gives the diffusion coefficients of Sr in compacted nuclear graphite with parameters $D_0=28 \text{ cm}^2/\text{s}$ and $E_a=210 \text{ kJ/mol}$. Calculate the time required for a uniform initial distribution of Sr to be achieved in spheres of the same material with $R=0.3 \text{ cm}$, at 1100°C .

- Open the Spherical Infusion Calculator/Simulator and select the “Sphere Loading” tab
- Enter the D_0 and E_a values into cells $E29$ and $E30$, respectively. Enter the loading temperature into cell $E28$. Enter the sphere radius into cell $E23$. The figure indicates the expected concentration profile at $t=20,000 \text{ s}$.



- Increase the time using the "Loading Time" scroll bar or spin button until the profile is approximately uniform. Cell E35 indicates the concentration at the center relative to the surface. Increasing the loading time to 120,000 s, one finds the concentration at the center is 95% of that at the surface, indicating an approximately uniform distribution of Sr should be achieved given these conditions (note the nearly flat concentration profile in the figure below).

Diffusion Calculator Spherical Release 4-9-15 Non-uniform with Loading and Actual - Excel

FILE HOME INSERT PAGE LAYOUT FORMULAS DATA REVIEW VIEW DEVELOPER

E29 fx 28

Variables:	Values:	Units:
M0=Material in sphere	1.502346	g
D=diffusivity	2.87E-07	cm ² /s
C1=loading concentration	0.000138	g/cm ³
C2=sphere average concentration	0.000134	
R=sphere radius	0.3	cm
t=time	1.3888	day
V0=sphere volume	0.110097	cm ³
V0q=Vial volume	2.5	cm ³
Q0=initial quantity of diffusant	0.000346	g
T=temperature	1100	°C
D0=diffusivity at infinite temperature	1373	K
Ea=activation energy	28	cm ² /s
R=gas constant	0.008314	kJ/mol K
Time multiplier	20000	
Time step	6	
Center/Surface Conc. Ratio	0.9541	

Sphere Loading Simulation

Concentration Profile, Sphere

Quartz Tube

LOADING TIME < >

TEMPERATURE/D < >

LOADING QUANTITY < >

Click/scroll to adjust:

Transformed Concentration

$$C(r,t) = C_1 - \frac{2C_1 R}{\pi r} \sum_{n=1}^{\infty} \frac{(-1)^{n+1} \sin\left(\frac{n\pi r}{R}\right)}{n - \sin\left(\frac{n\pi r}{R}\right)} e^{-\left(\frac{n\pi D}{R}\right)^2 t}$$

Concentration Related Variables: Values: Units:

r=distance from center: 0 to R: cm

C1,C2=concentration: 0 to C2: g/cm³

Fitting Coefficients: r: C1(x) y(x) n: 1 2 3 4 5 6 7 8 9 10 11 12 13 14 15 16 17 18 19 20

Cs Release Cs Sphere Loading Actual Distribution

READY 7:11 PM 7/13/2015

VITA

Lukas M. Carter was born on July 7, 1986 in Kansas City, KS. He grew up in mid-Missouri and graduated valedictorian of Community R-VI High School. He majored in chemistry at the University of Missouri and earned his bachelor of sciences degree in 2010. During this time he raced competitively for the MU Cycling Team, and became interested in radiochemistry and analytical chemistry. He was accepted into the Ph. D. program at the University of Missouri, and joined the Robertson group soon after. He will complete his Ph. D. in December, 2015.